Cape Peninsula University of Technology

Elemental Cu-doped Co_3O_4 thin film for highly sensitive non-enzymatic glucose detection

by

Micaela Lisa Harry

Thesis submitted in the fulfilment of the requirements for the degree

Master of Engineering: Chemical Engineering

In the Faculty of Engineering

at Cape Peninsula University of Technology

Supervisor: Dr. M. R. Chowdhury

Bellville Campus

Date Submitted: 1st July 2019

Declaration

I, Micaela Harry, hereby declare that this research dissertation is my own unaided work. It is being submitted for the MEng Degree at the Cape Peninsula University of Technology. It has not been submitted before for any degree or examination in any other University. Furthermore, it represents my own opinions and not necessarily those of the Cape Peninsula University of Technology.

…….. 13/10/2019 ……..

Signed **Date**

Elemental Cu-doped Co_3O_4 thin film for highly sensitive non-enzymatic glucose detection

M.L.Harry

Abstract

This thesis is a study and analysis of the non-enzymatic glucose sensing ability of elemental Cu-doped Co_3O_4 thin film deposited on FTO. A facile chemical solution method was utilized to substitute elemental Cu into the Co_3O_4 host lattice structure. The morphology of the electrode was characterized by XRD, SEM, HRTEM, SAED and EELS. The introduction of Cu resulted in increased electrical conductivity, charge density and decreased charge transfer resistance in Co_3O_4. This ultimately resulted in enhanced electrochemical activity when compared to pristine Co_3O_4. The as prepared thin film exhibited very high sensitivity, 1850 $\mu Acm^{-2}mM^{-1}$, and linear range up to 7.6 mM. The sensor showed a limit of detection of 153 nM at a signal to noise ratio of 3. The developed sensor was used successfully to measure glucose level in human serum and spiked saliva sample.

Acknowledgements

I am thankful to:

~Dr. Chowdhury, for the supervision and guidance on completion of my thesis. And for allowing me to pursue the research under his direction

~The staff at the *Flow Process and Rheology Centre* for creating an inclusive culture

~My family, for their continuous support and guidance throughout my journey always

The financial assistance of the National Research Foundation, CPUT & Mauerberger Foundation towards this research is acknowledged. Opinions expressed in this thesis and the conclusions arrived at are those of the author, and are not necessarily to be attributed to the National Research Foundation, CPUT & Mauerberger Foundation.

Dedication

This thesis is dedicated to my beautiful mother, *Indira Harry*, for her love, continuous support and guidance. My father, *Terry Chris Harry*, for his patience, love and support continually. And my sister, *Isobel Harry*, for her kindness, love, motivation and always being prepared to help me when required.

To all those struggling to find inspiration, this is what I tend to live by:

"We can't choose where we come from, but we can choose where we go from there."

- Stephen Chbosky

Table of Contents

List of figures

List of tables

List of equations

Glossary- Terms and Concepts

Biosensor	a device which uses a living organism or biological molecules, especially enzymes or antibodies, to detect the presence of chemicals
Electrochemical cell	a device capable of either generating electrical energy from chemical reactions or using electrical energy to cause chemical reactions
Fermi Level	(of a solid-state body) is the thermodynamic a device capable of either generating electrical energy from chemical reactions or using electrical energy to cause chemical reactions

List of abbreviations

AA	Acetic Acid
AC	Acetaminophen
CE	Counter Electrode
CV	Cyclic Voltammetry
DNS	Dinitro Salicylic Acid
EC	Electrochemical cell
EDS	Energy Dispersive Spectroscopy
EELS	Electron Energy Loss Spectroscopy
EIS	Electrochemical Impedance Spectroscopy
ELNEFS	Energy Loss Near Edge Fine Structure
FTO	Fluorine Doped Tin Oxide
HAADf	High-Angle Annular Dark-Field Imaging
LOD	Limit of Detection
RE	Reference electrode
RSD	Relative Standard Deviation

SEM	Scanning Electron Microscopy
TEM	Transmission Electron Microscopy
UA	Uric Acid
WE	Working Electrode
XRD	X-ray Diffraction

List of Symbols

Notation	Description	Unit
E	Emission Line Energy	-
Z	Atomic number	-
A	Ammeter	A
V	Potential difference	V
Z	Faraday Impedance	
I	Current	A
Rs	Electrolyte Resistance	Ω
Cdl	Double layered capacitance	F
Rct	Charge transfer resistance	Ω
n	No. of electrons for oxidation/ reduction	-
F	Faradays constant	C/mol
A	Area of electrode	m^2
C_j^0	Initial concentration of reducible analyte	mM
D_j	Diffusion co-efficient	-
s	Time	s
ŋ	Integer	-
d	Interplanar spacing	m
L	Length	m
B	Breadth	m
D	Depth	m
σ	Standard deviation	-
$C_{1/2}$	Constant	-
W	Warburg element	$mMho \cdot s^{1/2}$
N	Number of layers	-

Greek symbols

Θ	theta
λ	lambda
σ	sigma
μ	micro

~ *Chapter 1* ~

Introduction

This research comprises the study of a copper doped cobalt oxide thin film non-enzymatic glucose sensor, which is economically feasible for the purpose of depicting an enhanced detection of glucose.

This chapter comprises:

***Section 1.1**: Background of research*

***Section 1.2:** Problem statement*

***Section 1.3:** Aim and objectives*

***Section 1.4:** Research question*

***Section 1.5:** Delineation of study*

***Section 1.6:** Thesis structure*

Chapter 1: Introduction

1.1. Background of research

Currently, one of the major causes of death and disability in the world is diabetes mellitus. The frequent testing of physiological blood glucose levels to avoid grave emergencies is vital for the confirmation of effective diabetic treatment. According to Luo *et al*. (2012), glucose monitoring is also vital in the food industry, clinical diagnostics and medicine. According to the WHO (2016), the number of individuals diagnosed with diabetes has escalated from 108 million in 1980 to 422 million in 2014. As a result, effective and efficient glucose monitoring is a critical requirement.

The current glucose sensors used by diabetic patients are glucose oxidase sensors (enzymatic) (Si *et al*., 2012). The difference between enzymatic and non-enzymatic glucose sensors is that an enzyme is utilized as the electrocatalyst on the former, while for the latter; a metal or metal oxide deposited on a substrate functions as the electrocatalyst (Zhu *et al*., 2016). However, due to problems associated with high costs, chemical instability, constrained pH ranges, temperature and humidity levels for enzymatic sensors, non-enzymatic glucose sensors that provide excellent electrochemical detection to glucose have been the main focus in recent research (Si *et al*., 2012).

Previous studies have shown that non-enzymatic glucose sensors have been constructed utilizing precious metals and/or precious metal alloys (Doria *et al*., 2012; Xiang *et al*., 2011; Bansal *et al*., 2016; Lee *et al*., 2010). However, since it is costly to purchase these metals, cost-effective materials, such as metal oxides have been proposed as an alternative (Chowdhury *et al*., 2016).

Nanostructured metal oxide materials are more suitable for non-enzymatic glucose sensors as they have good electrocatalytic properties, large surface areas and fast electron transfer (Zhu *et al*., 2014). In addition, nanostructured materials are advantageous as they counteract drawbacks such as surface poisoning of the electrode and the reduction in potential of glucose oxidation due to the use of noble metal-based non-enzymatic glucose sensors (Si *et al*., 2012). Previous studies have shown that nano-structured materials can be used to produce highly selective and sensitive non-enzymatic glucose sensors (Si *et al*., 2012).

With respect to nanostructured metal oxides, Cu_2O, NiO_2, MnO_2 and Co_3O_4 have been tested and reported in previous studies in terms of glucose selectivity and sensitivity performance (Chowdhury *et al*., 2016). However, among the different oxides, Co_3O_4 demonstrated the optimum glucose sensing performance with a lower detection limit due to the material having a large surface area to allow for additional reactive sites. In the case of this research, Co_3O_4 will be utilized in the construction of the

glucose sensor, together with a dopant material (to improve the performance of the biosensor), i.e. Cu, to further escalate the electrochemical performance. Doping was proven to escalate the electronic conductivity by means of amending the electronic structure of the nanoparticle. This is evidenced in a number of studies including Zn-doped Co_3O_4, Mn and Fe doped Co_3O_4 and Sn doped Co_3O_4 (Kang *et al.*, 2007; Espro *et al.*, 2014; Zhuang *et al.*, 2011). Cu will be added to Co_3O_4 as it was found in previous studies to increase the charge transferability to allow for enhanced glucose detection in the non-enzymatic glucose sensor. This was proven in studies involving Cu nano particles, Cu and CuO (Kang *et al.*, 2007; Espro *et al.*, 2014; Zhuang *et al.*, 2011).

1.2. Problem statement

Commercially available glucose sensors have shown several drawbacks. The problems are associated with high costs, chemical instability, constrained pH ranges, temperature and humidity levels. Pristine Co_3O_4 suffers from a low electronic conductivity which results in a higher LOD, low sensitivity and low linear ranges.

1.3. Aim and objectives

The aim of this research project is to evaluate the electrochemical performance of Cu-doped Co_3O_4 thin film for glucose detection.

In accordance to the aim above, the following objectives that will be reached.

- A solution deposition of Cu-doped Co_3O_4 thin film on FTO substrate
- Sensing performance of the as-developed sensor

1.4. Research question

What effect does the doping of Cu into Co_3O_4 have on the electrochemical performance of the biosensor?

1.5. Delineation of study

This study will not use fresh blood sample for the testing of the biosensor.

1.6. Thesis structure

Chapter 1: Introduction

Chapter 1 provides a brief background to the research and contextualizes the problem statement. The chapter is a framework for the aim and objectives including the research questions and a delineation of this research study. The chapter inaugurates the quantitative analysis for biosensor performance.

Chapter 2: Literature review

Chapter 2 comprises a detailed literature review for the research problem. It details the progression of glucose sensors and the origin of non-enzymatic glucose sensors. Inclusive descriptions of the electrochemical cell, including the counter, reference and working electrode, are discussed. Thorough details of the different techniques used for electrochemical measurements and surface characterisation are discussed. A section on sensor fundamentals is provided for.

Chapter 3: Research methodology

Chapter 3 comprises the detailed research and experimental methodology for the development of the novel non-enzymatic glucose sensor utilizing a Cu-doped Co_3O_4 solution material as the electrocatalyst.

Chapter 4: Results and data analysis

Chapter 4 provides significant interpretations of the data retrieved from experimental work. A summary and evaluation of the electrochemical and surface characterisation results of the biosensor is conducted in order to achieve the objectives for this study.

Chapter 5: Conclusion

Chapter 5 includes a summary of the significant results obtained, conclusion, and recommendations for future research.

~ Chapter 2 ~

Literature Review

This chapter comprises:

Section 2.1: *Introduction*

Section 2.2: *Glucose sensors*

Section 2.3: *Material fabrication*

Section 2.4: *Method of fabrication*

Section 2.5: *Electrochemical cell*

Section 2.6: *Techniques for electrochemical measurements*

Section 2.7: *Surface characterisation*

Section 2.8: *Sensor characteristics*

Section 2.9: *Conclusion*

Chapter 2: Literature Review

2.1. Introduction

This chapter is a detailed review associated with glucose sensors. Literature on the fabrication materials and methods is discussed, including theory on the electrochemical cell, electrochemical measurements, surface characterisation, and sensor characterisation.

2.2. Glucose sensors

According to Zhu (2016) and Wang (2013), glucose sensors have broad applications and have been developed to a great extent for diabetes diagnosis. Currently, electrochemical enzymatic glucose sensors are frequently utilized for the detection of glucose and are a success as glucose meters commercially. This is due to their demonstrating high reliability and good selectivity. However, due to general shortcomings of the enzyme i.e. poor stability and a high fabrication cost, amplification to the research of non-enzymatic glucose sensors came about. This is owing to their extraordinary stability, minimal cost, low detection limit and rapid response. Additionally, Zhu and Park (2016) highlight that nanostructured electrodes offer improved performance for glucose sensing applications. With this in mind, the following subsections will provide insight on the timeline of glucose sensors. A perception and appraisal of the distinct types of glucose sensors i.e. enzymatic and non-enzymatic will be discussed.

2.2.1. Timeline of glucose sensors

According to Tian and co-authors (2014), the chronology of the development of glucose sensors can be isolated into four generations. The initial generation of glucose sensors was dependent on the immobilization of the glucose oxidase (GOx) catalytic enzyme. It is further explained that the GOx acted as a catalytic reagent for the oxidation reaction between glucose and oxygen at the surface of the electrode to generate gluconolactone and hydrogen peroxide (Tian *et al.,* 2014). From this, the concentration of glucose was regulated by perceiving the quantity of hydrogen peroxide formed at the electrode. Conversely, free oxygen is mandatory for the reaction, else the reaction mediator (natural mediator) will result in its being problematic. This is due to the sensor not functioning effectually for deficient oxygen blood samples (Wang *et al.*, 2013). Another disadvantage is that these glucose sensors suffer from the interference of electroactive species in the blood, specifically ascorbic acid, uric acid, etc. (Tian *et al.*, 2014).

In contrast, the second generation of glucose sensors utilizes an artificial mediator instead of the natural mediator for the augmentation of the electron transfer procedure. This sensor uses ferrocene derivatives or ferricyanide which is the GOx catalytic enzyme on an artificial mediator (Tian *et al.*,

2014). However, the performance and sensitivity of the sensor was highly reliant on fluctuations of pH for the intermediate, as well as fluctuations in humidity and temperature on the surface of the electrode.

According to Tian and co-authors, the third generation glucose sensors also utilize the GOx enzymatic catalyst; however, porous materials (nano and micro) were selected as the substrate for the immobilization of the GOx. This ensures a heightened surface area of the electrode, hence an escalation of the electron transfer rate. However, the enzyme activity is highly dependent on the temperature, humidity and interference. Due to these drawbacks, non-enzymatic glucose sensors (NEG), which allow glucose to be oxidized on the electrode surface, have come about as the fourth generation glucose sensors.

2.2.2. Enzymatic glucose sensing and its challenges

The variance between enzymatic and non-enzymatic glucose sensors is that the enzyme is utilized as the electrocatalyst on the electrode for the former, and for the latter, metal and/or metal oxide deposited upon the surface of the electrode functions as the electrocatalyst (Zhu *et al.*, 2016). There are several advantages pertaining to detecting glucose without utilizing an enzyme i.e. stability, simplicity, reproducibility and freedom from oxygen limitation (Park *et al.*, 2005). The following highlights the disadvantages of enzymatic glucose sensing.

i. Stability

One of the generic problems associated with enzymatic sensors is the insufficient stability of GOx (Park *et al.*, 2005). GOx is stable in comparison to the other enzymes; however during fabrication, storage or use, the glucose oxidase sensors are subjected to thermal and chemical deformation. According to Wilson and Turner (1992), the GOx enzyme misplaces its catalytic activity below the pH of 2 and beyond the pH of 8, and a temperature exceeding 40 °C could cause terminal damage as well. Park and co-authors (2005) further mentioned that due to the thermal and chemical instability, the GOx sensors are prevented from being used in human bodies, because they require sterilization and incessant observation of fermentation processes. In addition to temperature, pH and chemical instability, GOx sensors are also affected by humidity, as high and low humidity levels could affect the use and storage of these sensors (Park *et al.*, 2005).

ii. Simplicity and reproducibility

In order to develop an enzymatic electrode, one or more layers should be located on the raw substrate for complete optimization (Park *et al.*, 2005). Mohamed and co-authors (2015) reported that there are a variety of methods by which the enzyme can be immobilized, namely direct adsorption, sol-gel entrapment and cross linking, etc. However, since the aim is to develop the sensor for mass production

and commercialization, straightforward and supplementary reproducible methods have been sought (Park *et al.*, 2005). Since the sensitivity of the sensor highly hinges upon the catalytic activity of the enzyme immobilized, another vital aspect to be considered in terms of quality control is reproducibility. This is why electro-polymerization, where the enzyme is entrapped in the solution comprising enzymes or monomers, is expended due to electrical governing of the enzyme deposit depth. However, Park and co-authors (2005) further argue that regardless of the immobilization method, enzyme electrodes are not free of the uncertainty of biological constituents found in artificial surroundings. This justifies why non-enzymatic glucose sensors remain in consideration.

iii. Absence of oxygen limitation

A low concentration of oxygen is associated with the responses of the majority of enzyme electrodes (Park *et al.*, 2005). Generally, all glucose sensors generate an electric current by the oxidation of glucose on the electrode surface; hence the reductive oxygen current functions as interference. This reductive oxygen current interferes due to the thermodynamic reduction potential of oxygen being more positive than where glucose is oxidized. However, fortunately, this interference can be minimized by finding appropriate potential whereby the reduction kinetics of oxygen molecules is sluggish. This is another reason why non-enzymatic glucose sensors have replaced GOx sensors in research, as the former are less subject to oxygen limitation.

2.2.3. Overview of the advances in non-enzymatic glucose sensing

As previously mentioned, nanotechnology is causing an escalation in more innovative non-enzymatic glucose sensors (Park *et al.*, 2005).

A variety of nanostructured materials have been studied and reported for non-enzymatic glucose detection, such as Cu_2O, NiO_2 etc., providing substantiation that non-enzymatic glucose-sensing electrodes' are rapidly developing (Toghill and Compton, 2010). This is due to the enlarged surface area, improved glucose oxidation kinetics and improved selectivity. Particularly, nanoporous and microporous materials have raised interest in non-enzymatic glucose sensors alone. This is due to porous materials offering surfaces with a high surface-to-volume ratio (Toghill and Compton, 2010).

With their noticeable advantages, nanostructured metal oxides have acquired widespread use in the growth of economically feasible sensors that have attained an extraordinary stability, sensitivity and response time in relation to glucose detection via electrochemical oxidation (Zhu *et al.*, 2016). Hence, the following table summarizes a couple of innovations in non-enzymatic glucose sensors centred on diverse metal oxides.

Table 2. 1: Contrast of non-enzymatic glucose sensors presented with respect to type, sensitivity, response time, LOD and linear range

Biosensor	Sensitivity (uA/cm^2 mM)	Response time (s)	LOD	Linear range	Reference
Co_3O_4 nano-fibers	36.25	≤ 7	0.97 µM	---	(Ding *et al.*, 2010)
Co_3O_4/PbO_2	460	≤ 2	0.31 µM	5 µM-1.2 mM	(Chen *et al.*, 2013)
Co_3O_4-$Ni(OH)_2$	1.089	≤ 5	1.08 µM	5 uM-40 µM	(Rahman *et al.*, 2010b)
Sn: Co_3O_4	921/265	≤ 4	100 nM	2 µM-0.5 mM & 0.6 mM-5.5 mM	(Chowdhury *et al.*, 2017)
Zn: Co_3O_4	193	≤ 7	2 µM	5.5 mM-0.62 mM	(Chowdhury *et al.*, 2016)
Co_3O_4: TiO_2	2008.82	≤ 5	0.34 µM	3 mM	(Gao *et al.*, 2016)
Cu_2O-Cu	1620	---	49 µM	0-6 mM	(Wang *et al.*, 2013)
Cu-Cu_2O nanoporous nanoparticles	123.8	---	0.05 µM	0.01-5.5 mM	(Zhao *et al.*, 2013)
Graphene wrapped Cu_2O nanotubes	285	≤ 9	3.3 nM	0.3 -3.3 mM	(Luo *et al.*, 2012)
CuO nano-fibers	431.3	≤ 1	0.018 µM	0.006-2.5 mM	(Ding *et al.*, 2010)
Co_3O_4-$Ni(OH)_2$	1.089	≤ 5	1.08 µM	5-40 µM	(Mahmoudian *et al.*, 2016)

2.3. Material fabrication

Tian and co-authors (2014) highlighted that the behaviour of a non-enzymatic glucose sensor is related to the electrode material by which glucose is oxidized. Studies have shown that a variety of materials and processes utilizing metals, namely gold (Au), platinum (Pt), nickel (Ni) and copper (Cu), and metal oxides such as nickel oxide (NiO), iron (II) oxide (Fe_2O_3), cobalt oxide (Co_3O_4) etc. have been used in non-enzymatic glucose detection (Doria *et al.*, 2012; Xiang *et al*., 2011; Bansal *et al.*, 2016; Lee *et al.*, 2010). The metals and metal oxides have been studied due to their synergistic effect and good electrocatalytic activities. This is due to the metal/ metal oxides affecting the activity

Nanostructured metal-oxides have high sensitivity, rapid response times, and excellent stability with respect to glucose detection (Rahman *et al.*, 2010a). As mentioned above, although a variety of nanostructured metal oxides have been tested, Co_3O_4 shows promising results.

According to Zhu and co-authors (2016), Co_3O_4 is a widely used metal oxide with respect to non-enzymatic glucose sensors. The polymorphs of cobalt oxide include cobaltous oxide (CoO), cobaltic oxide (Co_2O_3) and cobaltosic oxide (Co_3O_4), with the latter depicting promising results with regard to glucose detection in several studies (Ding *et al.*, 2010). Co_3O_4 is advantageous to utilize in non-enzymatic glucose sensors as it is relatively inexpensive, depicts good conductivity and electrocatalytic properties, and it is environmentally friendly. This polymorph represents excellent electron conductivity, catalytic and electrocatalytic properties which results in the acceleration of the electron transfer between electrode surface and redox species.

2.3.1. Previous studies on cobalt oxide (Co_3O_4) based non-enzymatic glucose sensors

Developing an efficient and effective device for the frequent monitoring of glucose levels is vital analytically to manage diabetes and reduce the risk of serious problems.

Ding and co-authors (2010) reported that Co_3O_4 nano-fibers are fabricated by electrospinning and calcination, and show enhanced electrochemical glucose detection. The as-developed biosensor resulted in a fast response time, high selectivity and reproducibility, and a small lower detection limit (LOD) as can be seen in table 2.1. The selectivity of the as-developed sensor was also investigated against interference species that co-exist in the blood with glucose, namely ascorbic acid ($C_6H_8O_6$) and uric acid ($C_5H_4N_4O_3$). The blood glucose levels of the average human is between 4 mM and 7 mM (Park *et al.*, 2005), whereas, the concentration of endogenous ascorbic acid and uric acid is around 0.125 mM and 0.33 mM respectively in blood samples (Hrapovic and Luong, 2003). With the addition of uric and ascorbic acid, a negligible escalation in current response was observed i.e. 17 % and 14 % in

comparison to that of the addition of glucose. The sensor also demonstrated excellent inter- and intra-electrode reproducibility with standard deviations of 9.73 % and 3.99 %.

Further research was conducted whereby a biosensor was constructed using Co_3O_4/PbO^2 core-shell nanorod arrays as electrocatalysts (Chen *et al.*, 2013). The as-prepared electrode exhibited excellent electrochemical behaviour towards glucose as the resultant sensitivity was high with a small LOD. The characteristics of the sensor can be noted in table 2.1. The biosensor showed negligible interference with respect to current response for the detection of uric acid and merely a slight increase by 16.7% and 6.7 % in current density for ascorbic acid and fructose ($C_6H_{12}O_6$) respectively. In fact, these minor changes can be ignored when comparing to the current response value arising from glucose addition. In terms of the further classification of the sensor, the inter-electrode reproducibility of biosensor resulted in a relative standard deviation of 9.4 % and an excellent inter-electrode reproducibility with a relative standard deviation of 2.7 %.

Mahmoudian *et al*. (2016) reported the synthesis and characterisation of Co_3O_4 ultra-nanosheets with Ni $(OH)_2$ as a non-enzymatic electrochemical sensor for glucose discovery. The sensor confirmed the feasibility for the quantitative detection of glucose with a fast response time. Negligible interference of uric acid, ascorbic acid and dopamine ($C_8H_{11}NO_2$) were as compared to detection of glucose. The biosensor was found to be stable and viable.

Even though the previous studies as reported (see table 2.1) provide feasible strategies for fabrication and show promising electrode materials for the construction of practical non-enzymatic glucose sensors, the sensitivity and linear range of glucose detection can be improved for the purpose of further bulk manufacturing and commercialization. This is why Co_3O_4 will be used further in the fabrication of the biosensor for this research, as it is proven to provide enhanced electrochemical glucose detection.

2.3.2. Dopant materials

A variety of dopant materials have been added to Co_3O_4 electrodes for the purpose of enhancing electrochemical performance. Chowdhury *et al*. (2016) recently reported that zinc (Zn) as a dopant for Co_3O_4 showed enhanced electrochemical performance due to improved charge transferability. Further, Gao *et al*. (2016) tested titanium dioxide (TiO_2) as a dopant and the resultant effect showed a great sensitivity and minimal detection limit. This was due to the addition of TiO_2 which allowed for an increase in the specific surface area and additional reactive sites. Several studies based on Cu materials have been reported with respect to non-enzymatic glucose sensors; however none used Cu as a dopant material for Co_3O_4.

According to Kang *et al*. (2007), Cu nano-materials were used on electrodes that were made with Naflon carbon nanotubes. The results exhibited excellent selectivity, reproducibility, a high sensitivity and a high current response. Espro *et al*. (2014) also tested Cu, which resulted in a large oxidation peak after glucose was added in the electrolyte solution. Zhuang *et al*. (2007) reported that copper oxide (CuO) nano-materials were used on a Cu substrate for non-enzymatic glucose detection, which also proved that the CuO provided enhanced sensitivity, good stability, high current response and a truncated detection limit once again.

Since the utilization of Cu results in enhanced electrochemical performance, Cu will be added to Co_3O_4 for the purpose of increasing the charge transferability to allow for enhanced glucose detection in the non-enzymatic glucose sensor.

2.4. Method of fabrication

There are a variety of deposition techniques utilized to fabricate Co_3O_4 films such as pulsed layer deposition (PLD), plasma sputtering, atomic layer deposition (ALD). However, capital investment is demanding and it requires continuous maintenance (Donders *et al.*, 2011). There are other conventional procedures that are utilized to fabricate the films directly onto the substrate such as hydrothermal growth and electrode deposition; however these methods generally result in reduced electrocatalytic activity of Co_3O_4. Additionally, these techniques are not appropriate for the efficient, effective and economic production of glucose biosensors due to the lengthy processing time, cost and complexity of the methods (Jeon *et al*., 2015). The method of fabrication for the biosensor to be utilized in this study is spin coating and calcination (Wang *et al*., 2016). Hence, the purpose of this section is to detail the theory behind spin coating by touching on aspects of deposition, spin-up, stable fluid outflow and the evaporation steps, and thereafter elucidate calcination.

2.4.1. Spin-coating

According to Smith *et al*. (2013), spin coating is a quick and efficient process that exploits centrifugal forces by a rotating substrate in order to evenly disperse a coating solution across an area.

Typically, if a liquid solution is located on the substrate in the spin coater, and the sample spins at a particular speed and period, the centrifugal forces will cause the liquid to spread consistently and transversely across the sample. The spin coating technique can be fragmented into four key phases: stage 1 - fluid dispensing, stage 2 - spin-up, stage 3 - stable fluid outflow and stage 4 - evaporation (Sahu *et al*., 2009).

Generally, stage 3 and 4 are crucial as they will affect the final coating thickness of the electrode, and both stages underlie the two processes that must occur simultaneously (viscous flow and evaporation). Notably, the fluid flow on the flat spinning substrate i.e. in this case the FTO, is a vital physical process involved in spin coating (Sahu *et al*., 2009). The following is a depiction of the steps taken in spin coating.

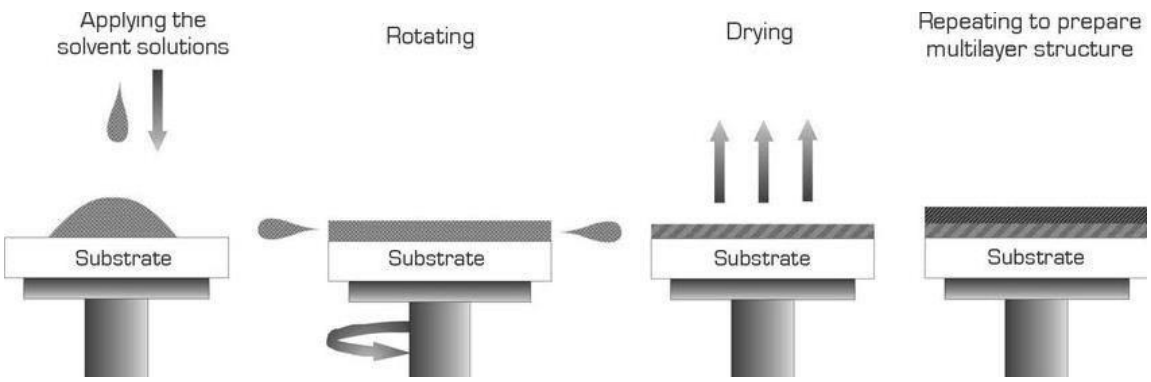

Figure 2. 1: Spin coating process (Kandjani *et al.*, 2015)

i. Deposition

Deposition is the initial stage of spin coating whereby a micro-syringe is utilized to displace a solution onto the raw substrate which is rotated at a predetermined speed. The desired solution is then dispersed due to the centrifugal force (Sahu *et al*., 2009).

ii. Spin-up

The subsequent stage of spin coating is when the substrate is accelerated to its ultimate rotation speed. Generally, this stage is distinguished by the fluid expulsion from the water surface by the rotational motion (Sahu *et al*., 2009). Owing to the complexity of fluid on the water surface, spiral vortices are existent at this stage, and are moulded due to the twisting motion that is caused by the fluid layer inertia of the surface that is exerted whilst the water below rotates. Ultimately, the fluid will be thin enough and co-rotated with the water, by which differences in fluid depth withdraw. Eventually, the water achieves its anticipated speed and the fluid is adequately thin, which results in viscous shear drag balancing the rotational acceleration (Sahu *et al*., 2009).

iii. Stable fluid outflow

The third stage of spin coating is when the substrate spins at a constant rate and the viscous forces of the fluid govern the fluid-thinning behaviour. Generally, this stage is characterized by a gradual fluid-thinning process. This process is uniform, though it slows down progressively as the coating thickness is

reduced. Typically, edge effects are observed as the fluid flows uniformly outward because droplets form at the edge and are flung off (Sahu *et al*., 2009).

iv. Evaporation

The fourth stage of spin coating occurs as the film drying period initiates. Throughout this period, the centrifugal flow halts, and due to solvent forfeiture, further shrinkage of the film occurs. This stage results in the formation of a thin film on the substrate. During this phase the substrate spins at a persistent rate and solvent evaporation controls the coat thinning behaviour. The suspended or dissolved solids become concentrated at the liquid surface and develop an elevated viscosity and a minimally diffused solid coat (Sahu *et al*., 2009).

2.4.2. Calcination

Calcination is the second step for the fabrication of the electrocatalyst onto the substrate. Calcination is defined as a thermal treatment process that is applied to substrates/solid materials, in the presence of air or oxygen to bring about thermal decomposition, phase transition or the removal of a volatile fraction (Vesuvius, 2019). It is vital that after each layer of material is coated onto the substrate, it is calcined to a temperature higher than the reaction temperature, for the purpose of removing impurities after synthesis. In the case of this research, calcination occurred at 350 °C, as reported in Chowdhury *et al*. (2017) and Ding *et al*. (2010). This was done to ensure that impurities were removed, the catalyst structure was not altered, and the surface area of the catalyst was not reduced.

2.5. Electrochemical cell

Generally, an electrochemical cell is utilized to generate current and voltage from a chemical reaction or input of electrochemical signals by induced chemical reactions. The most frequent utilized electrochemistry system is the three-electrode system which consists of a working, counter and reference electrode (Li and Miao, 2013). The following is an illustration of the three electrode system, depicting current (A) and voltage (V) flow between the relevant electrodes.

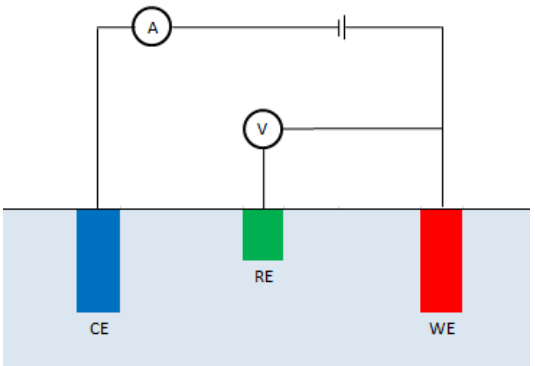

Figure 2. 2: Three-electrode cell depicting the counter (CE), reference (RE) and working electrode (WE)

In this setup, current flows between the counter and working electrode. Potential difference is controlled between the working and counter electrode and is measured between the reference and working electrode. The working electrode makes contact with the analyte. The surface of the working electrode is the location in which the reaction occurs (Li and Miao, 2013). Subsequently, when a specific potential is applied to the working electrode, the transfer of electrons amid the electrode and analyte transpires. The current at the electrode will transmit through the counter electrode for equilibrium. Generally, inert conducting materials such as platinum and graphite with large surface areas are utilized to make the counter electrode; hence in the case of this research, a graphite rod was chosen. The reference electrode has an acknowledged reduction potential and no current transmits through it. Thus, it only acts as a reference when quantifying the potential of the working electrode. Generally, silver-silver chloride (Ag-AgCl) and saturated calomel reference electrodes are utilized as the reference electrode (Li and Miao, 2013).

2.5.1. Counter electrode

The counter electrode is also acknowledged as the auxiliary electrode and is exploited to seal off the current circuit in the electrochemical cell (Metrohm, 2017). Generally, the electrode is constructed of an inert material e.g. graphite, platinum, gold, etc., and typically does not participate in the electrochemical reaction. Due to the current flowing between the working and the counter electrode, the overall surface area (i.e. source of electrons) of the counter electrode is obliged to be higher than the area of the working electrode. This is to ensure a termination of a restraining factor in the kinetics of the electrochemical process (Li and Miao, 2013).

2.5.2. Reference electrode

Notably, the reference electrode is one which has a steady and known electrode potential. It is used as a point of orientation in the electrochemical cell for the governing and quantifying of potential (Metrohm, 2017). The elevated stability of the reference electrode is typically reached by commissioning a redox system with perpetual concentrations of all participants of the redox reaction. In addition, the current movement through the reference electrode is reserved close to nil by permitting the counter electrode to seal off the current circuit in the electrochemical cell (Li and Miao, 2013).

2.5.3. Working electrode

The working electrode in the case of this research project consists of Co_3O_4: Cu and Co_3O_4 biosensors.

Conducting, high hydrophilic, porous substrates are beneficial in the applications of electrochemical biosensors as host electrodes. This is due to the fact that they offer fast charge transferability, large sensing surface area and wettability in aqueous analytes (Li and Miao, 2013). In this research project

commercial fluorine-doped tin oxide (FTO) glass is used as the substrate for the fabrication of the biosensors by means of a two-step process which was explained in the previous section.

FTO glass is a transparent conductive metal oxide which has a variety of applications including touch screen displays, heat glass, electromagnetic radio frequency interference shielding and biosensors. There are a variety of properties of the FTO glass that makes it suitable to be used as the substrate for the fabrication of the biosensor such as low surface resistivity, high optical transmittance, scratch and abrasion resistance, thermal stability, and it is inert to a range of chemicals. Below are a few vital properties and benefits of FTO glass (Sigma-Aldrich, 2018):

- Electrically conductive for heat and thermal control, electrostatic dissipation and reduced transmittance of electromagnetic radiation.
- Colour- neutral glass which impedes reflector colour and results in an escalation of light transmittance. Due to this property, it also minimizes haze for an optimum visibility.
- Simple fabrication as the pyrolytic surface can be managed, insulated, cut, heat-strengthened and annealed by normal techniques.
- Durable pyrolytic surface of the glass provides an unlimited shelf life and does not oxidize nor change colour over time.
- Availability in numerous depths and surface resistivities which range from 7-13 Ω/sq.

2.6. Techniques for electrochemical measurements

For the electrochemical analysis of materials/substances, a range of electrochemical signals must be generated. These signals are current, potential, charge and impedance, which are further related to the concentrations of the analyte to be used (glucose) (Li and Miao, 2013). Hence, the most frequently used electrochemical measuring techniques, i.e. cyclic voltammetry, chronoamperometry and electrochemical impedance spectroscopy, are briefly discussed below.

2.6.1. Cyclic voltammetry

Cyclic voltammetry stipulates the thermodynamic information of redox and adsorption processes and the kinetics of electron transfer reactions. Generally, voltage is swept between two values at a fixed scanning rate; however, when voltage reaches V_2, the scan is inverted and the voltages are swept back to V_1 (Andrienko, 2008). This can be seen in figure 2.3. During cyclic voltammetry scanning, the analytes will undergo certain electron communication with the electrode (in this case, the biosensor) under various potentials and the currents obtained will be proportional to the concentration of the analytes. For reversible electrochemical reactions, the cyclic voltammetry that is documented has distinct traits, i.e.:

- The ratio of peak currents is equivalent to one.
- The peak currents are proportionate to the square root of the scan rate.
- The position of the peak voltage does not change as a function of voltage scan rate (Andrienko, 2008)

The voltage scan rate has a great influence on the current for a reversible electron transmission process as visualized in figure 2.3. This proves that cyclic voltammetry is an acceptable qualitative analytical method for this research project dissertation.

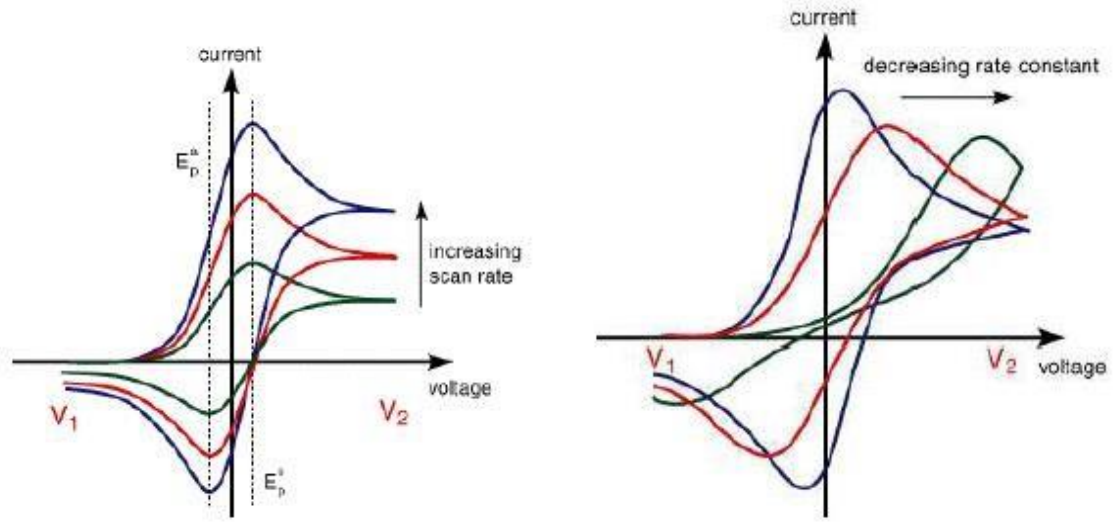

Figure 2. 3: Scan rate and rate constant dependence of the I-V curves

2.6.2. Electrochemical impedance spectroscopy (EIS)

Electrochemical impedance spectroscopy is utilized to detect the dielectric properties of a particular medium over a range of frequencies. Generally, the data is represented by a Bode impedance plot, Bode phase plot and a Nyquist plot. The electrochemical process of the electrode (in this case, biosensor) is then simulated to an equivalent circuit that consists of resistors and capacitors.

Electrochemical impedance spectroscopy is utilized in this research to conform to the electrochemical results of the electrode. The EIS measurement is a simple method that is conducted utilizing a Frequency Response Analyzer (FRA) which is coupled to a potentiostat (Fasmin & Srinivasm, 2017) Generally, an applied alternating voltage can generate alternating current from an electrochemical reaction on the electrode, and that same alternating current can be produced if the voltage is applied on an equivalent circuit. Hence, the electrochemical behaviour of the electrode is equivalent to resistance

i.e. Faraday impedance (Z), which is equivalent to the ratio of voltage (V) and current (I) in an alternative current circuit (MacDonald, 2006);

$$Z = \frac{V}{I}$$

Equation 2. 1

Generally, when conducting an EIS experiment, a fixed sinusoidal voltage is applied by means of a potentiostat across a three-electrode system comprising an electrolytic solution with the molecule to be invested. The EIS experiment entails constructing a composite upon the electrode surface that attracts target analytes which in turn affect the conductivity of the system. In such cases, it is expected that the impedance measurements be conducted in a blank buffer solution such as potassium ferricyanide (II) (K_4Fe (CN_6)) (Brownson *et al*., 2012).

Figure 2.4.a is an illustration of a Nyquist plot and a basic equivalent circuit of the electrochemical impedance spectroscopy of an electrolytic cell also known as Randall's circuit. This plot measures charge transfer resistances, solution resistances, time constants and Warburg impedances. Randall's circuit is one of the most basic cell models describing electrochemical interface processes and comprises an active electrolyte resistance (Rs) in series with the parallel combination of a double layered capacitance (Cdl), the impedance of a faradaic reaction consisting of an active charge transfer resistance (Rct), and an electrochemical element of diffusion (W), Warburg element.

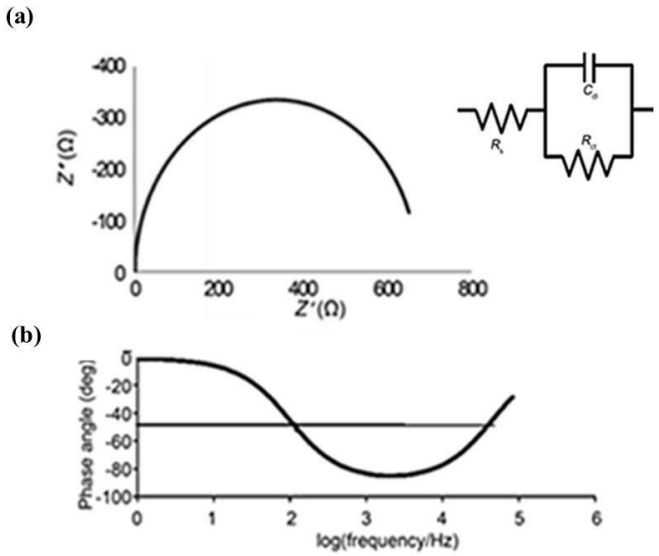

Figure 2. 4: (a) Nyquist plot and its basic equivalent circuit and (b) Bode phase plot (AMS, 2018)

On the other hand, figure 2.4.b, depicts Bode plots which provides information regarding capacitance, phase angles and charge transfer resistance.

Electrochemical impedance spectroscopy is utilized to provide information regarding the reaction mechanism of an electrochemical process. Generally, the application of different layers of coatings on the electrode allows for valuable electron transfer enhancements and sensitivity (Li *et al.*, 2009). A variety of authors, including Gao and Yang (2016), all establish that EIS can be utilized to identify the effects of the different layers including polar, ionic and dielectric relaxation processes within the electrolyte, electrode, electrode surface and double layered region. This method enables the ability to investigate key constraints of an electrochemical system such as charge transfer resistances, double layered capacitance and exchange current densities.

2.6.3. Chronoamperometry

Generally, chronoamperometry is an electrochemical analysis by which the potential of the working electrode (biosensor) is stepped and the subsequent current due to faradaic processes transpiring at electrode is measured against time (Bard and Faulkner, 2000).

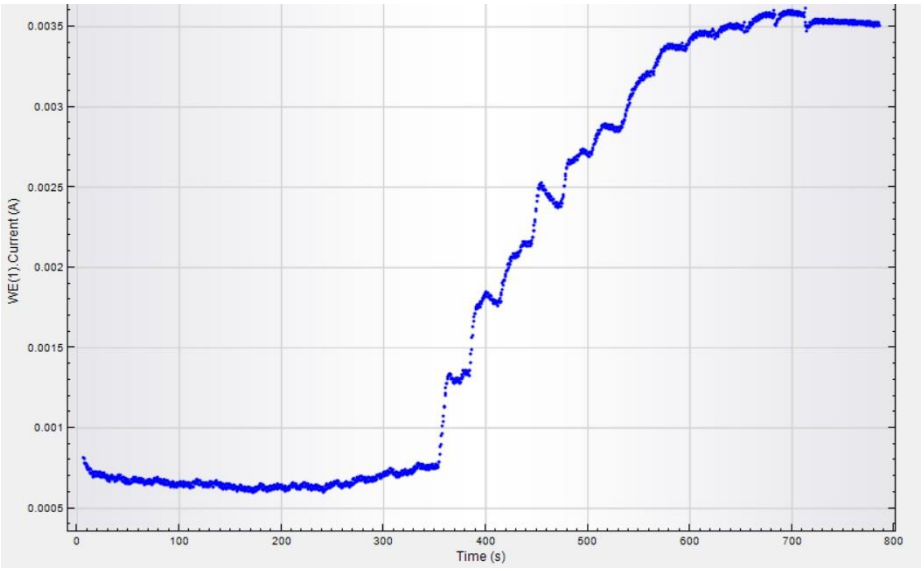

Figure 2. 5: Example of a chronoamperometric graph (Current vs. time)

The faradaic current is due to the occurrence of electron transfer, and decays as defined by the Cottrell equation. The Cottrell equation given below outlines the variation in current against time with a controlled potential (Zoski, 2007), while the current measured is dependent on the rate at which the analyte (glucose) diffuses to the electrode (biosensor) film (Zoski, 2007).

$$i = \frac{nFAc_j^0\sqrt{D_j}}{\sqrt{\pi t}}$$

Equation 2. 2

Whereby, I represents the current, n, the number of electrons for reduction or oxidation, F is Faraday (96485 C/mol), A is the area of the electrode, c_j^0 is the initial concentration of the reducible analyte, D_j is the diffusion coefficient and t, is the time (Bard and Faulkner, 2000).

The chronoamperometry is vital for effective biosensor characterisation. It assists in obtaining the sensitivity, glucose linear concentration range, limit of detection (LOD) and response time of the biosensor.

2.7. Surface characterisation

2.7.1. X-ray diffraction (XRD)

According to Cullity (1978), X-ray diffraction (XRD) is a technique utilized for the exploration of the fine structure of matter. It is also utilized in the study of crystal structures and atomic spacing (Bunaciu *et al*., 2015). The technique of X-ray diffraction is centred on constructive interference of monochromatic X-rays and a crystalline sample. Generally, the X-rays are produced by a cathode ray tube, filtered to generate monochromatic radiation, and focussed in the direction of the sample.

Typically, the contact of the incident rays with the sample will produce constructive interference i.e. and a diffractive ray, only when the circumstances satisfy the Braggs Law:

$$n\lambda = 2dsin\theta$$

Equation 2. 3

Whereby, n is an integer, λ is wavelength of the X-rays, d is the interplanar spacing that generates the diffraction and Θ is the angle of diffraction.

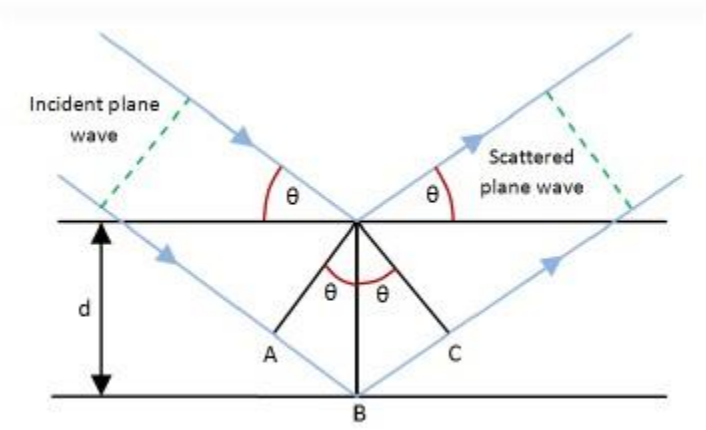

Figure 2. 6: The Bragg description of diffraction in terms of reflection of an incident wave (Kriedemann, 2014)

Braggs Law depicts a relationship between the wavelength of electromagnetic radiation to the diffraction viewpoint and the lattice arrangement in a crystalline sample. When the diffracted X-rays are perceived, they are administered and then counted. Notably, by scanning the tester through an array of 2Ɵ angles, all diffraction directions of the lattice can be obtained due to the random alignment of the material. A transition of the diffraction peaks to d-spacings permits the identification of the compound as each has a unique set of d-spacings. This is normally obtained by comparing the d-spacings obtained to standard reference patterns (Bunaciu et al., 2015).

A distinctive X-ray diffractometer comprises three basic elements which are an X-ray tube, sample holder and an X-ray detector. The X-rays are then generated in a cathode ray tube by heating a filament for the production of electrons, and fast-tracking the electrons toward a target by the application of a voltage. This bombards the target material with electrons. Hence, when the electrons have adequate energy to extricate the inner shell electrons of the objective material, X-ray spectra are generated (Bunaciu *et al*., 2015).

2.7.2. Electron microscopy

According to Voutou and Stefanaki (2008), electron microscopes are a valuable tool in material sciences and the development of scientific theory. Electron microscopes are scientific instruments that utilize a ray of active electrons for the purpose of examining materials on a fine scale. This inspection provides evidence regarding the topography (surface features), morphology (shape and size), composition and crystallographic structure of the material examined.

The frequent utilization of electron microscopes is centred around the fact that they permit observations and characterisation of materials on a nanometre and micrometre scale (Voutou and Stefanaki, 2008). The following subsections contain basic theory on two basic types of electron microscopes that are utilized for material characterisation for this research project i.e. TEM and SEM.

i. Transmission electron microscopy (TEM)

Transmission electron microscopy (TEM) is utilized for the purpose of providing information regarding the morphology (size, shape, particle arrangement) and crystallographic information (arrangement and order of atoms from diffracted electrons) of a material (Egerton, 2005).

Egerton (2005) further explains that transmission electron microscopy is a microscopy technique where a ray of electrons is transmitted through an ultra-thin specimen that causes an interaction with the specimen as it passes through. An image is produced, enlarged and focused onto an imaging device such as fluorescent screen, photographic film or registered on a CCD camera sensor. Typically, only the transmitted beams are utilized to form the diffraction contrast image.

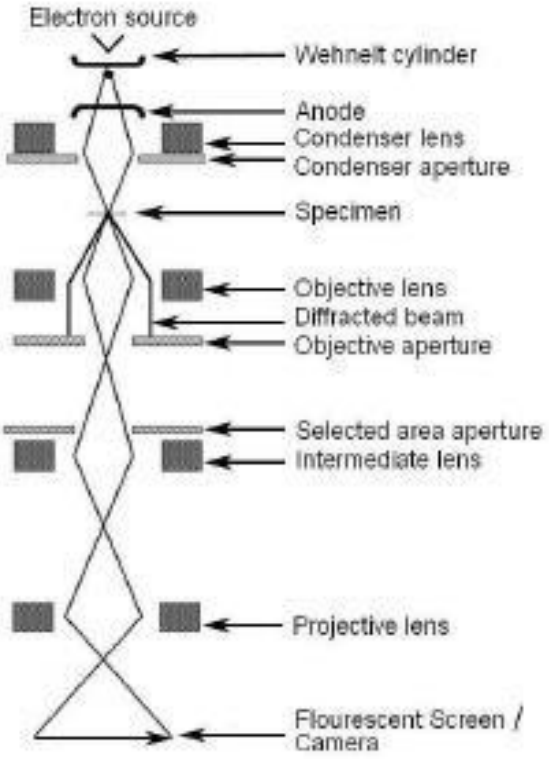

Figure 2. 7: Graphic of the fundamental electron components of a TEM (Almeida, 2010)

ii. Scanning electron microscopy (SEM)

Scanning electron microscopy (SEM) utilizes a focussed beam of high-energy electrons to generate an assortment of signals at the surface of solid specimens. These signals provide evidence about the external morphology (texture), chemical configuration and crystalline structure of the sample (signals that derive from the electron-sample interactions). Notably, SEM images have a three-dimensional exterior which is highly useful for the examination of the surface structure of a sample (De Gree, 2015).

According to Khursheed (2011), the focal apparatuses of a scanning electron microscope are an electron column, scanning system, detector, display, vacuum system and electronic control. Generally, the electron column of the microscope comprises an electron gun with two or more electromagnetic lenses functioning in vacuum. This electron gun then produces free electrons and causes an acceleration of these electrons to energies in the range of 1-40 keV. The objective of the electron lenses is to generate a minor, fixated electron probe on the specimen.

For an image to be produced, the electron ray is fixated into a fine probe which is scanned through the surface of the specimen by the aid of scanning coils. Every point of the specimen will emit a signal in the configuration of electromagnetic radiation if it is struck by the accelerated electrons. Thereafter, designated portions of this radiation are composed by a detector and the resultant signal is amplified and exhibited on a screen i.e. SEM image.

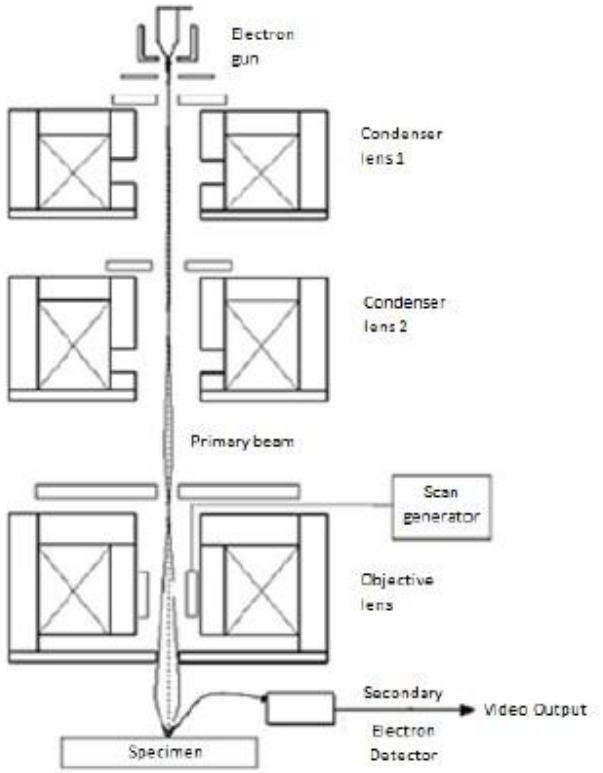

Figure 2. 8: Graphic of the basic electron optical components of a SEM (Khursheed, 2011)

2.7.3. Energy dispersive spectroscopy (EDS)

A custom method for identifying elements within a sample in a SEM or TEM is by means of energy dispersive spectroscopy (EDS) analysis. According t o Almeida (2010) & Ellmer *et al.*, (2001), the emission of a photoelectron is caused by the interaction with the innermost electron shell of an

atom by the high energy electron beam. Subsequently, an electron from the outer orbiting shell moves into the core level vacancy and emits energy in the form of an X-ray photon.

Ellmer *et al.*, (2001) further mentions that the energy of the X-rays rising from the differential energy amid the shells is representative of the atomic number, hence can be utilized to determine the elemental composition of a specific sample. Notably, the relationship between the atomic number and energy for a given X-ray is provided by Moseley's Law:

$$\sqrt{E} = C_1(Z - C_2)$$

Equation 2. 4

Whereby E is the emission line energy for a given X-ray series i.e. Kα, Kβ, Lα, Mα, and Z represent the atomic number and C_1 and C_2 are constants.

2.7.4. Electron energy loss spectroscopy (EELS)

Electron energy loss spectroscopy is the examination of the vibrational motion of atoms and molecules on and adjacent to the surface by means of analysing the energy spectrum of low-energy electrons scattered from it (Ibach and Mills, 1982).

Electron energy loss spectroscopy (EELS) is a practice that analyses the energy lost by the rapid incoming electrons when they move through a sample. Notably, diffraction effects in TEM are due to the interaction of the fast electrons with the nucleus; however, EELS diffraction effects are due to the electro-electron interaction. The latter interaction occurs due to the electron beam and the electrons in the sample (Hofer *et al*., 2016). Hence, the EELS study provides information about the electronic structure of the desired sample. Subsequently, the imaging provides an image of the specimen with electrons that have lost energy characteristics for a certain atom. This provides a cartographic image of the partition of this atom in the sample i.e. chemical mapping (Riviere, 1990).

Generally, an electron beam in a TEM is inelastically scattered whenever there are interactions with atomic electrons in the specimen. The electron beam then loses energy and is bent through a minor angle, usually 5-100 milli-radians. The energy dissemination of all the inelastically disseminated electrons specifies evidence regarding the native area of the atomic electrons, which narrates the physical and chemical properties of the specimen (Hofer *et al*., 2016). This highlights the basis of EELS.

A distinctive electron energy-loss spectrum can be observed in figure 2.9. The initial peak generally transpires at 0 eV and is known as the zero-loss peak. This peak illustrates the electrons which have not been scattered in the specimen i.e. transmitted electrons, and the electrons which have been elastically scattered by means of the interaction with the atomic nuclei.

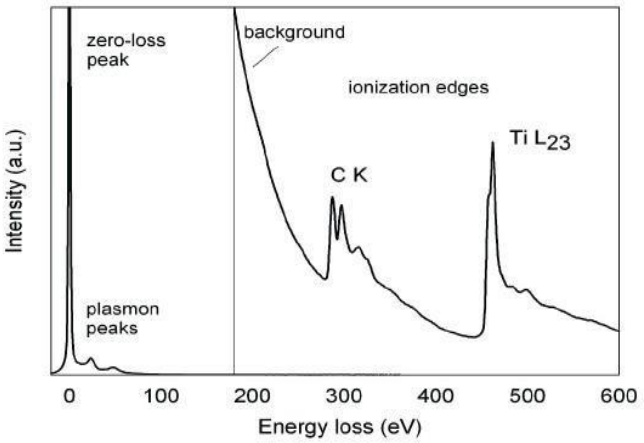

Figure 2. 9: Typical electron energy-loss spectrum (Hofer *et al.*, 2016)

The low-loss/valence region of the spectrum i.e. $<$ 50 eV, specifies evidence about the band structure and the dielectric properties of the material e.g. band gap, surface plasmon. Notably, the signal intensities in the low-loss area are superior to the high-loss area of the spectrum.

In the high energy loss region i.e. $>$ 50 eV, the quantity of inelastically scattered electrons is minor and the spectrum depicts ionisation edges owing to the shape i.e. a prompt upsurge trailed by a gradual decline. Notably, the edges are formed when the inner-shell electron absorbs sufficient energy from an electron beam to be excited to a state above the Fermi level. Generally, not all ionisation edges are saw-tooth in shape as can be noted in figure 2.9, but rather display complex edge shapes such as the $L_{2,3}$-edge.

The $L_{2,3}$-edge comprises piercing excitations at the beginning of the ionisation edge known as white-lines which represent elements in the initial row of transition and rare earth elements. Generally, the ionization edges are utilized in analysing chemical elements as the edge onset provides ionisation energy and allows for a qualitative investigation as for thin samples; the edge intensities are proportional to the concentration of the conforming elements.

2.7.5. Hall Effect measurement

The Hall Effect measurement is one which depicts the behaviour of the free carriers in a semi- conductor when applying an electric and magnetic field. It is a vital tool for material characterisation and can be perceived when the arrangement of a magnetic field through a sample and current along the extent of the sample generates an electrical current that is perpendicular to the magnetic field and current (Green, 2017). This then produces an oblique voltage that is perpendicular to the magnetic field and current as can be noted in figure 2.10. The fundamental principle is Lorentz force which is the force on a point charge owing to electromagnetic fields.

Figure 2. 10: Illustration of the Hall Effect

Green (2017) further notes that the Hall Effect measurement can be utilized to regulate some material parameters such as Hall voltage, carrier mobility, bulk carrier concentration, Hall co- efficient, resistivity, magneto resistance and the conductivity type (n or p). However, for this research, the conductivity, bulk carrier concentration and conductivity type will be reported on.

i. N-type and p-type semi-conductors

Generally, the conductivity of a material can be increased by adding certain impurities to the specific material. Once this is completed, the semi-conductor is known as a doped semiconductor. According to Armen (2007), there are two classifications of impurities that are utilized which are donor and acceptor impurities. A semiconductor that is doped with a donor impurity is known as an n-type semiconductor and one that is doped with an acceptor impurity is termed a p-type semiconductor (Bobrow, 1996).

- N-type semiconductor

The n-type semiconductor is formed by the addition of a donor impurity, such as arsenic or antimony, etc., to an inherent semiconductor. Generally, all donor atoms have five valence electrons, and when a donor atom substitutes an atom in the crystal lattice, four valence electrons are communed with the adjacent atoms. The fifth valence electron converts to a free electron (Bobrow, 1996).

Notably, the quantity of free electrons contributed by the donor atoms is greater than the quantity of free electrons and holes in the inherent semiconductor. Due to this, the conductivity of the n-type semiconductor is greater than the conductivity of the inherent semiconductor. Hence, due to the quantity of free electrons being greater than the quantity of holes, the free electrons are the mainstream carriers. The semiconductor is classified as n-type because the bulk of carriers have a negative charge (Bobrow, 1996).

It is vital to note that the donor atom will remain electrical neutral if the fifth valence electron does not convert to a free electron in the lattice. As, if the fifth valence electron becomes a free electron, the quantity of protons in the atom will be larger than the quantity of electrons and the donor atoms converts to a bound positively charged ion (Bobrow, 1996).

- P-type semiconductor

The p-type semiconductor is created by the addition of an acceptor impurity such as boron or gallium to an intrinsic semiconductor. Generally, each acceptor atom has three valence electrons, so when the acceptor atom substitutes an atom in the crystal lattice, there will only be three valence electrons bordering the adjacent atoms. This then causes a hole in the lattice. Hence, the quantity of holes produced by the acceptor atoms is greater than the quantity of free electrons and holes in the intrinsic semiconductors (Bobrow, 1996).

Due to the quantity of holes being larger than the number of electrons, the holes are the majority carriers. The semiconductor is classified as n-type because the majority of the carriers have a positive charge (Bobrow, 1996).

It is vital to note that the acceptor atom will remain electrical neutral if the hole produced by the absence of its fourth valence electron is not filled by an electron from an adjacent atom in the lattice. Hence, once an electron fills the hole, the quantity of electrons is greater than the number of protons, and the acceptor atom becomes a bound negatively charged ion (Bobrow,
1996).

2.8. Sensor characteristics

In this section, various static and dynamic characteristics of sensors are introduced. Their significance is highlighted, followed by their influence on the operation of the sensor.

2.8.1. Calibration curve

Notably, a sensing system has to be standardised in relation to a known measurand for the purpose of assuring that the sensing outcomes in accurate results. The relationship amid the measured variables and the signal variables as a resultant of the system is known as the calibration curve (Kalantar-Zadeh, 2013). An example of a calibration curve can be noted in figure below.

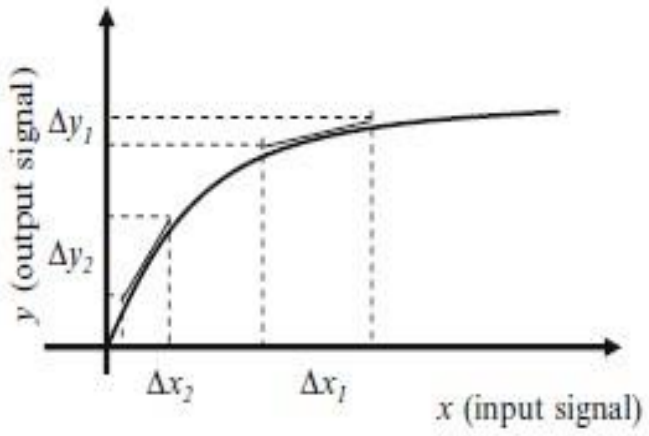

Figure 2. 11: Case of a y-x calibration curve

2.8.2. Sensitivity

The sensitivity of a sensor is the incremental alteration in the sensor's output to the incremental alteration of the measured input (Kalantar-Zadeh, 2013). Notably, the sensitivity represents the slope of the transfer function i.e. slope of the calibration curve. In this case, the sensitivity of the biosensor for this research dissertation is the slope of the graph of current density (uA cm^{-2}) against glucose concentration (mM).

From figure 2.11, it can be noted that the sensitivity can be changed subject to the calibration curve. The sensitivity of the lower values is larger than the sensitivity of the higher values. Generally, an ideal sensor has a great and continual sensitivity in the particular operating (linear) range. Also, the ideal sensor ultimately reaches saturation i.e. a state by which the sensor no longer responds to any changes.

2.8.3. Linearity

Linearity can be described as the proximity of the calibration curve to a specific straight line for the sensor (Kalantar-Zadeh, 2013). Its degree of similarity to a straight line depicts how undeviating the system is. Linearity can be used for indication of the measurement range (section 2.7.4).

2.8.4. Measurement range

The maximum and minimum quantities of the analyte (glucose) that can be measured with a sensor is called the linear concentration range in the case of this research dissertation. Linear/measurement range is also known as the dynamic range or span. Generally, all sensors are designed to execute the desired function over a specific range. Signals outside the specific range are incoherent results and could cause inaccuracies and damage to the sensor (Kalantar-Zadeh, 2013).

2.8.5. Limit of detection (LOD)

With respect to sensors, the minimum signal growth that can be obtained from the system, when all interfering influences are taken into consideration, is known as the limit of detection (LOD) (Kalantar-Zadeh, 2013).

2.8.6. Response time

In general, when a sensor is subjected to a measurand i.e. analyte, the duration it takes to reach a stable value is known as the response time. This is articulated as the time by which the output reaches a convinced percentage (95%) of its ultimate value, in response of a step alteration of the input (Kalantar-Zadeh, 2013).

2.8.7. Selectivity

Generally, selectivity is defined as the sensor's aptitude to quantify an objective measurand. i.e. analyte, in the presence of other interference species (Kalantar-Zadeh, 2013). In the case of this research, glucose is the target measurand and the interference species it will be tested against are sucrose, fructose, uric acid, ascorbic acid, acetaminophen, sodium chloride and potassium chloride. If the glucose biosensor does not depict any response to the interference species, it is considered a highly selective biosensor.

2.8.8. Repeatability and shelf life

A repeatability analysis for a sensor is required to determine the intra-electrode reproducibility of the sensor. Generally, when all the operating and environmental circumstances are continual, repeatability is defined as the sensor's aptitude to bring about the same response for succeeding measurements. Precision is vital when conducting a repeatability analysis. Both long (shelf life) and short term repeatability approximates are vital for a sensing system (Kalantar-Zadeh, 2013).

2.8.9. Reproducibility

A reproducibility analysis is utilized for the inter-electrode characterisation. Reproducibility is the sensor's capacity to exhibit similar responses after measurement conditions have been altered.

2.8.10. Stability

The chemical stability of a sensor is vital for biosensor characterisation. Stability is a sensor's ability to produce a similar output value when measuring the same measurand over a number of cycles.

2.8.11. Noise

Noise is defined as unsolicited fluctuation in the output signal of the biosensor when the measurand is not changing. The mean value of the signal per the standard deviation of the noise strength is generally used in sensing applications as a good benchmark (Kalantar-Zadeh, 2013).

See below, for signal to noise ratio (*S/N*) (Kalantar-Zadeh, 2013):

$$\frac{S}{N} = \frac{Mean\ \ value\ \ of\ signal}{Standard\ \ \ deviation\ \ \ of\ noise}$$

Equation 2. 5

Generally, noise is caused by external or internal sources. External noises include electromagnetic signals such as those brought about from mechanical vibrations, transmission circuits and ambient temperature changes which could result in a systematic error. Internal noises are those originating from electronic noises, i.e. thermal energy causes resulting in variations in current and voltage, and shot noises, i.e. random fluctuations instigated by the carriers' (electrons, photons etc.) random arrival time. Generation-recombination noises (g-r noises) produced from the generation of electrons in semi-conductors is an example of internal noises as well (Kalantar-Zadeh, 2013).

2.9. Conclusion

This chapter presented a review of the literature associated with glucose sensors and nanotechnology i.e. glucose oxidase and non-enzymatic glucose sensors.

It was found that nanostructured metal oxide materials are more suitable for non-enzymatic glucose sensors as they have good electrocatalytic properties, large surface areas and fast electron transfer. With respect to nanostructured metal oxides, among the different oxides reported, the Co_3O_4 biosensor portrayed the optimum glucose sensing performance with a lower detection limit due to the material having a large surface area to allow for additional reactive sites. As previously mentioned, in the case of this research Co_3O_4 will be utilized in the construction of the glucose sensor, together with a dopant material i.e. Cu to further escalate the electrochemical performance. This was reported to result in an increase in the charge transferability to allow for enhanced glucose detection in the non-enzymatic glucose sensor.

The method of fabrication for the biosensor was also discussed. This included spin coating and calcination. The technical aspects of the electrochemical cell to be used in this research were also discussed followed by detailed explanations of the techniques utilized for characterizing the biosensor.

~ Chapter 3 ~

Research Methodology

This chapter comprises:

Section 3.1: *Introduction*

Section 3.2: *Materials and consumables*

Section 3.3: *Substrate preparation*

Section 3.4: *Fabrication of the biosensor*

Section 3.5: *Surface characterisation*

Section 3.6: *Electrochemical measurements*

Section 3.7: *Detection of glucose in human serum*

Section 3.8: *Detection of glucose in human saliva*

Section 3.9: *Reliability and validity of results*

Section 3.10: *Data analysis and presentation of results*

Section 3.11: *Health and safety precautions*

Section 3.12: *Conclusion*

Chapter 3: Research Methodology

3.1. Introduction

This chapter includes detailed research methodology for the development of a novel non-enzymatic glucose sensor utilizing a Cu-doped Co_3O_4 solution material as the electrocatalyst. It comprises descriptions of the test procedures as well as sensor characterisation for the biosensor analysis.

3.2. Materials and consumables

The experiments conducted for the development of the non-enzymatic glucose biosensor comprised the usage of a variety of chemicals and consumables for the objectives to be achieved without any further purification.

Cobalt (II) chloride hexahydrate ($CoCl_2.6H_2O$), sodium oleate ($C_{18}H_{33}NaO_2$), de-ionized water (H_2O), hexane (C_6H_{14}), ethanol (C_2H_5OH), toluene (C_7H_8), cupric chloride ($CuCl_2.2H_2O$), ethanol (C_2H_5OH), sodium hydroxide pellets (NaOH), D (+) glucose ($C_6H_{12}O_6$), D (+)- sucrose, D (-) fructose ($C_6H_{12}O_6$), sodium chloride (NaCl), potassium chloride (KCl), acetaminophen ($C_8H_9NO_2$), uric acid ($C_5H_4N_4O_3$), ascorbic acid ($C_6H_8O_6$), human serum albumin and fluorine doped tin oxide (FTO) glass (properties noted in table 3.1) were obtained from Sigma Aldrich, South Africa. Human saliva samples were collected from an anonymous individual following a specific ethical protocol.

Table 3. 1: FTO glass properties

Description	Haze: 5 %
Composition	SnO_2/F
Surface resistivity	~7 Ω/sq
L×B×D	300 mm×300 mm× 2 mm
Transmittance	80-82 % (Visible)

3.3. Substrate preparation

Fluorine-doped tin oxide (FTO) glass was the substrate used in making the non-enzymatic glucose sensor. Rectangular pieces of FTO glass were cut, using a diamond glass cutter, in accordance to the measurement of ±4 cm length and ≥1.2 cm breadth.

The pre-cut FTO glass was then cleaned for the removal of adsorbed particles by being positioned in a 100 ml beaker with the addition of Mucasol universal detergent. This was placed in the ultrasonic bath for 10 min. The FTO glass was then taken out of the beaker and rinsed with deionized water.

For further cleansing, the procedure above was repeated using ethanol (10 min) and thereafter Mucasol universal detergent (10 min) once again. For drying, the clean FTO glass slides were blown with air and then placed in a petri dish and covered with aluminium foil, to prevent contaminants from being in contact with it. The FTO glass in the petri-dish was left in the oven at 60 °C for overnight drying. The conductive sides of the FTO glass were obtained by utilizing a multimeter. A schematic for the substrate preparation for developing the biosensor can be observed in *figure 3.1*.

Figure 3. 1: Schematic diagram of the cleaning process of FTO glass

3.4. Fabrication of the thin film Co_3O_4:Cu layers on the FTO glass electrodes

The following is a schematic illustration of the deposition of the Co_3O_4: Cu thin film on the FTO glass to develop the biosensor. Theoretical details are explained in *section 3.4.1 and 3.4.2*.

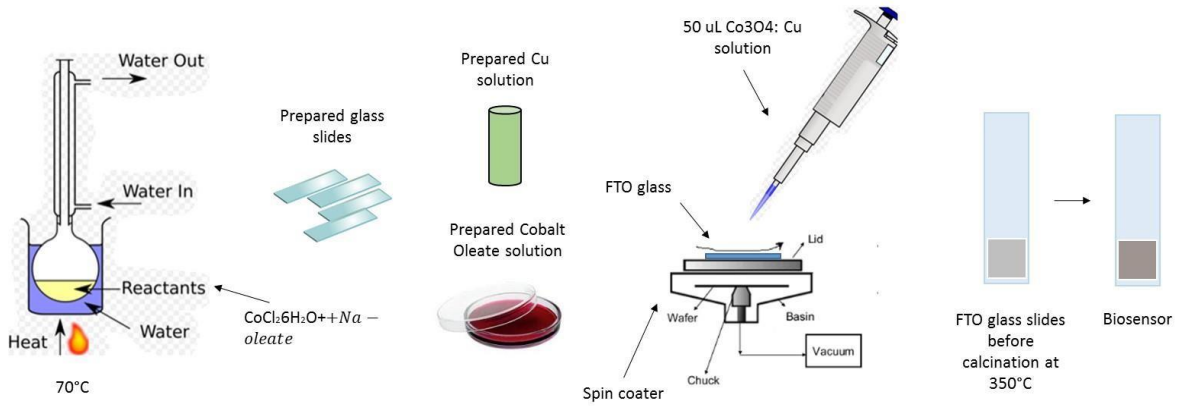

Figure 3. 2: Schematic diagram of the electrode fabrication of Co_3O_4: Cu thin film on the FTO glass

3.4.1. Synthesis of Co_3O_4

The synthesis of Co_3O_4 was conducted in adaption to the work published by Wang *et al.*, (2016).

In order to synthesize the oleate complex, 40 mmol cobalt (II) chloride hexahydrate ($CoCl_2.6H_2O$) and 120 mmol sodium oleate ($C_{18}H_{33}NaO_2$) were prepared. This was dispersed in a mixture of 80 ml ethanol (C_2H_5OH), 60 ml deionized water (H_2O) and 140 ml hexane (C_6H_{14}). The solution was then placed into a round bottom flask and heated under reflux at 70 °C for 4 hours. This ensured that the reaction between sodium oleate ($C_{18}H_{33}NaO_2$) and cobalt (II) chloride hexahydrate ($CoCl_2.6H_2O$) produced the oleate complex.

$$Metal\ chloride + Na - oleate \rightarrow Metal - oleate\ complex + NaCl$$

Equation 3. 1

After the refluxing period was complete, the upper organic layer containing cobalt oleate complex was washed 3 times in 30 ml distilled water in a seperatory funnel. The cobalt oleate complex was then poured in a petri dish and left to dry in an oven at 60 °C overnight. The residue, the bottom layer from refluxing, was discarded appropriately.

The oleate complex solution was prepared in a vial, together with the addition of toluene (C_7H_8) in accordance with the ratio of 0.09 g: 0.5 ml. The resultant solution was then placed in an ultrasonic bath for 40 minutes. The copper dopant solution was prepared by dispersing cupric chloride ($CuCl_2.2H_2O$) with ethanol (C_2H_5OH) in the ratio of 0.53 g: 1 ml. This mixture was then stirred using a spatula continuously until properly dispersed.

3.4.2. Spin coating and calcination

A surface area of $1cm^2$ was prepared and made noticeable with tape on the cleaned FTO glass. The cleaned FTO glass was then placed towards the centre of the spin coater. The furnace was preheated to 350 °C.

The spin coating technique was utilized for the purpose of obtaining a thin film of the desired material on the substrate. Generally, the substrate together with the material is positioned inside the spin coater on the air hole. When the vacuum pump is switched for the purpose of holding the substrate at the centre, the substrate rotates at a high speed causing the centripetal force and the surface tension of the solution to pull the liquid coating into an even covering. During this time, the solvent evaporates for the purpose of leaving the desired material on the substrate in an even covering. The spin coater utilized for experiments can be seen in *figure 3.3*.

Figure 3. 3: Spin coater utilized for the development of the biosensors

In order for the objective of the study to be achieved, three categories of tests regarding spin coating and calcination had to be achieved. Firstly, for preparation of the pristine Co_3O_4 electrode, 50 uL of the Co_3O_4 solution was spin coated on clean FTO glass. This was conducted within the surface area of $1cm^2$. Four layers of the solution were coated on the clean FTO glass. The electrodes were spin coated for 60 s at 4000 rpm. During the spin coating of each of the fours layers, the electrode was placed in the furnace for 10 min at 350 ℃ before the next layer was coated. After the fourth layer, the electrodes were dried in the furnace at 350 ℃ for 4 hours.

Table 3. 2: Volume ratios required to make the precursor solution for the fabrication of the biosensor

Electrode composition (wt %)	**Co_3O_4 (µL)**	**Cu (µL)**
98: 2	49	1
90: 10	45	5
85: 15	42.5	7.5
80: 20	40	10

Secondly, for the Co_3O_4:Cu electrode, 50 uL of a Co_3O_4: Cu at different ratios (see table 3.2) were spin coated on cleaned FTO glass to determine the optimal biosensor based on concentration of the material of fabrication. Thereafter, once the optimum concentration of the precursor solution was established (results from the second analysis), a layer study was conducted for the purpose of determining the optimum number of layers required to construct the sensor to achieve the optimal electrochemical activity. Once the optimum concentration Co_3O_4: Cu solution was prepared, 50 uL was spin coated on a cleaned FTO glass. All categories of analysis were spin coated within the same duration, speed and surface area of 1 cm^2, and calcined in the same manner as the first analysis.

3.5. Surface characterisation

X-ray diffraction (XRD) was utilized for the purpose of identifying the cobalt oleate and copper phase present in the as prepared electrode. The XRD patterns were recorded utilizing a PANalytical X'Pert PRO PW3040/60 diffractometer with Fe filtered Cu-Kα (λ=0.154 nm) monochromated radiation source. Scanning electron microscopy (SEM) and energy dispersive X-ray spectroscopy (EDS) was conducted utilizing a Zeiss Auriga field-emissions SEM, operated at 5 kV for imaging and 20 kV for EDS analysis. High resolution transmission electron microscopy (HR-TEM), selected area electron diffraction (SAED) and electron energy loss spectroscopy (EELS) data of the samples were collected using an FEI Tecnai F20 field emission gun TEM operated at 200 kV, equipped with a Gatan GIF- 2001 energy filter. EELS was utilized to study the electron energy loss near edge fine structure (ELNEFS) signals of cobalt and oxygen ionisation edges. Each spectrum was collected in normal parallel beam, bright-field TEM mode for 5 seconds. Atomic force microscopy was also used to analyse the surface roughness of the Co_3O_4 thin film electrode. The SEM top and side views and profilometry measurements were obtained for the Co_3O_4:Cu and pristine electrode for comparison. TEM micrographs and SAED patterns were used for analysis. HAADf images of the electrode were obtained with an area selected for EDS mapping. EELS analysis was conducted by a plot of normalized intensity against energy loss.

3.6. Electrochemical measurements

All the electrochemical measurements were measured utilizing an Autolab PGSTAT302N Potentiostat. Autolab software Nova 1.1 and 2 were utilized for the electrochemical tests.

A three electrode cell system was set up for the purpose of measuring both current and potential. The reference electrode utilized was Ag/AgCl (3 M), the counter electrode was a graphite rod and the working electrode was the sensor fabricated. The electrolyte utilized was 0.1 M NaOH solution for the cell set-up to be complete. The electrolytic cell was placed on top of a magnetic stirrer. *Figures 3.4 and 3.5* depict the apparatus utilized for the electrochemical measurements.

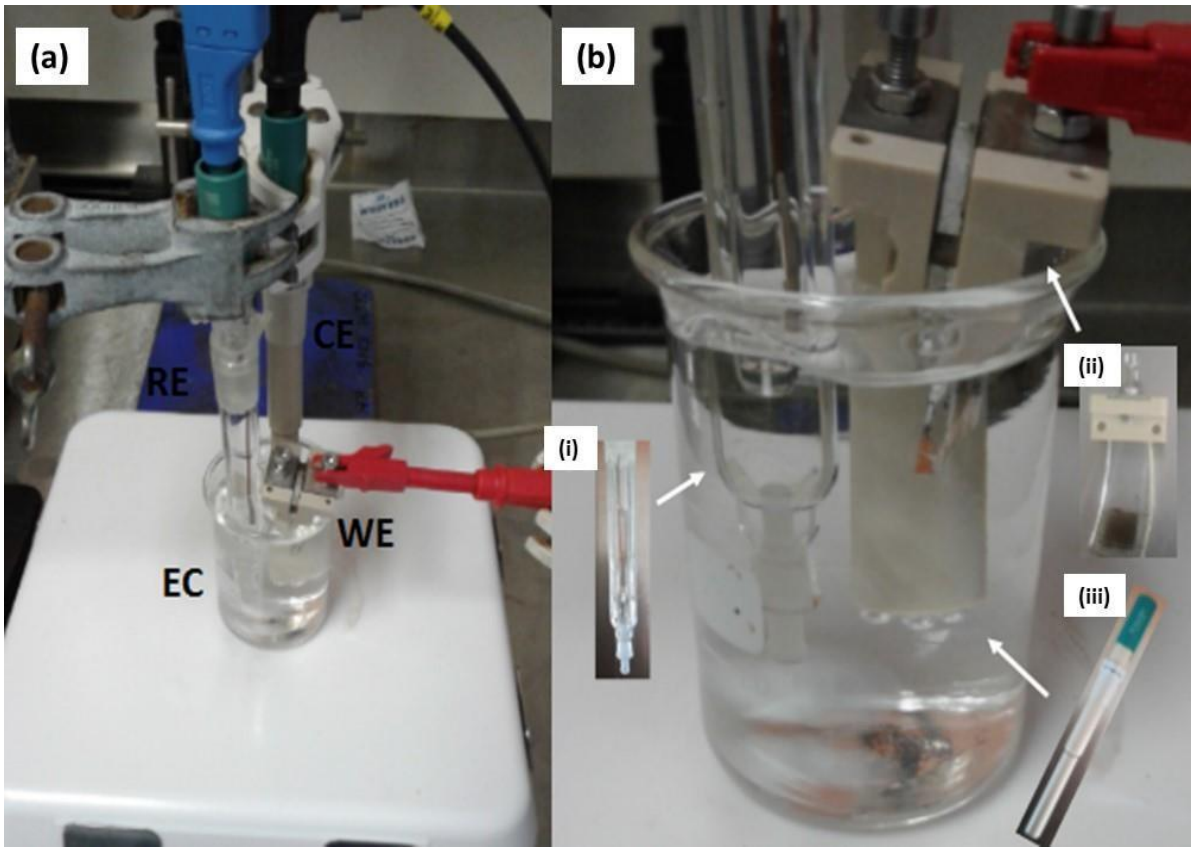

Figure 3. 4: The three-electrode cell (a) Electrolytic cell (EC), the reference (RE), counter (CE) and working (WE) electrode (b) zoomed view of the three-electrode cell (insets: (i) RE (ii) the as prepared film on FTO setup (iii) CE electrode)

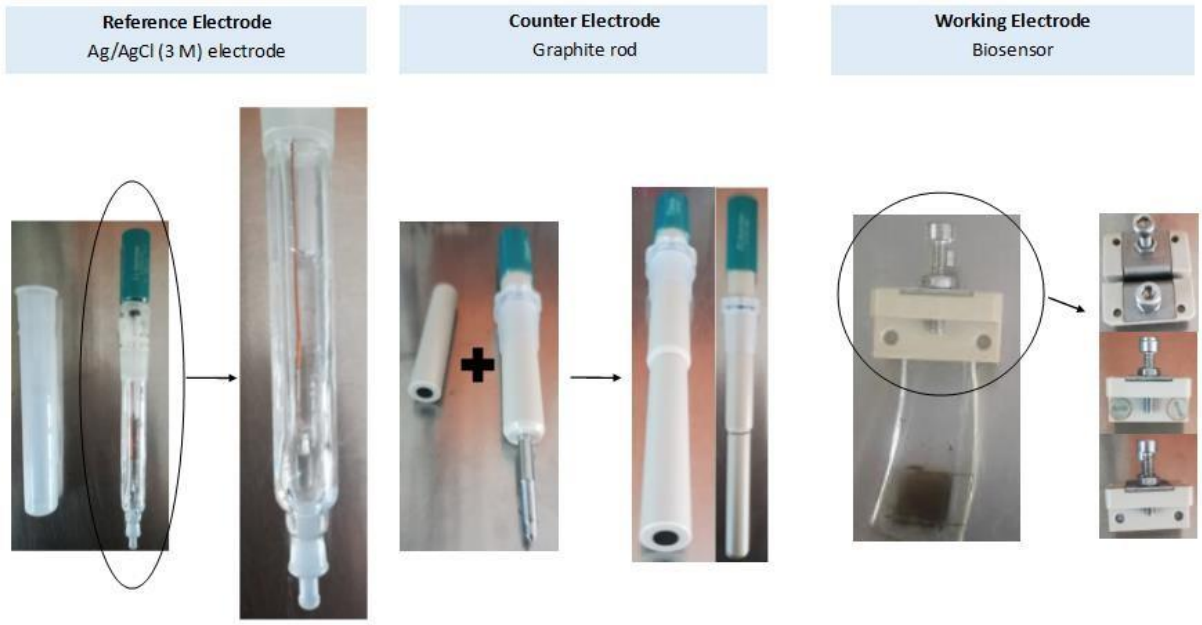

Figure 3. 5: Reference, counter and working electrode utilized for the 3-electrode cell

3.6.1. Electrochemical detection of glucose

Cyclic voltametry (CV) was utilized for determining the electrochemical detection of glucose. Cyclic voltametry was used to determine the peak oxidation current of the pristine Co_3O_4 electrode, the optimum concentration Co_3O_4:Cu electrode and the optimum number of layers of the Co_3O_4:Cu electrode (CV was conducted for each electrode fabricated).

50 ml of 0.1 M NaOH was correctly measured and added into the electrolytic cell. The number of cycles was set to 2 to ensure an oxidation and reduction curve was obtained. A set potential between 0.2 V and +0.8 V vs. Ag/AgCl was used for the cyclic voltametry set up-up in order to obtain oxidation and reduction. The scan rate for the electrochemical measurements was adjusted accordingly. In a blank solution of 0.1 M NaOH the scan rates tested were 25 mV/s, 30 mV/s, 50 mV/s, 100 mV/s and 200 mV/s.

Once the above data were captured, the addition of 1 ml to 5 ml of a prepared 51 mM glucose solution was added into the electrolytic cell. After every successive addition of glucose, the magnetic stirrer was switched on for the purpose of ensuring that the glucose was properly dispersed into the electrolytic solution. The magnetic stirrer was then switched off to prevent interferences when the CV was performed. The scan rate of the electrochemical detection of glucose was 25 mV/s and did not vary unless stated otherwise.

3.6.2. Chronoamperometric detection of glucose

45 ml of 0.1 M NaOH was correctly measured and added into the electrolytic cell. The chronoamperometry tests were conducted at applied potentials of +0.6 V, +0.65 V, +0.7 V, +0.75 V and +0.8 V vs. Ag/AgCl. (These potentials were taken from the CV data where the optimum electrode displayed a peak oxidation current of 0.65 V.)

In order to evaluate the chronoamperometric response of the Co_3O_4:Cu electrode, a successive addition of 1 ml of 1.67 µM glucose solution at intervals of 30 s were added into the electrolytic cell. Before the addition of glucose, the system needed to be stabilized. Hence, the glucose addition was added at 200 s. The electrolytic solution together with the successive addition of glucose was stirred continuously for the duration of the chronoamperometry measurements.

3.6.3. Interference study

45 ml of 0.1 M NaOH was correctly measured and added into the electrolytic cell. The interference study was conducted at the optimum potential (+0.65 V) obtained from the chronoamperometric tests i.e. the potential as a result of which the chronoamperometry results exhibited a high sensitivity, low LOD and broad linear range.

In order to conduct the interference study, a successive addition of a variety of chemicals were added into the electrolytic cell at intervals of 30 s as follows: 0.51 mM glucose, 0.05 mM sucrose, 0.05 mM fructose, 0.05 mM acetic acid, 0.05 mM acetaminophen, 54 mM sodium chloride, 64 mM potassium chloride, 0.05 mM uric acid and then 0.51 mM glucose, once again, was added accordingly.

Before the addition of the first solution, the system needed to be stabilized i.e. constant. Hence, the addition occurred at 200 s. The electrolytic solution together with the successive addition of solutions was stirred continuously for the duration of the interference study.

3.6.4. Reproducibility study

The reproducibility of the glucose sensor is vital for the accurate measurement of analyte concentrations. Four individual electrodes were prepared accordingly and tested with 1 mM – 5 mM glucose at 25 mV/s. Cyclic voltammetry tests were conducted for each electrode following the procedure in sub *section 3.6.1*.

3.6.5. Stability study

A stability test was conducted to determine the number of times the glucose sensor could be used without losing its catalytic activity. Cyclic voltammetry was performed for 100 cycles at a scan rate of 25 mV/s.

3.6.6. Repeatability study

Repeatability tests were conducted to ensure that the same sensor could be utilized multiple times without large deviations in glucose detection. Before each measurement, the sensor was washed with distilled water and dried under air flow to be tested in a fresh 1 mM glucose solution immediately. Cyclic voltammetry tests were conducted for each electrode following the procedure in *section 3.6.1*.

3.6.7. Electrochemical impedance spectroscopy (EIS) and Hall Effect Measurements

A 5 mM $K_4Fe(CN)_6.3H_2O$ solution was prepared. 50 ml was added into the electrolytic cell. The Autolab PGSTAT302N potentiostat and cell were switched on. The bias potential was set at 0.25 V by applying an AC voltage with 5 mV amplitude in the frequency range from 0.1 Hz to 100 kHz. This was plotted in the form of plane diagrams i.e. Nyquist plots and Bode plots. A Randalls circuit was used to fit the data accordingly.

The Hall Effect Measurement for conductivity and bulk concentration was imported from the ECOPIA Hall Effect Measurement System software.

3.6.8. Shelf life study

A shelf life test was conducted to determine the length of time for which the glucose sensor remains usable without losing its catalytic activity. Cyclic voltammetry tests were conducted with the addition of 1 mM glucose every week for a month.

3.7. Detection of glucose in human serum

Glucose in human serum was measured utilizing the chronoamperometric method of analysis as discussed in *section 3.6.2*; however, two successive additions of 1 ml human serum sample were added to the electrolytic cell. The human serum was then further prepared for analysis on the UV Spectrophotometer in order to determine the initial concentration of glucose.

1 ml of the sample was placed in individual plastic vials. 3 ml of dinitro salicylic acid (DNS) solution was then dispersed in the sample. The sample was then placed in a water bath for 15 min at 100 °C. From there, the sample was removed and left to cool for ≤ 5 min. A laboratory glucose test kit was utilized as a standard for determining the concentration of glucose in the human serum sample. The glucose content of prepared human serum sample was determined by the absorbance of 540 nm utilizing a Cintra 2020 UV Spectrophotometer.

A minor quantity of human serum was also tested utilizing the sensor from a commercial Glucose Meter for comparison purposes.

3.8. Detection of glucose in saliva

The following section explains the methodology followed for the detection of glucose in human saliva.

3.8.1. Saliva sampling protocol for test subject

One healthy volunteer in the age group of 20-30 years was utilized in this study following the ethical procedures of Cape Peninsula University of Technology, with his or her identity withheld. In order to obtain the sample of saliva required for testing, the following protocol was adopted:

The volunteer:

- Waited for 2 min after rinsing the mouth with water.
- Minimized swallowing and held saliva in mouth for 30 s.
- Placed dental sterilized cotton sponge in mouth and chewed it until soaked with saliva (≤ 1 min).
- Deposited the sponge into a syringe directly from the mouth without touching it to avoid contamination.

- Inserted the plunger in the syringe and squeezed the saliva through the bottom of the syringe into clean vials.
- Preserved the sample tube at 4 °C in a refrigerator.

Three sample vials were collected from the same person ≈ 10 ml.

3.8.2. Saliva sample preparation and analysis

Two types of saliva samples were tested i.e. a raw and a spiked saliva sample. Both samples were collected via the above procedure (sub *section 3.8.1*.); however, 1 ml of a 51 mM glucose solution was added to the other i.e. the adjusted sample. Each sample was placed in the centrifuge at 10 000 g for 5 min for the purpose of removing particulate materials. The resultant supernatant was then transferred to new vials for further tests. Glucose in human saliva was measured utilizing the chronoamperometric method of analysis as explained in *section 3.6*.; however instead of the addition of glucose, a successive addition of 1 ml of the saliva sample was added to the electrolytic cell.

The saliva samples were then analysed on the UV Spectrophotometer whereby 1 ml of each sample i.e. raw and adjusted, was placed in individual plastic vials, and 3 ml of dinitro salicylic acid (DNS) solution was dispersed in each saliva sample. The samples were then placed in a water bath for 15 min at 100 °C. From there, the samples were removed from the water bath and left to cool down for ≤ 5 min. A laboratory glucose test kit was utilized as a standard for determining the concentration of glucose in the saliva samples. The glucose content of prepared saliva sample was determined by the absorbance of 540 nm utilizing a Cintra 2020 UV Spectrophotometer.

3.9. Reliability and validity of results

Since the outcome of this study highly depends on the quantitative data collected, to ensure reliability and validity of the results, it is assumed that the instruments utilized provided accurate results. Also, since no one glucose sensor will produce the same results, repeatability, reproducibility and stability studies will be completed; a standard deviation of less than 15 %, according to the ISO 15197: 2013 will be accepted where the results are close to the mean and are clinically accurate (Kim *et al.*, 2019). A larger standard deviation than 15 % will mean that there is a large variance in the results and that it is a clinically irrelevant deviation.

3.10. Data analysis and presentation of results

A range of literature was utilized for the qualitative analysis of the fabrication material for the non-enzymatic glucose sensor construction. With respect to the quantitative analysis, the data for the electrochemical and chronoamperometric measurements were imported from the Autolab Nova 1.1 and 2 software.

Cyclic voltammetry graphs of current density against potential were plotted in order to obtain the current peak and optimum biosensor. The amperometric responses of the biosensor to glucose were plots of current density against time, whereby the corresponding calibration curves were obtained by the current density against glucose concentration. This data provides characterisation of the sensor i.e. sensitivity, linear concentration range, potential, limit of detection and response time. For the selectivity study analysis, a chronoamperometric plot of current density against time was utilized to examine the current response escalation for inference species that can be found in the blood.

The intra- and inter-electrode reproducibility was displayed on a histogram and the standard deviation between the peak currents was calculated. The shelf life of the biosensor was analysed by utilizing the peak current obtained from the cyclic voltammetry plots over a period of four weeks. This data is represented by a histogram and percentage difference between initial and final current peak over the four week period.

3.11. Health and safety precautions

The *Nanotechnology* and *Engineering laboratories, Cape Peninsula University of Technology (CPUT)* facilities, were utilized for completion of this research project. The individual housekeeping rules of each of the laboratories were abided by accordingly. In order to be permitted to work in the laboratories, the *Flow Process and Rheology Centre (FPRC)* induction and safety test needed to be completed.

In order to promote health and safety during the course of this research project, the correct personal protective equipment (PPE) was worn at all times in the laboratory. Gloves, safety glasses, lab coats and safety footwear were worn when conducting experiments. This was done in order to protect the user against health and safety risks.

With respect to the chemicals and consumables utilized in this research project, material safety data sheets (MSDS) were read. Generally, working safely with chemicals requires the proper use of laboratory equipment, hence training and reading the work instructions and user manuals of equipment and apparatus were conducted.

3.12. Conclusion

This chapter has described the research and experimental methodology undertaken for completion of the study. The research design techniques, materials and consumables were outlined accurately. Experimental methodology for the preparation of the substrate and synthesis of the Co_3O_4 were explained. Preparation of the Co_3O_4 solution and Cu-doped material were clarified. The procedure followed for spin coating and calcination were explained thoroughly. The electrochemical measurement test procedures i.e. electrochemical and amperometric detection of glucose, interference, reproducibility,

stability, repeatability, electrochemical impedance spectroscopy and shelf life study were explained in detail. Surface characterisation methodology was clarified. The techniques utilized for the detection of glucose in human serum and saliva was described. The reliability, validation of data, data analysis and presentation of data was explicated. Thereafter, ethical compliance measures and health and safety precautions were briefly touched upon with respect to this study. The analysis of these tests is depicted and discussed in Chapter 4.

~ Chapter 4 ~

Results and Discussion

This chapter comprises:

Section 4.1: *Introduction*

Section 4.2: *Surface characterisation*

Section 4.3: *Electrocatalytic oxidation of glucose*

Section 4.4: *Electrochemical Impedance Spectroscopy*

Section 4.5: *Chronoamperometric detection of glucose*

Section 4.6: *Human serum and salivary glucose analysis*

Section 4.7: *Selectivity study of the Cu-doped Co_3O_4 biosensor*

Section 4.8: *Reproducibility analysis*

Section 4.9: *Repeatability and stability analysis*

Section 4.10: *Conclusion*

Chapter 4: Results and discussion

4.1. Introduction

The aim of this study was to develop a non-enzymatic glucose sensor that achieves an enhanced detection of glucose utilizing a Cu-doped Co_3O_4 electrode. In this chapter, the results obtained from Chapter 3 were analysed and placed into context.

4.2. Surface characterisation

The morphology and structure of the solution deposited film was evaluated utilizing high resolution SEM and TEM. *Figure 4.1 a–c* represents the SEM micrograph of the pristine electrode and *figure 4.1 d–f* represents the SEM micrograph of the deposited film. It can be perceived from *figure 4.1 a–c* that the deposited film on the pristine electrode is uniformly dispersed on the FTO, with no cracks or holes are observed on the film. In *figure 4.1 d–f*, it is observed that the deposited film of the Cu-doped electrode has a rough surface. The roughness of the surface can provide increased surface area for electrochemical catalytic oxidation of glucose (Chowdhury *et al.*, 2016). The average film thickness on the Cu-doped electrode is 1697 nm and for the pristine electrode, the average film thickness is 357 nm, as seen in *figure 4.2*. This suggests successful incorporation of Cu into the Co_3O_4 host lattice.

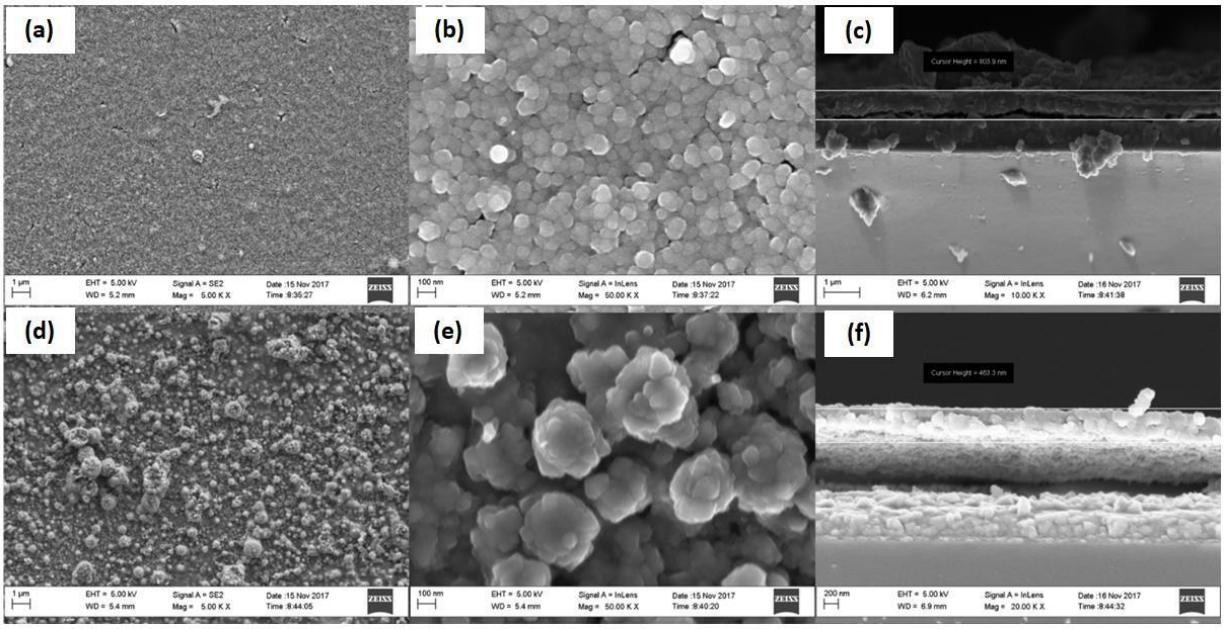

Figure 4. 1: SEM top and side views of (a-c) Pristine Co_3O_4 sample (d-f) Co_3O_4: Cu sample

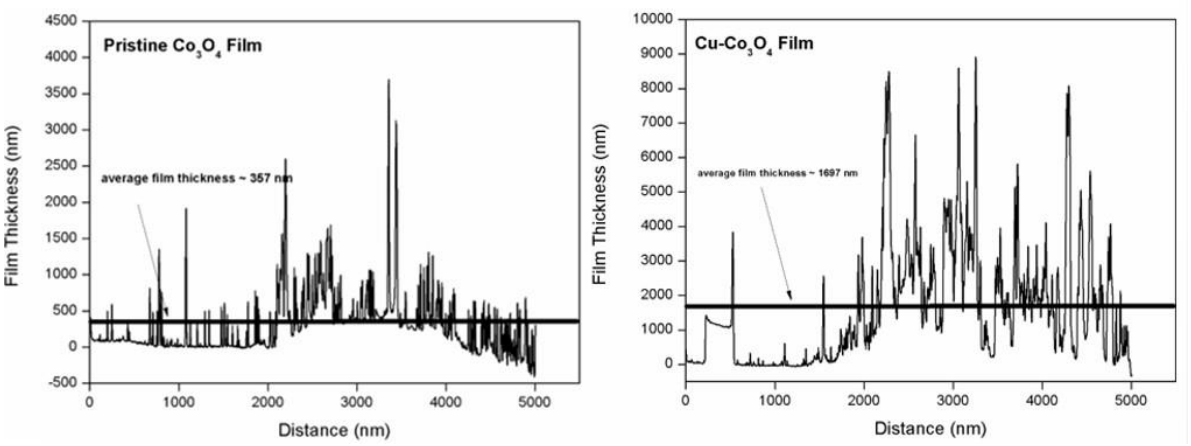

Figure 4. 2: Average film thickness of the Co_3O_4 : Cu and pristine Co_3O_4 electrode

Figure 4.3 d & e depicts the TEM images of the Cu doped Co_3O_4 biosensor film. A uniform distribution of Cu was found in *figure 4.3* from the elemental X-ray mapping.

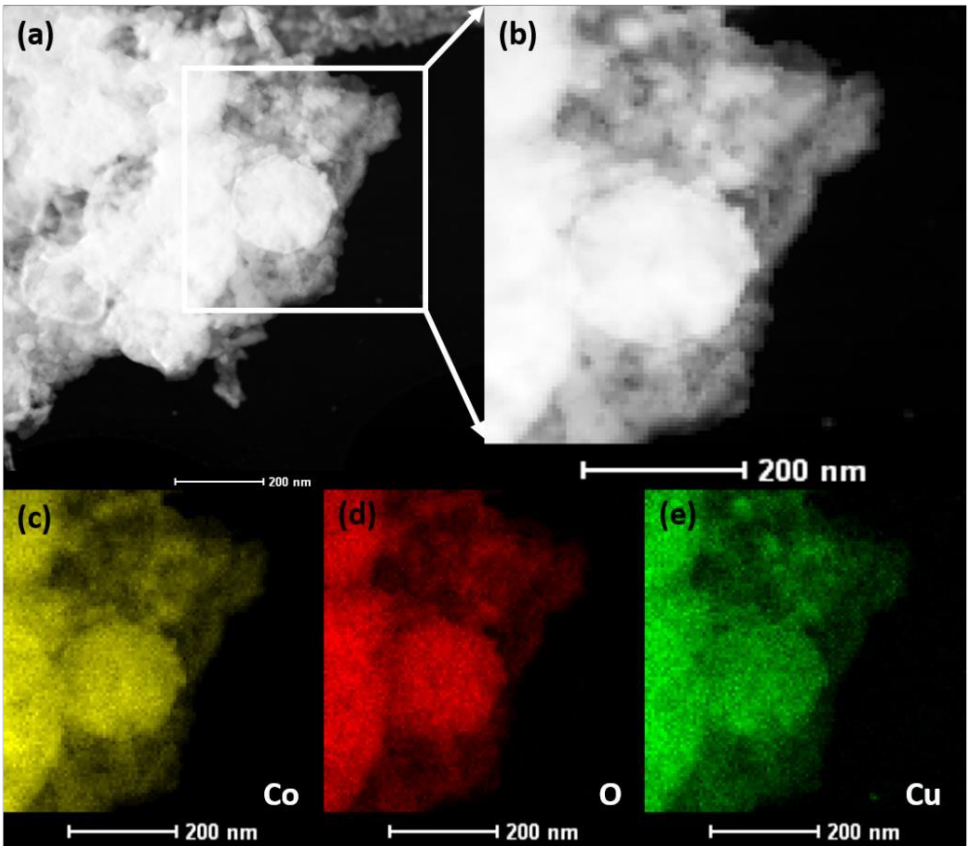

Figure 4. 3: (a) HAADF image of the Co_3O_4: Cu with the area selected for EDS mapping indicated by the square, (b) resultant STEM spectral image from the highlighted area in (a), (c)–(e) extracted Co, O and Cu maps, respectively

Figure 4.4 a–c represents the TEM micrographs and SAED patterns of the pristine electrode. The first four diffraction rings (*figure 4.3 c*) is identified as that from the face centred cubic (fcc) Co_3O_4 crystal structure yielding d(111)=0.474 nm, d(220)=0.291 nm, d(311)=0.249 nm and d(400)=0.205 nm respectively. From these values an average lattice constant of a=0.822 ± 0.003 nm was determined. Correspondingly, the Cu-doped electrode sample exhibited the fcc crystal structure of Co_3O_4 but with a slight increase in the respective d-spacing to d(111)=0.475 nm, d(220)=0.293 nm, d(311)=0.250 nm and d(400)=0.206 nm (*figure 4.4 f).* Due to this, there is a small expansion of the average lattice constant compared to the pristine Co_3O_4 sample, a=0.826 ± 0.003 nm.

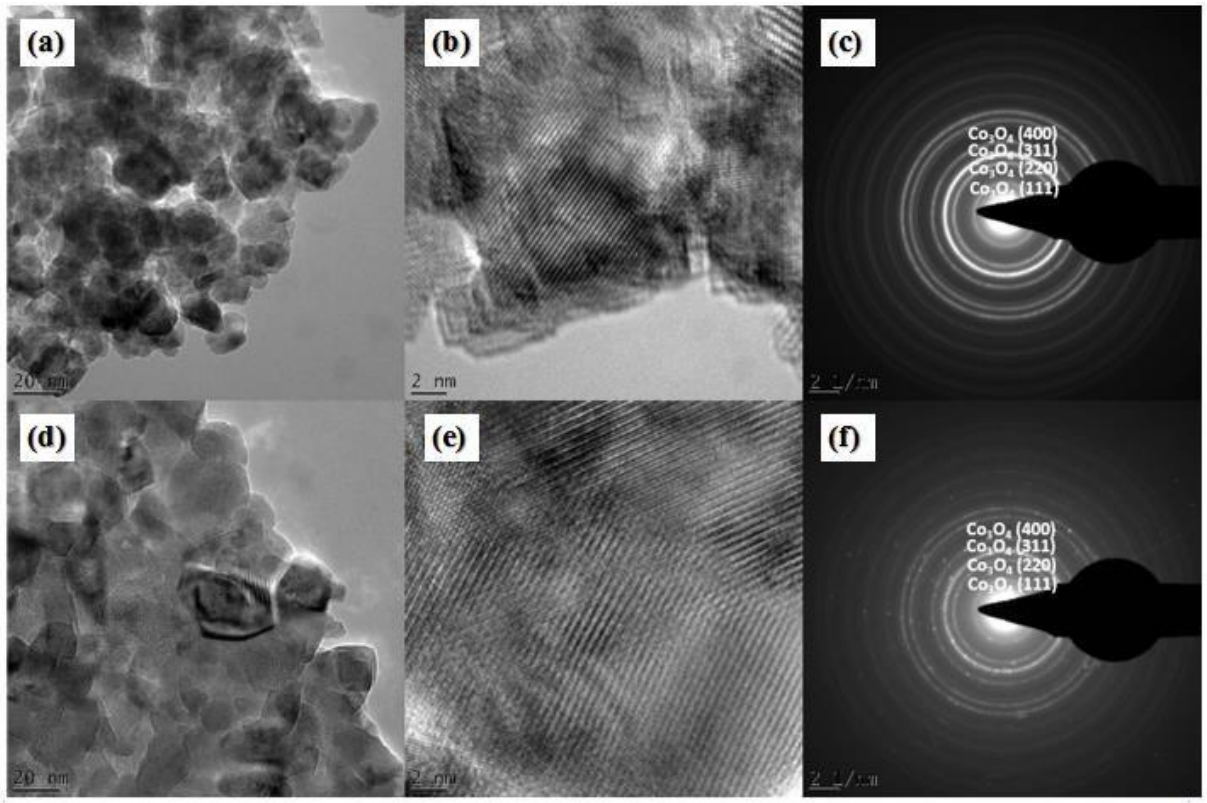

Figure 4. 4: TEM micrographs and SAED pattern of (a-c) Pristine Co_3O_4 (d-f) Co_3O_4: Cu samples

It can be observed from the XRD pattern that the film contains the Co_3O_4 structure regardless of the Cu doping. The slight increase in the lattice constant can further be explained by the XRD patterns in *figure 4.5*. It can be observed that the Co_3O_4 crystalline matrix experiences a slight shift to higher Bragg angles upon doping with Cu. This phenomenon causes a strain in the Co_3O_4 matrix due to the successful addition of elemental Cu ions into the Co_3O_4 lattice. Hence, the addition of the Cu^{2+} ions into the Co_3O_4 causes a slight expansion in the unit cell of Co_3O_4 as observed in the XRD. Also, the presence of (111), (220), (311) and (400) peaks complements the observation from the TEM and SAED analysis.

***FTO**

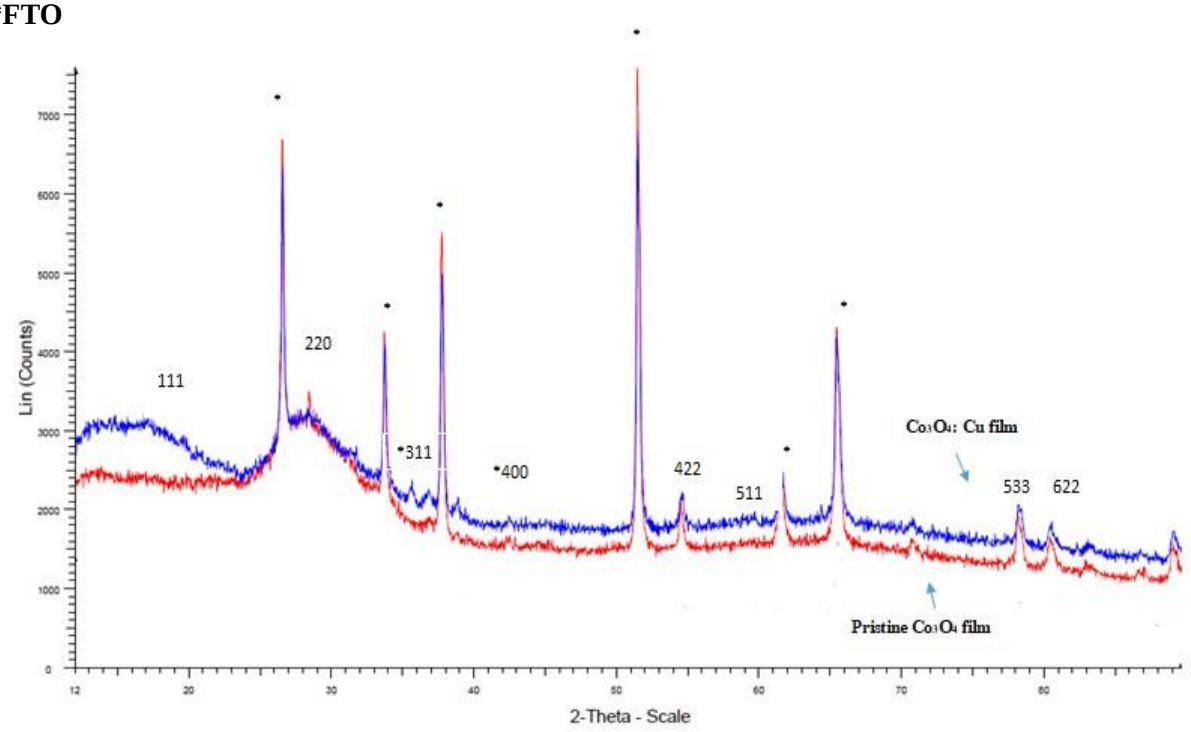

Figure 4. 5: XRD pattern of the Co_3O_4: Cu and pristine Co_3O_4 film

Figure 4.6 compares the energy loss near edge fine structure (ELNEFS) data of the Co $L_{3,2}$ ionization edge of the pristine (black curve) and Co_3O_4: Cu (red curve) samples. Both materials show two sharp peaks at 783 (L_3) and 798 eV (L_2), which correspond to the Co $2p_{3/2}$ and Co $2p_{1/2}$ spin–orbit peaks of the Co_3O_4 spinel (Wang *et al*., 2000), respectively. In addition, it can be seen that the characteristic Cu $L_{3,2}$ edge at 931 eV is absent in the Co_3O_4:Cu specimen, indicating that the Cu as identified in the X- ray maps of *figure 4.3*, do not exist in either oxide or metallic form in the hybrid material. Rather, at closer inspection of the L_3/L_2 of the Co $L_{3,2,}$ widely considered a fingerprint method for determining the Co valence state (Wang *et al*., 2000; Hagelin-Weaver *et al*., 2004; Abu Zied *et al*., 2015 & Barrec *et al*., 2010), a clearer understanding of the effect of the incorporation of the Cu in the Co_3O_4 matrix is developed. From *figure 4.6* an L_3/L_2 ratio of 2.49 and 3.89 is determined for the pristine Co_3O_4 and Co_3O_4:Cu, respectively. The ratio of 2.49 is typical for cobalt oxides exhibiting cobalt ions, and exists in two oxidation states: one-third of the Co atoms being Co^{2+} in a tetrahedral coordination to oxygen, and two thirds Co^{3+} in an octahedral oxygen environment (Wang *et al*., 2000; Hagelin-Weaver *et al*., 2004). The increase in the L_3/L_2 ratio for the Cu modified Co_3O_4 proves that a change in the $1/3Co^{2+}$ + $2/3Co^{3+}$ coordination occurred upon incorporation of the Cu ions in the Co_3O_4 matrix. The value of 3.89 is typical of pure Co^{2+} and in some instances Co^{4+} valence states (Abu-Zied *et al*., 2015; Barrec *et al*., 2010). However, considering the expansion in lattice parameter measured from the SAED results of *figure 4.4* and the distribution of the Cu elements in the X-ray maps of *figure 4.3*, the

increase in L_3/L_2 ratio, and subsequent change in valence state of the Co oxide, is attributed to doping by the Cu atoms.

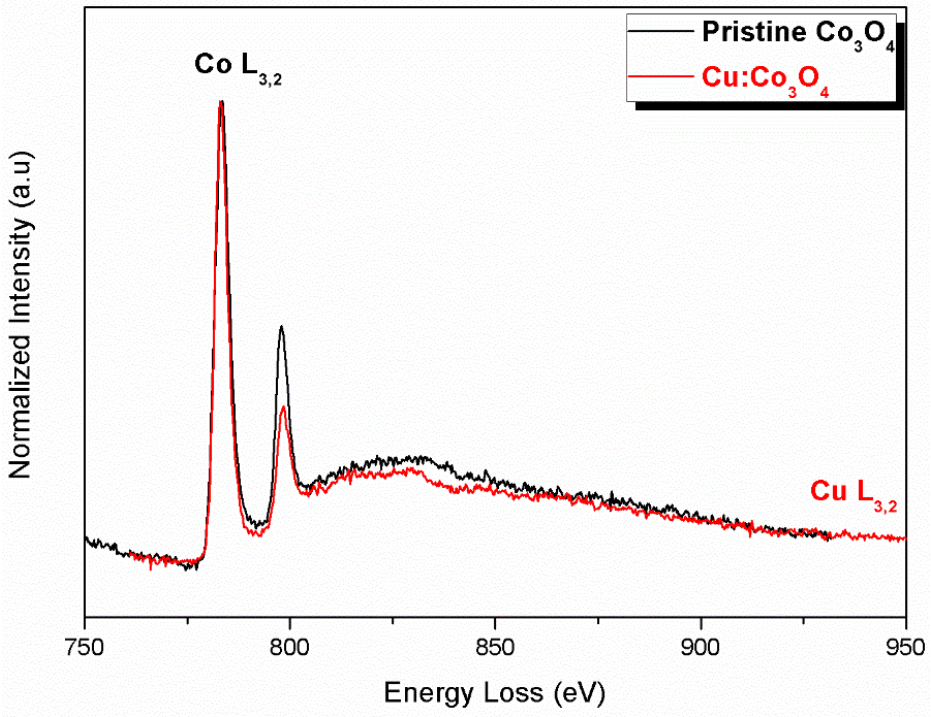

Figure 4. 6: Electron energy loss spectroscopy results comparing the Co $L_{3,2}$ ionization edge of the pristine Co_3O_4 sample to that of the Cu incorporated Co_3O_4 material

4.3. Electrocatalytic oxidation of glucose

Cyclic voltammetry (CV) was utilized to evaluate the performance of the Co_3O_4:Cu electrode for electrocatalytic oxidation of glucose in a low concentration alkaline solution of 0.1 M NaOH. The electrodes were evaluated in the potential range between -0.2 V to 0.8 V vs. Ag/AgCl.

Various amounts of Cu concentrations into the Co_3O_4 host lattice were introduced for electrochemical characterisations. This was conducted to find the optimum level of Cu doping for enhanced electrochemical activity. The figure below depicts the CV outcomes for the Co_3O_4:Cu composition ratios tests, i.e. 98: 2 wt %, 90: 10 wt %, 85: 15 wt % and 80: 20 wt % in the absence and presence of 1- 5mM glucose at 25 mV/s.

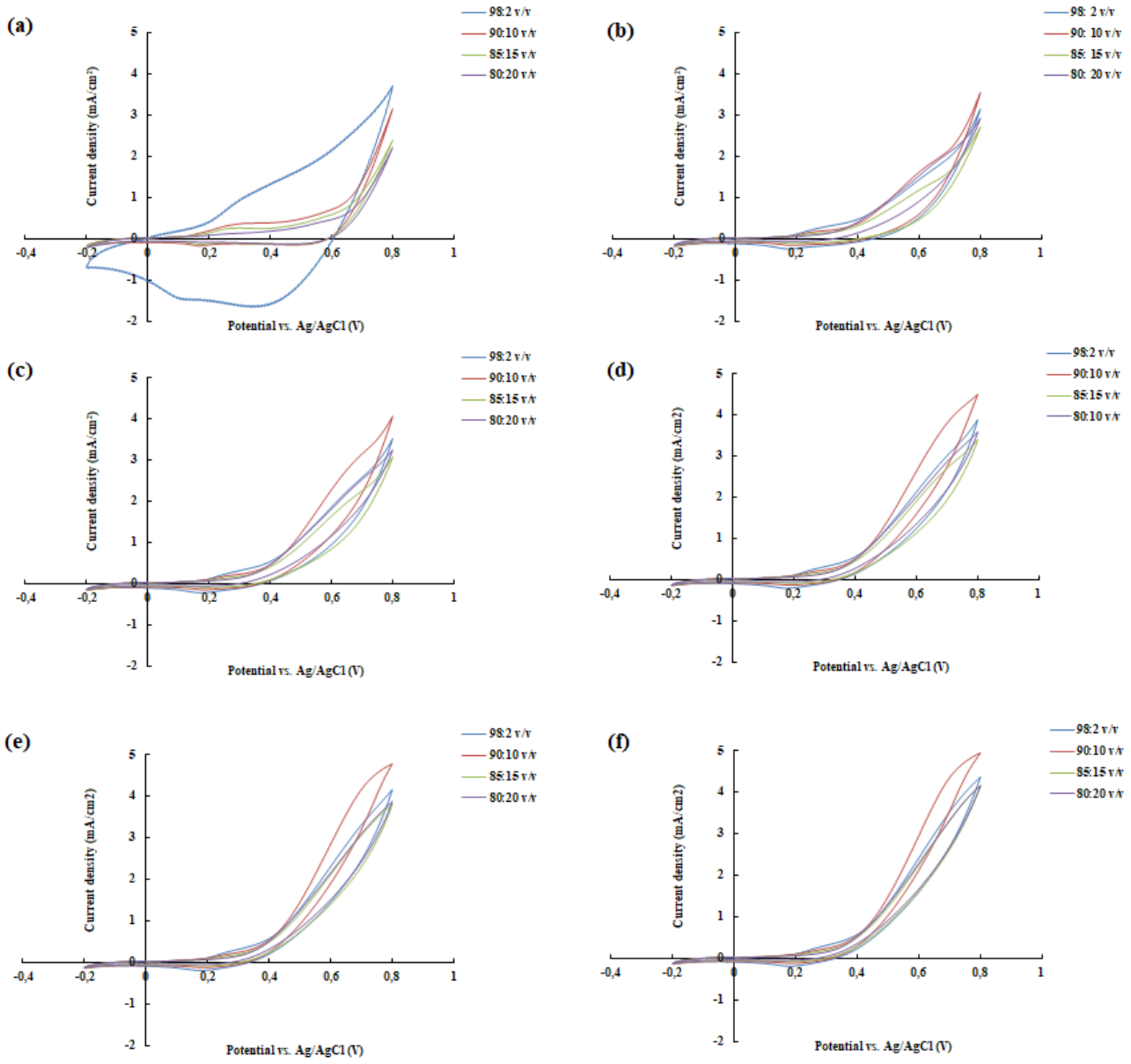

Figure 4. 7: Comparison of the varying rations of the Co_3O_4: Cu electrodes in the (a) absence of glucose and presence of (b) 1 mM (c) 2 mM (d) 3 mM (e) 4 mM and (f) 5 mM glucose in a 0.1 M NaOH solution at 25 mV/s

On comparison of the various CVs, as portrayed above, the results substantiate that the 90: 10 wt % Co_3O_4: Cu provides the highest electrochemical activity (current density response) with respect to glucose detection. This is due to the significant anodic current increase/anodic peak for the 90: 10 wt % Co_3O_4: Cu biosensor with the reduction peaks diminished. This highlights that a biosensor fabricated with 90: 10 wt % Co_3O_4: Cu would be more effective in terms of detecting glucose than the other Co_3O_4: Cu compositions analysed. In order to further optimize the biosensor, an analysis of the electrode film thickness was conducted.

The electrode film thickness (N=1 to 6) also has a substantial effect on the electrochemical performance as can be seen in *figure 4.8.a–f.* Displayed below are the CV comparisons for the Co_3O_4:Cu layer study i.e. 1- 6 layers of 90: 10 wt % Co_3O_4: Cu in the absence and presence of 1-5mM glucose at 25 mV/s.

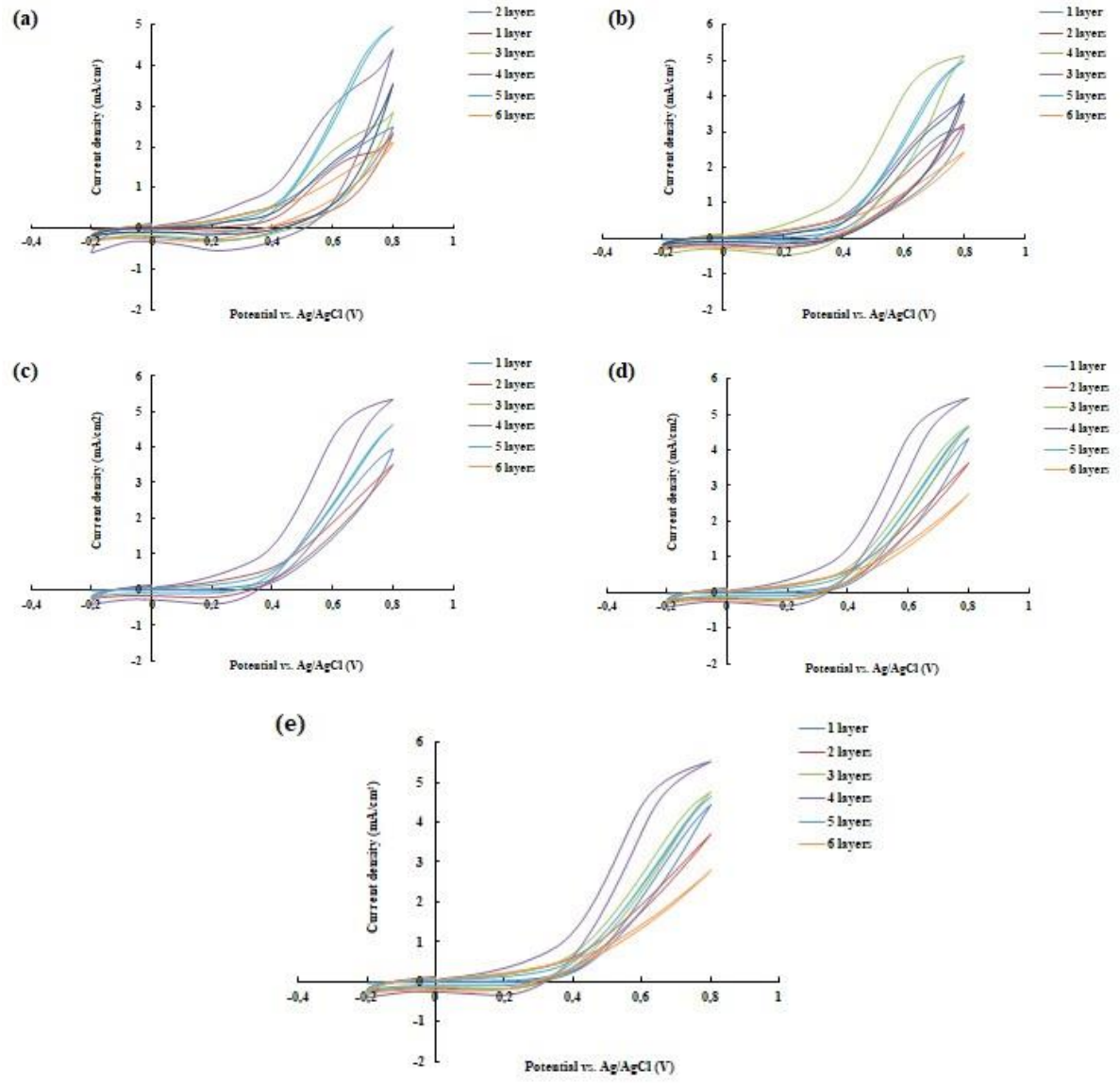

Figure 4. 8: A comparison the various layers of the Co_3O_4: Cu biosensor in the presence of (a) 1 mM (b) 2 mM (c) 3 mM (d) 4 mM (e) 5 mM glucose in 0.1 M NaOH solution at 25 mV/s

It can be noted that the four-layered electrode exhibited the highest electrochemical performance as the anodic current was significantly higher in contrast to the other layers studied with the successive addition of glucose. The Co_3O_4:Cu electrode (N=4) also showed enhanced electrochemical activity when compared to the pristine Co_3O_4 electrode respectively. This can be observed in *figure 4.9.*

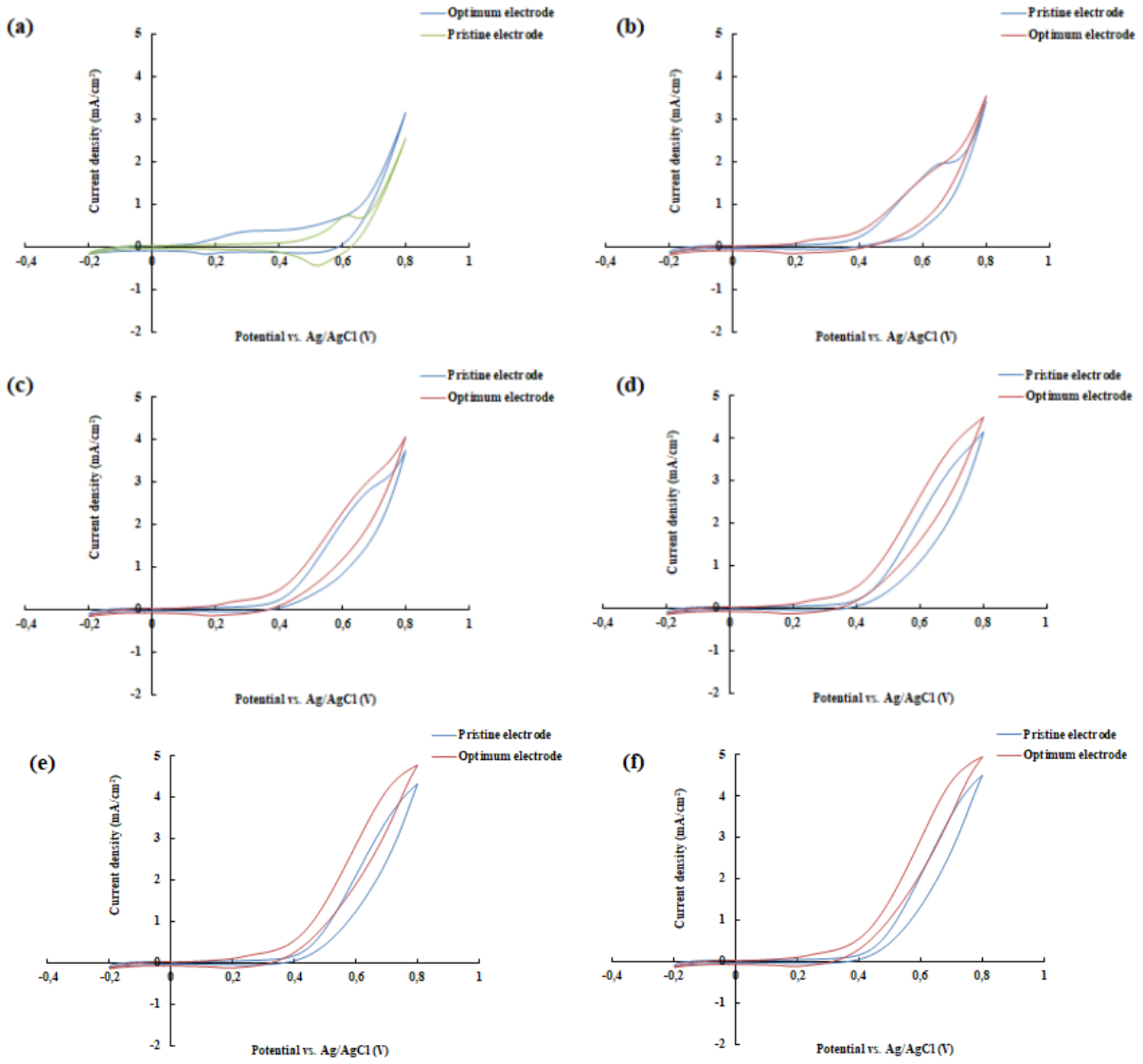

Figure 4. 9: Cyclic voltammetry comparison of the optimum Co_3O_4: Cu electrode with the pristine electrode in the (a) absence of glucose and presence of (b) 1 mM (c) 2 mM (d) 3 mM (e) 4 mM (f) 5 mM glucose at 25 mV/s in 0.1M NaOH solution

It is clear that the Co_3O_4:Cu electrode exhibits enhanced electrochemical activity compared to its pristine counterpart in the absence and presence of 1- 5 mM glucose. This proves that the electrochemical activity of the Co_3O_4 electrode is influenced by the presence of Cu doping in the Co_3O_4 lattice host. The FTO alone does not show any glucose oxidation behaviour, hence it can be postulated that a synergistic effect is present between the Cu and Co_3O_4. Also, The Co_3O_4 electrode exhibited a current density around 2.85 mA/cm^2 with 5 mM glucose, whereby the Cu doped electrode exhibited a higher current density around 3.78 mA/cm^{2,} with 5 mM glucose, at a 25 mV/s scan rate at a potential of 0.65 V vs. Ag/AgCl. The process showed a percentage enhancement of the catalytic oxidation current around 0.65 V of the Cu-doped electrode was 33 % higher than the Co_3O_4 electrode.

Figure 4.10 depicts the CVs of the pristine and Cu-doped Co_3O_4 (*N*=4) electrode at various scan rates (25 -200 mV/s). It can be observed from the figures that there is an increase in both the anodic and cathodic oxidation current peaks, as the scan rate increases from 25 - 200 mV/s. A linear correlation exists between the peaks and the scan rate as can be seen from figure insets. This provides indication of a fast electrochemical process and that the process is a diffusion-based, surface-controlled electrochemical reaction (Kung *et al.*, 2011).

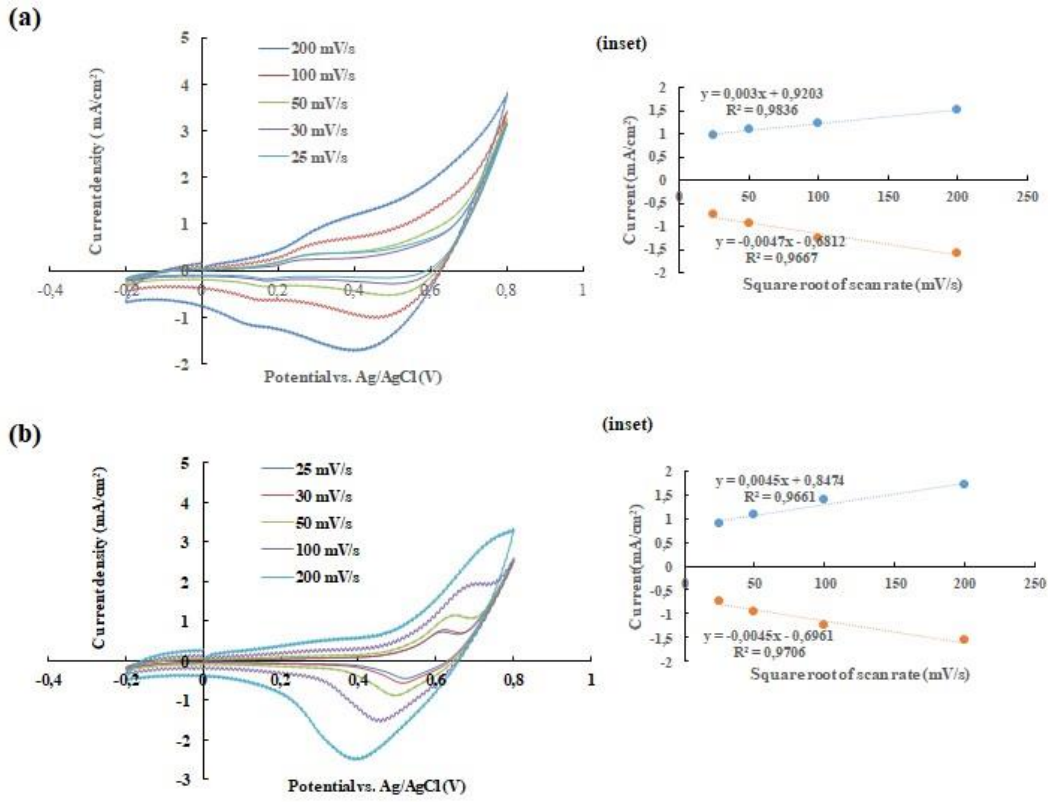

Figure 4. 10: Effect of scan rate on the electrochemical behaviour of the (a) Cu-doped Co_3O_4 thin film electrode (inset: relationship between scan rate and peak current) and the (b) pristine Co_3O_4 electrode (inset: relationship between scan rate and peak current)

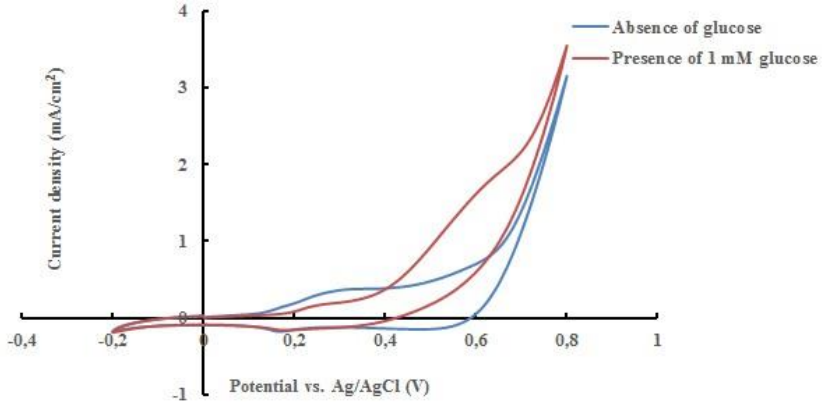

Figure 4. 11: Co_3O_4: Cu electrode in the presence and absence of 1 mM glucose in 0.1 M NaOH solution

Two pairs of clear redox peaks were found in alkaline solution due to the electrochemical redox reaction between Co_3O_4 and OH^- ions. The first pair of redox peaks appeared in the relative low potential zone between +0.1 V to +0.3 V vs. Ag/AgCl, and can be ascribed to the reversible transition between Co_3O_4 and CoOOH and the other redox peak can be assigned to the conversion of CoOOH to Co_3O_4 (equation 4.1).

$$Co_3O_4 + OH^- + H_2O \leftrightarrow 3CoOOH + e^-$$

Equation 4. 1

$$CoOOH + OH^- \leftrightarrow 3CoO_2 + + H_2O + e^-$$

Equation 4. 2

$$2CoO_2 + glucose \rightarrow CoOOH + C_6H_{10}O_6$$

Equation 4. 3

After the injection of 1 mM glucose in *figure 4.11*, the anodic peak shifted in a positive direction between +0.55 V to +0.65 V vs. Ag/AgCl and the current density underwent an apparent increase. This indicates that the Co_3O_4:Cu modified thin film electrode can be used for the electrochemical detection of glucose. This mechanism can be explained using equation 4.3, such that the electrochemical oxidation reaction from glucose to gluconolactone is catalysed by the Co_3O_4:Cu coating. Notably, with the CoO_2 consumption and the CoOOH production, the extent of reaction (equation 4.2) favours the forward reaction, thus resulting in an enhanced oxidation peak upon the addition of glucose.

With the addition of Cu to the Co_3O_4, there is an escalation of the number of reactive sites for redox reaction and biological electrical signal transmission. As Cu is doped onto Co_3O_4, the specific electroactive surface area is increased. Hence, more reactive sites are provided where the redox reaction occurs. Thus the Cu doped electrode has more reactive sites than the pristine Co_3O_4 electrode, proving that the synergistic effect results in an improved electrochemical performance when detecting glucose.

4.4. Electrochemical impedance spectroscopy (EIS) and the Hall Effect Measurement

The interfacial properties of the pristine Co_3O_4 and the modified Co_3O_4: Cu electrodes were studied by electron impedance spectroscopy (EIS). *Figure 4.12* depicts the Nyquist plots of the pristine Co_3O_4 and the Co_3O_4: Cu electrode and their equivalent circuits (inset i and ii) in 5 mM $K_4Fe(CN)_6.3H_2O$ solution.

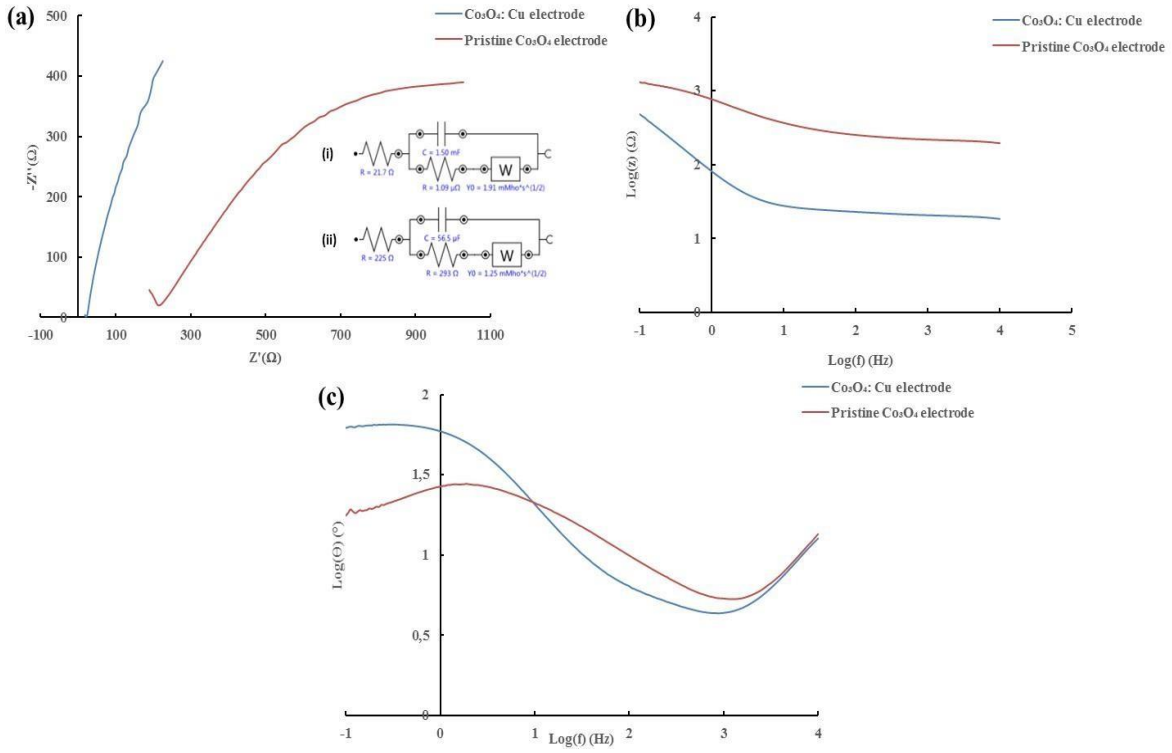

Figure 4. 12: (a) Nyquist plot (inset: Resultant Randall's circuit for (i) Co_3O_4: Cu and (ii) Pristine Co_3O_4 electrode) (b) Bode impedance plots (c) Bode phase plots of the pristine and Cu-doped electrode film

The Nyquist diagrams show that the pristine Co_3O_4 electrode has a roughly semicircle/curve-shaped Nyquist plot with a large diameter which in turn suggests the hindrance to the electron transfer kinetics at the electrode (Chen *et al.*, 1996). However, for the Cu-doped electrode, a smaller semi-circle/curve was observed, which indicates higher electron transfer kinetics. These semi-circles are a result of the charge transfer resistance (R_{ct}) at the electrode interface, which provides an indication of the electron transfer kinetics. It can be noted that the R_{ct} value decreased substantially for the Cu-doped electrode as to the pristine electrode. For the Co_3O_4: Cu electrode the R_{ct} =1.09 uΩ and for the pristine Co_3O_4 R_{ct} = 292 Ω, as can be seen in *figure 4.12*. This is attributed to the catalytically active Cu-doped material on the electrode surface. Notably, the double layered capacitance is directly related to surface area, and the surface area in turn increases with the surface roughness. The Cu-doped electrode exhibited a double layer capacitance of 56.5 µF whereby the pristine Co_3O_4 electrode exhibited 1.5 mF.

The conducting nature of the pristine Co_3O_4 and Co_3O_4: Cu electrode facilitates the peak shifting in the Bode plots (Chowdhury *et al.*, 2016). The Bode impedance plot, shown in *figure 4.12 b*, of the Co_3O_4: Cu electrode compared to the pristine Co_3O_4 showed a lower log (z) value in the frequency range of 0.1 Hz to 10 000 Hz. The comparison for the log (z) of the pristine and Cu-doped electrode distinctively shows that the charge transfer resistance decreases significantly with the presence of Cu, highlighting good electrochemical activity. In *figure 4.12 c*, the Bode-phase plot of the electrodes were

collected in the frequency range of 0.1 Hz to 10 000 Hz. The Bode-phase plot of the Co_3O_4: Cu electrode compared to the pristine Co_3O_4 showed a lower log (-Θ) in the frequency range of 100 Hz to 10 000 Hz. It can be seen that around 2.5-3.5 Hz, the phase angle for the Cu-doped electrode is lower than that of the pristine electrode. It is also evident that the doping of the Cu particles in the Co_3O_4 allows for greater electrochemical and catalytic reactions, and improves the efficiency of the composite electrode. This result confirms that the Co_3O_4: Cu electrode has a higher charge transfer rate and electroactive surface area, leading to a high conductance as compared to the pristine electrode. This proves that the introduction of Cu as a dopant material in the Co_3O_4 lattices has increased the material's charge transfer ability, thus resulting in an enhanced electrochemical activity.

The interfacial properties of the different layers of the Co_3O_4: Cu electrodes were also studied by electrochemical impedance spectroscopy (EIS). This was conducted in order to confirm the electrochemical CV results for the electrode that depicted an enhanced electrochemical performance in the detection of glucose. The EIS data for each of the varied film thickness electrodes (N=1 to 6) has a substantial effect on the interfacial proprieties of the electrode.

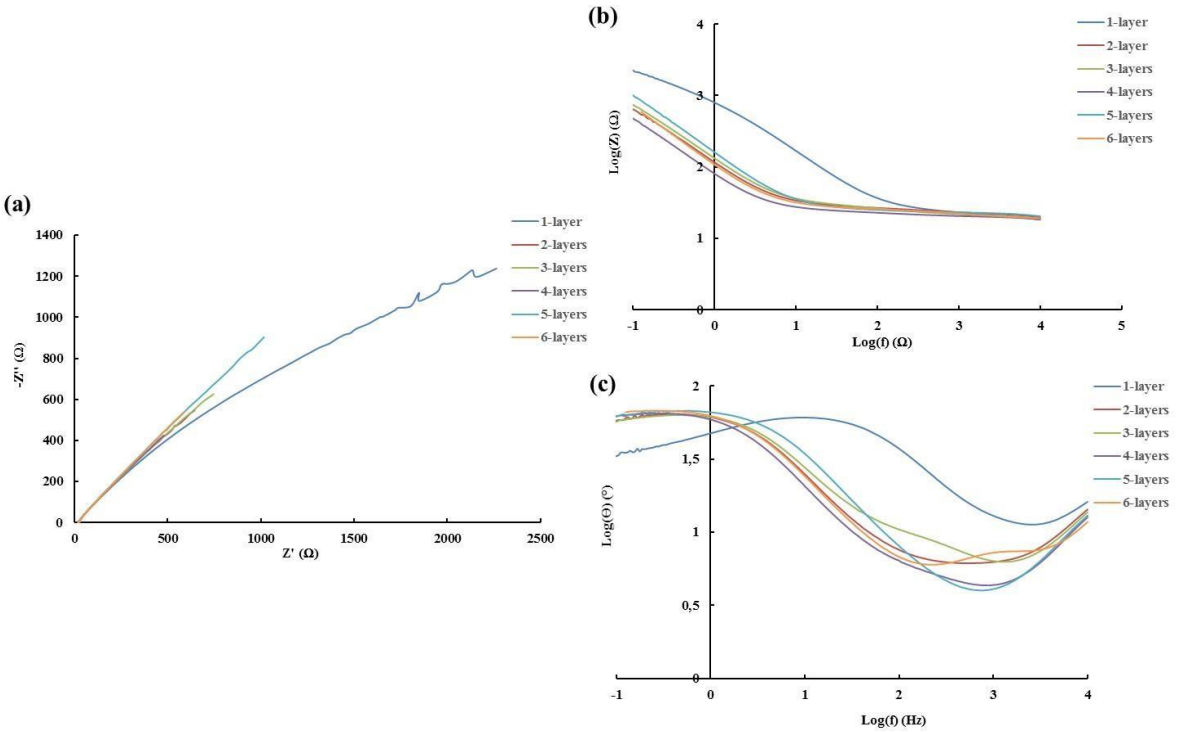

Figure 4. 13: Comparison of the (a) Nyquist plots (b) Bode impedance plots (c) Bode phase plots of the various layers of Co_3O_4: Cu film electrodes

Figure 4.13a depicts the Nyquist plots of the Co_3O_4: Cu electrode (*N*=1 to 6) in 5 mM $K_4Fe(CN)_6.3H_2O$ solution. It can be noted from *figure 4.13 a* that a depressed semi-circular/curve and linear pattern exists at high and low frequencies respectively. The semi-circular/curve and linear part at high and low frequency can be attributed to the charge transfer resistance (R_{Ct}) at the electrode interface which provides an indication of the electron transfer kinetics. It can be noted that the R_{Ct} value obtained is 1.09 uΩ (*N*=4) respectively. The Bode impedance plot, shown in *figure 4.13 b*, of the various layered Co_3O_4: Cu electrodes showed that the four layered Co_3O_4: Cu electrode resulted in a lower log (z) value in the frequency range of 0.1 Hz to 10 000 Hz. The comparison for the log (z) of the various layers of Cu-doped electrodes distinctively depicts that the charge transfer resistance decreases significantly with the presence of four layers of the Cu dopant material, highlighting better electrochemical activity than the rest of the other layered electrodes. This result also proves that the four layered Cu-doped electrode is the optimum biosensor.

The Bode-phase plot of the electrodes was collected in the frequency range of 0.1 Hz to 10 000 Hz. The Bode-phase plot of the five layered Co_3O_4: Cu electrode proved to be the lowest log (-Θ) in the frequency range of 100 Hz to 10 000 Hz. The four layered Co_3O_4: Cu electrode evidenced a slightly higher log (-Θ) in the frequency range of 100 Hz to 10 000 Hz, which can be considered negligible. Hence, the four layered Co_3O_4: Cu electrode produced a more enhanced electrochemical performance (CV), a lower log (z) value in the frequency range of 0.1 Hz to 10 000 Hz, small R_{ct}=1.09 uΩ value and low log (-Θ) in the frequency range of 100 Hz to 10 000 Hz. Its useability as the optimal Co_3O_4: Cu biosensor is therefore justified.

Hall Effect measurements were also conducted for the pristine and Cu-doped electrodes for the purpose of measuring the conductivity and bulk concentration of the sample electrodes. The pristine Co_3O_4 sample was not very conductive, hence the input current was very low i.e. 0.2 uA. The Cu-doped sample on the other hand displayed a greater conductivity thus the input current could be given as 25-150 uA. The conductivity and bulk concentration increased significantly with the addition of the Cu to the material. This translates to the fact that the addition of a dopant improves the electrochemical performance of the sensor. And since the bulk concentrations are both negative, it can be noted that both the materials are n-type semiconductors i.e. electrons are the majority carriers. The Hall Effect measurements can be seen in *table 4.1*.

Table 4. 1: Hall Effect Measurement results

Electrode Co_3O_4: Cu	
Current (uA)	
25	Bulk concentration: $-2.44 \times 10^{19}/cm^3$ Conductivity: $7.99 \times 10^{1}/\Omega$ cm
50	Bulk concentration: $-2.67 \times 10^{19}/cm^3$ Conductivity: $8.00 \times 10^{1}/\Omega$ cm
70	Bulk concentration: $-3.43 \times 10^{19}/cm^3$ Conductivity: $7.99 \times 10^{1}/\Omega$ cm
100	Bulk concentration: $-2.94 \times 10^{19}/cm^3$ Conductivity: $7.99 \times 10^{1}/\Omega$ cm
150	Bulk concentration: $-3.25 \times 10^{19}/cm^3$ Conductivity: $8.03 \times 10^{1}/\Omega$ cm
Electrode Co_3O_4	
Current (uA)	
0.2	Bulk concentration: $-1.69 \times 10^{16}/cm^3$ Conductivity: $3.72 \times 10^{-2}/\Omega$ cm

4.5. Chronoamperometric detection of glucose

It is depicted in *figure 4.11* that the oxidation peak current increases with an increase in the glucose concentration. The oxidation peak current was observed at a potential around + 0.65 V vs. Ag/AgCl. Hence, the chronoamperometry method, at a potential range of +0.6V to +0.8 V vs. Ag/AgCl, was utilized to evaluate the response of the Co_3O_4: Cu electrode to the successive addition of glucose at intervals of 30 s in 0.1 M NaOH solution. The potential range was selected to confirm the results from the CV analysis. The electrolytic solution was stirred continuously for the duration of the chronoamperometry measurements. The +0.65 V vs. Ag/AgCl potential exhibited the optimum performance in terms of sensitivity (*figure 4.14)* as compared to the other potentials tested (*table 4.2*).

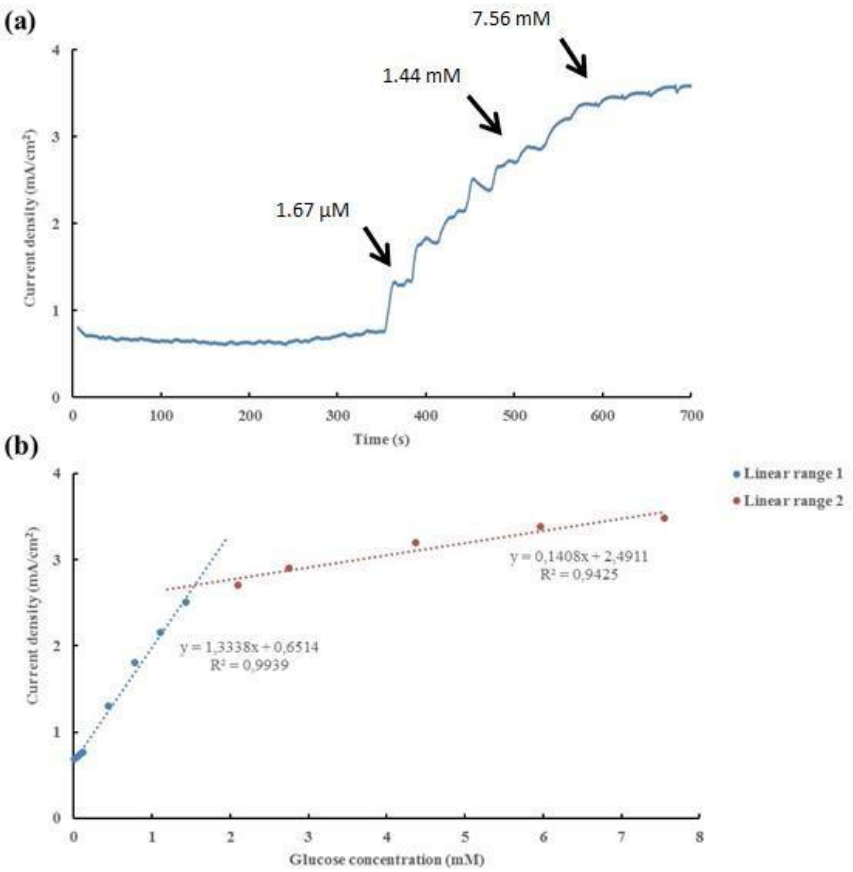

Figure 4. 14: (a) Amperometric response of the Co_3O_4: Cu electrode with successive addition of glucose from 150 mM stock solution of glucose (b) Calibration curve of the Co_3O_4: Cu electrode at an applied potential of +0.65 V in 0.1 M NaOH solution

The sensor displayed a good glucose sensing performance as a classical step style increase in current density with a response time of ≤ 10 s, the time taken for the system to react to the addition of glucose and to reach steady state current.

The optimum response curve at 0.65 V of the Co_3O_4:Cu electrode is shown in *figure 4.14*. Two distinctive linear ranges were observed from the response curve. The initial linear range is from 18.3 µM up to 1.44 mM (R^2=0.99) and the second is from 2.1 mM up to 7.6 mM (R^2=0.94). The sensor exhibited a sensitivity of 1333 µA/cm^{2}mM and 141 µA/cm^{2}mM for the linear ranges of 18.3 µM up to 1.44 mM and 2.1 mM up to 7.6 mM respectively. The limit of detection (LOD) was calculated utilizing the following equation:

$$LOD = \frac{3\sigma}{m}$$

Equation 4. 4

σ b is the standard deviation of the sample linear range obtained after the addition of the glucose; m is the slope of the calibration curve. The extrapolated LOD was calculated to be 0.153 µM (*S/N*=3).

A comparison (*figure 4.15*) of the chronoamperometric responses of the pristine Co_3O_4 and the optimum Co_3O_4:Cu biosensor was completed (*table 4.2*).

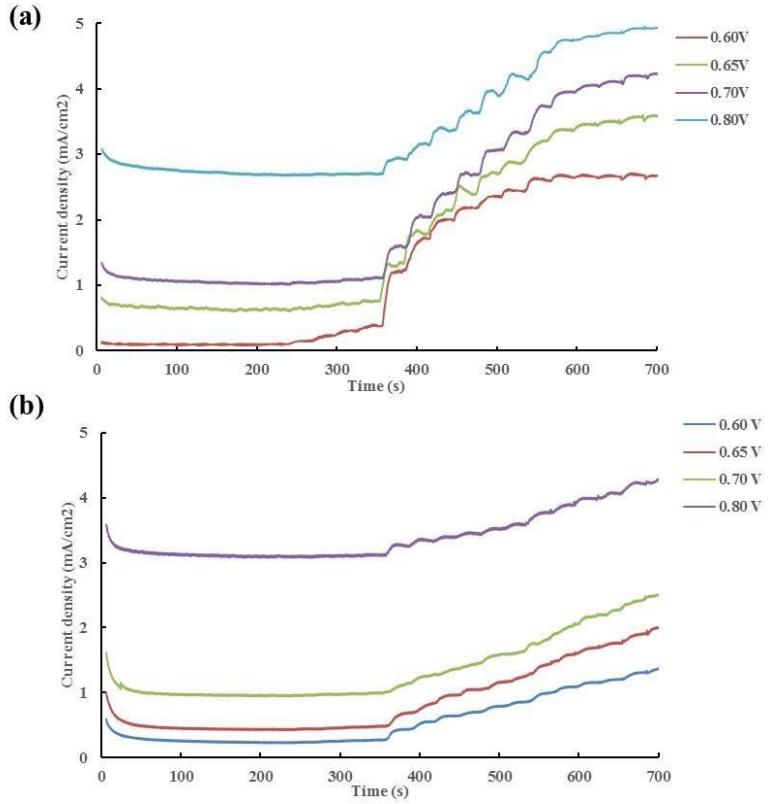

Figure 4. 15: Comparison of the amperometric response to glucose of the (a) Co_3O_4: Cu biosensor and (b) pristine Co_3O_4 electrode in 0.1 M NaOH solution

Table 4. 2: Sensitivity, linear range, LOD and response time results for the Co_3O_4: Cu and pristine Co_3O_4at various potentials

Potential (V vs Ag/AgCl)	**Sensitivity** (μA/mmcm^2)	**Concentration range**	**LOD** (μM)	**Response time** (s)
		Co_3O_4:Cu		
0.60	1850.4	18.3 μM – 1.44 mM	0.210	≤ 20
	76.1	2.1 mM – 7.56 mM		
0.65	1333	18.3 μM – 1.44 mM	0.153	≤ 10
	141	2.1 mM – 7.56 mM		
0.70	1215.3	18.3 μM – 1.44 mM	0.134	≤ 20
	181.6	2.1 mM – 7.56 mM		

0.80	687.5 153.4	18.3 µM – 1.44 mM 2.1 mM – 7.56 mM	0.09	≤ 20
		Pristine Co_3O_4		
0.60	392.8 74	18.3 µM – 1.44 mM 2.1 mM – 7.56 mM	0.264	≤ 10
0.65	488 105.3	18.3 µM – 1.44 mM 2.1 mM – 7.56 mM	0.155	≤ 20
0.70	373.8 115.3	18.3 µM – 1.44 mM 2.1 mM – 7.56 mM	0.143	≤ 20
0.80	277.7 88.2	18.3 µM – 1.44 mM 2.1 mM – 7.56 mM	0.436	≤ 20

The amperometric responses were conducted at a potential range of +0.6V to +0.8 V, and were utilized to evaluate the response of the pristine Co_3O_4 electrode to the successive addition of glucose at intervals of 30 s in 0.1 M NaOH solution. These results compared to the Co_3O_4: Cu biosensor resulted in two linear ranges with a lower sensitivity and a negligible higher LOD for all potential range of +0.6V to +0.8 V vs. Ag/AgCl tests. The pristine Co_3O_4 electrode at +0.65 V exhibited a sensitivity of 488 uA/cm^{2}mM and 105 uA/cm^{2}mM for the linear ranges of 18.3 µM up to 1.44 mM and 2.1 mM up to 7.6 mM, with a LOD of 0.155 µM (*S/N*=3) respectively. Hence, it can be resolved that the Co_3O_4:Cu biosensor exhibits improved chronoamperometric response to glucose than the pristine Co_3O_4 electrode.

Even though the response time of the as-developed biosensor is not the lowest as compared to previously reported cobalt based non-enzymatic electrodes, the ease of fabrication and scalability of production ensures the sensor will be a potential candidate for commercial application. A comparison of the non-enzymatic glucose sensors utilizing Co_3O_4 is summarized in *table 4.3*.

Table 4. 3: Contrast of non-enzymatic glucose sensors presented with respect to type, sensitivity, response time, LOD and linear range

Biosensor	**Sensitivity (uA/cm^2 mM)**	**Response time (s)**	**LOD**	**Linear range**	**Reference**
Co_3O_4 nano-fibers	36.25	≤ 7	0.97 µM	---	(Ding *et al.*, 2010)
Co_3O_4/ PbO_2	460	≤ 2	0.31 µM	5 µM-1.2 mM	(Chen *et al.*, 2013)
Co_3O_4-$Ni(OH)_2$	1.089	≤ 5	1.08 µM	5 uM-40 µM	(Rahman *et*

					al., 2010b)
Sn: Co_3O_4	921/265	≤ 4	100 nM	2 µM-0.5 mM & 0.6 mM-5.5 mM	(Chowdhury *et al*., 2017)
Zn: Co_3O_4	193	≤ 7	2 µM	5.5 mM-0.62 mM	(Chowdhury *et al*., 2016)
Co_3O_4: TiO_2	2008.82	≤ 5	0.34 µM	3 mM	(Gao *et al*., 2016)
Cu_2O-Cu	1620	---	49 µM	0-6 mM	(Wang *et al*., 2013)
Co_3O_4-$Ni(OH)_2$	1.089	≤ 5	1.08 µM	5-40 µM	(Mahmoudian *et al*., 2016)
Cu: Co_3O_4	1333/ 141	≤ 10	0.153 µM	18.3 uM-1.44 mM & 2.1 mM-7.6 mM	This work

The Co_3O_4:Cu biosensor has a greater improved sensitivity than Chowdhury *et al*. (2017), Ding *et al*. (2010) and Zhenfei *et al*. (2015) reported, and wider linear range than previous studied reported. The sensor also has a lower LOD as compared to the findings of Chowdhury *et al*. (2017), Zhenfei *et al*. (2015) and Ding *et al*. (2010).

4.6. Human serum and salivary glucose analysis

The developed sensor was also applied to detect glucose in human serum samples. *Figure 4.16* exhibits the chrono amperometric response of the proposed sensor after successive addition of 1mL serum (6.26 mM glucose concentration) in 46 mL of electrolyte solution.

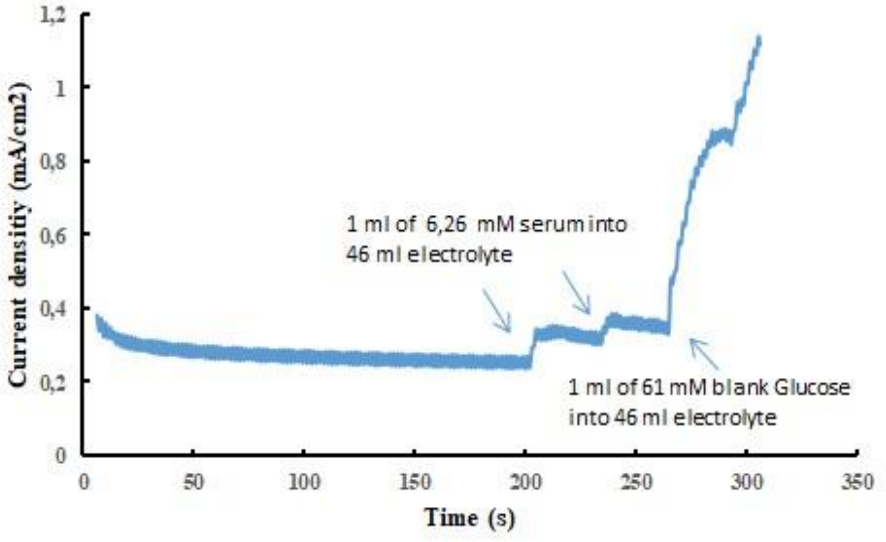

Figure 4. 16: Comparison of sensor data with conventional glucose detection technique

Clear increase in current response was observed after addition of human serum. The concentration of glucose in serum was measured by UV-vis spectrophotometry. The good agreement (*table 4.4*) between our proposed sensor and UV-vis spectrophotometry technique highlights the potential application of the non-enzymatic glucose sensor.

Table 4. 4: Human serum results

	UV-Vis Spectrophotometry (mM)	**As-developed sensor Test 1 (mM)**	**As-developed sensor Test 2 (mM)**
Result	6.26	6.60	6.30

In order to develop a non-invasive route for glucose detection, the sensor was used to detect glucose in spiked human saliva as a proof of concept. The saliva samples were spiked with different amounts of known glucose concentration for electrochemical analysis. *Table 4.5* shows that the obtained recovery was in the range of 92 – 97%. This highlights the sensor's potential application in glucose detection of real samples.

Table 4. 5: Detection of glucose in saliva sample (n=3)

Spiked (mM)	Measured by as-developed sensor (mM)	% Recovery
0.311	0.32	102
0.615	0.58	94.3
1.678	1.55	92.39

4.7. Selectivity study for the Co_3O_4: Cu biosensor

An interference study was conducted to evaluate the selectivity of the sensor in glucose detection as the human blood contains other key species i.e. ascorbic acid, acetaminophen, uric acid, fructose, sucrose, sodium chloride and potassium chloride.

The interference study was conducted using a 0.51 mM glucose, 0.05 mM fructose, 0.05 mM sucrose, 0.05 mM ascorbic acid, 0.05 mM acetaminophen, 0.05 mM uric acid, 54 mM sodium chloride and 64 mM potassium chloride solutions respectively, at an applied potential of +0.65 V. It can be seen from *figure 4.17* that the sensors' response to that of glucose if significantly higher than the addition of the other interference species. The slight current responses from the addition of fructose, sucrose, acetic acid, acetaminophen, uric acid, sodium chloride and potassium chloride can be neglected if compared to the current response obtained from the addition of glucose.

The sensor also maintained an excellent response when glucose was added successively after the addition of the interference species. This proves that the developed sensor can be used for reliable measurement of glucose in physiological samples. The good selectivity of the Co_3O_4: Cu towards glucose and against fructose, sucrose, acetic acid, acetaminophen, uric acid, sodium chloride and potassium chloride at +0.65 V vs. Ag/AgCl can be attributed to the repelling effect at the Co_3O_4: Cu surface (Ying et al., 2010).

Co_3O_4 has an isoelectric point ~8 and when in 0.1 M NaOH, it is negatively charged. The uric acid and ascorbic acid also have a negative charge due to the loss of protons in the presence of hydroxyl ions and phenolic groups, hence the electrocatalytic oxidation of the uric acid and ascorbic acid at the Co_3O_4: Cu electrode surface is decreased by the charge repelling effect.

The results obtained from the interference study confirm that the developed method for electrode fabrication is suitable for making biosensors for the detection of glucose.

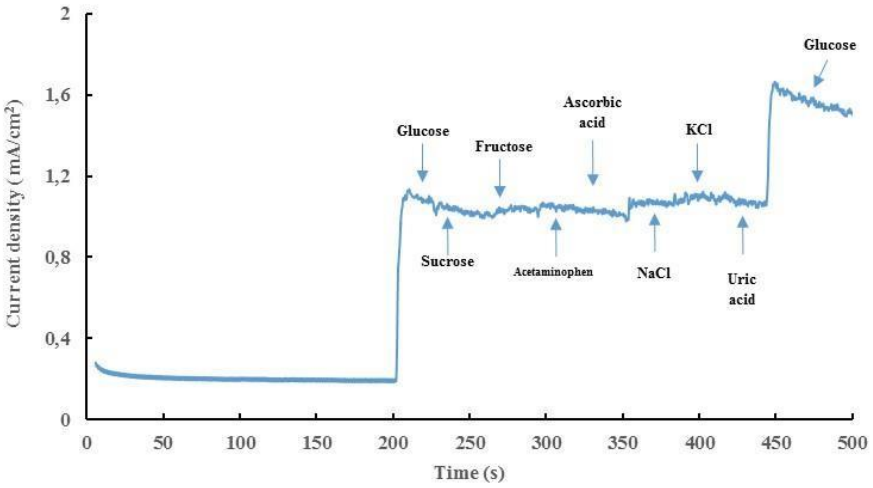

Figure 4. 17: Selectivity performance of the Co_3O_4: Cu thin film

4.8. Reproducibility analysis of the Co_3O_4: Cu biosensor

The reproducibility of glucose sensors is vital for the accurate measurement of analyte concentrations. Four individual electrodes were prepared accordingly and tested with 1 mM glucose at 25 mV/s. The results are depicted in *figure 4.18*.

The anodic oxidation current peak was then compared for inter electrode reproducibility. The percentage relative standard deviation (% R.S.D) was calculated to be 9 % for four sensors (1 mM glucose concentration). These results indicate good inter-electrode reproducibility for the method utilized to fabricate the electrodes for the application of glucose sensing as the % R.S.D reported by Chowdhury *et al*. (2016) is slightly higher.

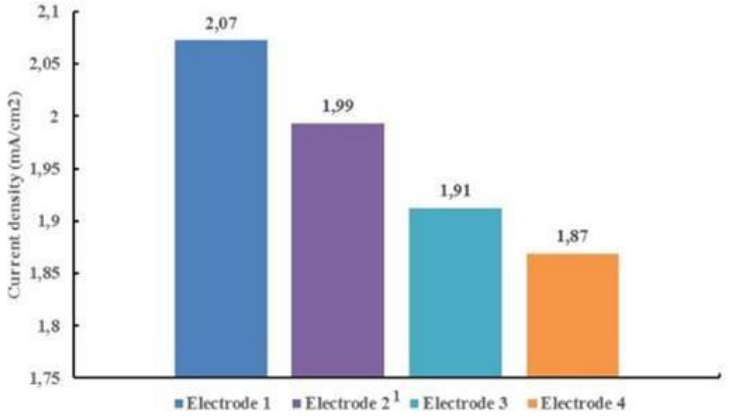

Figure 4. 18: Inter electrode reproducibility of the Co_3O_4: Cu electrode with the addition of 1 mM glucose solution

4.9. Repeatability and stability analysis of the Co_3O_4: Cu biosensor

Repeatability tests are vital to ensure that the same biosensor can be utilized multiple times without large deviations in glucose detection. Before each measurement for analysis, the sensor was washed with distilled water and dried under air flow to be tested in a freshly new 1 mM glucose solution immediately. The results are depicted in *figure 4.19*.

The anodic oxidation current peak was then compared for intra electrode repeatability. The percentage relative standard deviation (% R.S.D) was calculated to be 10 % between five repeats of the same electrode with 1 mM glucose. These results indicate good intra-electrode repeatability for the method utilized to fabricate the electrodes for the application of glucose sensing in comparison to literature.

The chemical stability and repeatability of the Cu-doped sensor was also determined by cyclic voltammetry for 100 cycles in a 1 mM glucose solution at a scan rate of 25 mV/s as seen in *figure 4.20*. It can be noted that no new redox pairs were found even though the anodic current decreases slightly hence it can be concluded that the chemical stability and repeatability of the sensor is good.

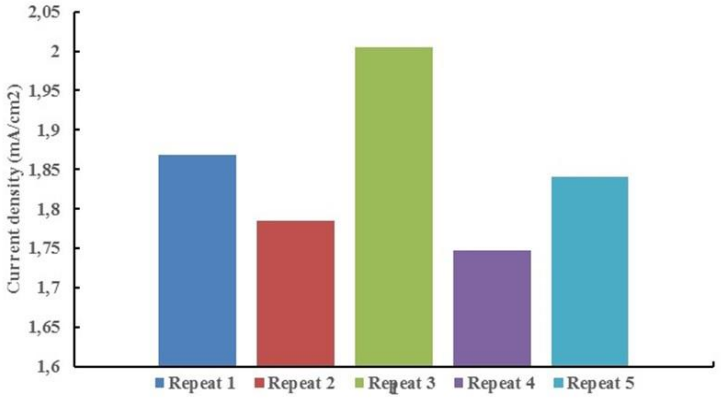

Figure 4. 19: Intra electrode repeatability of the Co_3O_4: Cu electrode at 25 mV/s in 0.1 M NaOH with the addition of 1 mM glucose

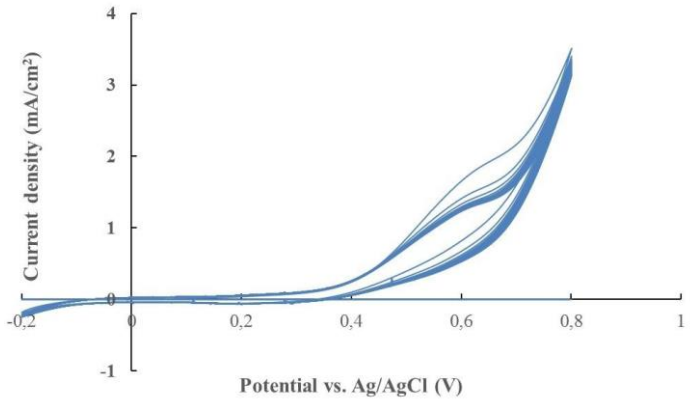

Figure 4. 20: Chemical stability of the Co_3O_4: Cu electrode

4.10. Conclusion

The Co_3O_4: Cu showed excellent electrocatalytic activity towards the oxidation of glucose in an alkaline medium. The electrode can be utilized to detect glucose in specific concentration ranges utilizing cyclic voltammetry and chronoamperometric techniques. The biosensor displayed an excellent sensing ability with a minimal LOD, appropriate response time, high sensitivity and acceptable shelf life and stability. The sensor also proved to be applicable to other species with minimal interference in the analytical sample. The ease of fabrication and economic feasibility for the fabrication of the biosensor substantiates the development of the next generation of non-enzymatic glucose sensors. It also withstands detection of glucose in human serum and saliva applications.

All data in this chapter was thoroughly interpreted to impart a precise conclusion which is provided in the next chapter.

~ Chapter 5 ~

Findings, contributions, conclusion & recommendations

This chapter comprises:

Section 5.1: *Introduction*

Section 5.2: *Findings- Summary of results*

Section 5.3: *Research significance*

Section 5.4: *Research contributions*

Section 5.5: *Conclusion*

Section 5.6: *Recommendations/future research*

Chapter 5: Findings, contributions, conclusion and recommendations

5.1. Introduction

This final chapter comprises a summary of the results obtained for the Cu-doped Co_3O_4 non-enzymatic glucose biosensor which was fabricated. The potential contributions of this study are discussed, and a final conclusion and recommendations for future research are formulated.

5.2. Findings: Summary of results

A facile solution-based process comprising spin coating and calcination was utilized for the fabrication of electrodes for bio-sensing applications. Cu-doped Co_3O_4 was utilized as a catalytic material to directly oxidise glucose without the presence of an enzyme. The presence of Cu in the Co_3O_4 host lattice enhanced the electrocatalytic activity of the electrode material as compared to its pristine counterpart.

Evaluation of the research proved that the film thickness and presence of Cu in the Co_3O_4 host enhanced the charge transferability of the Co_3O_4: Cu material compared to the pristine Co_3O_4 as confirmed by the EIS measurements. The modified glucose sensor exhibited two distinctive linear ranges (18.3 uM-1.44 mM and 2.1 mM-7.6 mM) at an applied potential of + 0.65 V vs. Ag/AgCl in 0.1 M NaOH solution. The sensor demonstrated good repeatability (R.S.D of <10%), stability and reproducibility (R.S.D of <10%). The as-prepared sensor showed a sensitivity of 1333 uA/cm^2 mM (lower concentration range) and 141 uA/cm^2 mM (upper concentration range), with a lower detection limit of 0.153 uM (S/N=3). The response time was concluded to be <10 s and the sensor was very selective towards glucose in the presence of various interference species i.e. acetic acid, acetaminophen, uric acid, fructose, sucrose, sodium chloride and potassium chloride.

The study also confirmed that the biosensor can be utilized to detect glucose in both saliva and human serum. This study thus demonstrated that the non-enzymatic glucose sensor is a promising candidate for non-enzymatic glucose detection.

5.3. Research significance

The Cu-doped Co_3O_4 biosensor exhibited a high electrochemical performance in its use as a non-enzymatic glucose sensor which is applicable to the medical industry in detection of glucose levels with respect to diabetes.

5.4. Research contributions

This research was published in journal *Sensing and Bio-Sensing Research*, and is made available to the academic industry. The design, development and optimization of a Cu-doped Co_3O_4 biosensor

that can be utilized for glucose detection in synthetic samples, human serum and saliva was accomplished. This research can be utilized in academic dissertations, conferences and further discussions.

This research project has contributed to the comprehensive reports in literature regarding the several drawbacks experienced in current glucose sensors. This involves specifically the pristine Co_3O_4 biosensors which suffer from a low electronic conductivity, which in turn results in a higher LOD, low sensitivity and low linear ranges, as detailed in the research project proposal. Therefore, this research proves that the application of a dopant material in Co_3O_4 enhanced its electronic and electrochemical properties. This work can be used for evaluation and further optimization with respect to nanotechnology and biosensor due to the potential of the biosensor.

5.5. Conclusion

The current study provides a feasible approach for the synthesis and development of the Cu-doped Co_3O_4 non-enzymatic glucose sensor.

The development and optimization of a non-enzymatic glucose sensor that can detect glucose in human saliva, human serum and synthetic samples has been provided to the academic industry. This sensor has excellent intra- and inter-electrode reproducibility and a long shelf life. It also provides a high sensitivity, low limit of detection and a broad linear range for glucose for detection, with an acceptable response time.

This study has extended and initiated a novel possibility for developing solution deposited nanostructured electrodes, utilizing copper and cobalt oxide, for sensing applications.

5.6. Recommendations/future research

The following are recommendations are for future research:

- The commercialization of non-enzymatic glucose sensors for glucose detection in human blood requires further ethical analysis with actual clinical diabetic patients.
- Since the as-prepared sensor was tested for glucose in human saliva, further knowledge and research needs to be conducted on a large scale to determine the correlation of diabetic patient's blood glucose concentrations and human saliva glucose concentrations. This will then result in the use of this biosensor to determine the glucose levels in diabetic patients.
- In order to conclude whether the as-prepared biosensor can be manufactured on a larger scale for commercial use, the material of construction and techniques should be conducted on SPE electrodes. These electrodes can be inserted directly into the current commercial glucose meters for glucose detection.

- A quantitative analysis can be conducted comparing Cu as a dopant, to other materials in Co_3O_4, as only a qualitative analysis was completed for this research. This could result in optimization of the sensor.

~ References ~

References

Almeida, T. 2010. *Hydrothermal Synthesis and Characterisation of α-Fe_2O_3 Nanorods.* Doctoral dissertation, University of Nottingham.

AMS. 2018. *Electrochemical Impedance Spectroscopy*. Available: *www.ams.org.cn*. 12th April 2019.

Andrienko, D. 2008. Cyclic Voltammetry.

Armen, B. 2007. Hall Effect Experiment. Department of Physics and Astronomy: The University of Tennessee. Available*: http://www.phys.utk.edu/labs/modphys/Hall%20Effect.pdf*. 2nd June 2018.

Awongo, M. A. 2016. Simple solution deposited Co_3O_4 electrode for rapid and selective nonenzymatic glucose detection. *In:* Chowdhury, M. R. (ed.). *Bachelor of Technology Research Project*. Cape Peninsula University of Technology.

Bahaa, M. A.Z., Bawaked, S. M., Kosa, S. A. & Schwiegerwilhelm. 2015. Effect of microwave power on the thermal genesis of Co3O4 nanoparticles from cobalt oxalate micro-rods. *Applied Surface Science*, 351(1)**,** 600-609.

Bansal, A. & Verma, S. S. 2016. Optical properties of bimetallic (Ag-Cu) core-noble metal shell nanoparticles. *Journal of Optics*, 45(1), 7-10.

Bard, A. J. & Faulkner, L. R. 2000. *Electrochemical Methods: Fundamentals and Applications* New York: Wiley.

Barreca, D., Gasparotto, A., Lebedev, O. L., Maccato, C., Pozza, A., Tondello, E., Turner, S. & Van Tendeloo, G. 2010. Controlled vapor-phase synthesis of cobalt oxide nanomaterials with tuned composition and spatial organization. *CrystEngComm*, 12(7)**,** 2185-2197.

Bobrow, L. S. 1996. Chapter 6: Diodes. *Fundamentals of Electrical Engineering.* New York: Oxford UP.

Brownson, D. A. & Kampouris, D. K. 2012. Graphene electrochemistry: fundamental concepts through to prominent applications. *Chemical Society*, 41(21)**,** 6944-6976.

Brundie, R.C., Charles, A. & Wilson, S. 1964. *Encyclopedia of Materials Characterisation.* Butterworth-Heinemann Publications.

Bunaciu, A. A., Udristioiu, E. G. & Aboul-Enein, H. Y. 2015. X-ray Diffraction: Instrumentation and Applications. *Analytical Chemistry*, 45(4)**,** 289-299.

Chen, P. & McCreery, R. 1996. Control of Electron Transfer Kinetics at Glassy Carbon Electrodes by Specific Surface Modification. *Analytical Chemistry,* 68(22)**,** 3958-3965.

Chen, X., Wu, G., Cai, Z., Oyama, M. & Chen, X. 2013. Advances in enzyme-free electrochemical sensors for hydrogen peroxide, glucose, and uric acid. *Microchimica Acta,* 181(7-8)**,** 689-705.

Chowdhury, M., Cummings, F., Kebede, M. & Fester, V. 2016. Binderless solution processed Zn doped Co_3O_4 film on FTO for rapid and selective non-enzymatic glucose detection. *Electroanalysis,* 28(1)**,** 1-10.

Chowdhury, M., Ossinga, C., Cummings, F., Chamier, J. & Kebede, M. 2017. Novel Sn Doped Co_3O_4Thin Film for Nonenzymatic Glucose Bio-Sensor and Fuel Cell. *Electroanalysis,* 29(1)**,** 1-12.

Cullity, B. D. 1978. *Elements of X-ray Diffraction,* Philippines, Addison-Wesley Publishing Company INC.

De Gree, A. 2015. The History and Working Principle of the Scanning Electron Microscope (SEM). *Azo Nano19*. Available: *https://www.azonano.com/article.aspx?ArticleID=3995*. 15th March 2018.

Ding, Y., Wang, Y., Su, L., Bellagamba, M., Zhang, H. & Lei, Y. 2010. Electrospun Co_3O_4 nanofibers for sensitive and selective glucose detection. *Biosensors and Bioelectronics,* 26(1)**,** 542-548.

Dong, X. C., Xu, H., Wang, X. W., Huang, Y. X., Chan-Park, M. B., Zhang, H., Wang, L. H., Huang, W. & Chen, P. 2012. 3D Graphene Cobalt Oxide Electrode for High-Performance Supercapacitor and Enzymeless Glucose Detection. *Acsnano,* 6(4), 3206-3213.

Doria, G., Conde, J., Veigas, B., Giestas, L., Almeida, C., Assuncao, M., Rosa, J., & Baptista, P.V. 2012. Noble metal nanoparticles for biosensing applications. *Sensors (Baseline),* 12(2), 1657-1687.

Egerton, R. F. 2005. *Physical Principles of Electron Microscopy.* New York: Springer Science and Business Media, Inc.

Ellmer, K., Miientus, R., Rossner, H. 2001. In situ investigation by energy dispersive X-ray diffraction (EDXRD) of the growth of magnetron sputtered ITO films. Surface and Coating Technology, 142(144), 1094-1099.

Espro, C., Donato, N., Galvagno, S., Aloisio, D., Leonardi, S. G. & Neri, G. 2014. CuO Nanowires-based Electrodes for Glucose Sensors. *AIDIC The Italian Association of Chemical Engineering,* 41(1)**,** 415-420.

Fasmin, F. & Srinivasan, R. 2017. Electrical Impedance Spectroscopy. *Journal of The Electrochemical Society, 1*64(7)**,** 303-325.

Gao, Z., Zhang, L., Ma, C., Zhou, Q., Tang, Y., Tu, Z., Yang, W., Cui, L. & Li, Y. 2016. TiO_2 decorated Co3O4 acicular nanotube arrays and its application as a non-enzymatic glucose sensor. *Biosensors and Bioelectronics,* 80 (2016)**,** 511-518.

Green, R. 2017. *Hall Effect Measurements in Materials Characterisation*. Cleveland, Ohio: Keithley Instruments, Inc.

Guo, C., Wang, Y., Zhao, Y., & Xu, C. 2013. Non-enzymatic Glucose Sensor Based on Three Dimensional Nickel Oxide for Enhanced Sensitivity. *Electronic Supplementary Material (ESI) for Analytical Methods*. 5(7), 1644-1647.

Hofer, F., Schmidt, F. P., Grogger, W. & Kothleitner, G. 2016. Fundamentals of electron Energy-Loss Spectroscopy. *Materials Science and Engineering C,* 109(1)**,** 1-9.

Hrapovic, S. & Luong, J. 2003. Picoamperometric Detection of Glucose at Ultrasmall Platinum-Based Biosensors: Preparation and Characterisation. *Analytical Chemistry* 75(14)**,** 3308-3315.

Ibach, H. & Mills, D. L. 1982. *Electron Energy Loss Spectroscopy and Surface Vibration.* New York: Academic Press.

Ibupoto, Z. H., Khun, K., Beni, V. & Willander, M. 2013b. Non-Enzymatic Glucose Sensor Based on the Novel Flower like Morphology of Nickel Oxide. *Soft Nanoscience Letters,* 3(1)**,** 46-50.

Kun, T., Prestgard, M. & Tiwari, A. 2014. A review of recent advances in nonenzymatic glucose sensors. *Materials Science and Engineering C,* 41(2014)**,** 100-118.

Kalantar-Zadeh, K. 2013. Sensors: An Introductory Course. *Springer***,** 11-28.

Kang, X., Mai, Z., Zou, X., Cai, P. & Mo, J. 2007. A novel glucose biosensor based on immobilization of glucose oxidase in chitosan on a glassy carbon electrode modified with gold–platinum alloy nanoparticles/multiwall carbon nanotubes. *Analytical Biochemistry,* 369(1)**,** 71–79.

Khursheed, A. 2011. *Scanning Electron Microscope Optics and Spectrometers.* Singapore: World Scientific.

Kriedemann, B. C. 2014. *The critical process conditions for controlled growth of iron oxide nanoparticles synthesized using continuous hydrothermal synthesis.* Master of Technology dissertation, Cape Peninsula University of Technology.

Kung, C. W., Lin, C. Y. & Lai, Y. 2011. Cobalt oxide acicular nanorods with high sensitivity for the non- enzymatic detection of glucose. *Biosensors and Bioelectronics,* 27(1)**,** 125-131.

Li, G. & Miao, P. 2013. Electrochemical Analysis of Proteins and Cells, Chapter 2: Theoretical Background of Electrochemical Analysis. Berlin: Springer.

Luo, J., Jiang, S., Zhang, H., Jiang, J. & Liu, X. 2012a. A novel non-enzymatic glucose sensor based on Cu nanoparticle modified graphene sheets electrode. *Analytica Chimica Acta,* 709(1)**,** 47-53.

Luo, J., Zhang, H., Jiang, S., Jiang, J. & Liu, X. 2012b. Facile one-step electrochemical fabrication of a non-enzymatic glucose-selective glassy carbon electrodemodified with copper nanoparticles and graphene. *Microchimica Acta,* 177(1)**,** 485–490.

Macdonald, J. R. 1987. *Impedance Spectroscopy: Emphasizing Solid Materials and Systems.* New York: Wiley.

Mahmoudian, M. R., Basirun, W. J., Woi, P. M., Sookhakian, M., Yousefi, R., Ghadimi, H. & Alias, Y. 2016. Synthesis and characterisation of Co_3O_4 ultra-nanosheets and Co_3O_4 ultra-nanosheet - $Ni(OH)_2$ as non-enzymatic electrochemical sensors for glucose detection. *Materials Science and Engineering C,* 59(1)**,** 500-508.

Metrohm, A. B. V. 2017. Basic overview of the working principle of a potentiostat/galvanostat (PGSTAT) – Electrochemical cell setup. *Metrohm Autolab*. BV, 1-3.

Mirershadi, S., Nikniaz, A. & Kandjani, S. 2015. *Solar Cells: New Approaches and Review*. Available: *https://www.intechopen.com.com/books/solar-cells-new-approaches-and-reviews/inorganic-organic-perovskite-solar-cells.* 12th April 2019.

Mohamad, N. R., Marzuki, N. H. C., Wahab, R. A., Buang, N. A. & Huyop, F. 2015. An overview of technologies for immobilization of enzymes and surface analysis techniques for immobilized enzymes. *Biotechnology, Biotechnological Equipment,* 29(2)**,** 205-220.

Park, S., Boo, H. & Chung, T. D. 2005. Electrochemical non-enzymatic glucose sensors. *Analytica Chimica Acta,* 556(1)**,** 46-57.

Rahman, M., Ahammad, A., Jin, J., Ahn, S. & Lee, J. 2010a. A Comprehensive Review of Glucose Biosensors Based on Nanostructured Metal-Oxides. *Sensors,* 10(5)**,** 4855-4886.

Riviere, J. C. 1990. *Surface Analytical Techniques,* Oxford, Oxford Science Publications, Clarendon Press.

Sahu, N., Parija, B. & Panigrahi, S. 2009. Fundamental understanding and modeling of spin coating process: A review. *Indian Journal of Physics,* 83(4)**,** 493-502.

Si, P., Huang, Y., Wanga, T. & Ma, J. 2012b. Nanomaterials for electrochemical non-enzymatic glucose biosensors. *RSC Advances*, 3(11), 3487-3502.

Sigma-Aldrich. 2018. *Fluorine doped tin oxide coated glass slide*. Sigma-Aldrich. Available: *https://www.sigmaaldrich.com/catalog/product/aldrich/735221?lang=en&region=ZA*. 2nd October 2017.

Smith, R., Inomata, H. & Peters, C. 2013. Chapter 4: Historical Background and Applications. *Supercritical Fluid Science and Technology*. Amsterdam: Elsevier.

Tian, K., Prestgard, M. & Tiwari, A. 2014. A review of recent advances in non-enzymatic glucose sensors. *Materials Science and Engineering C,* 41(1)**,** 100-118.

Toghill, K. & Compton, R. 2010a. Electrochemical Non-enzymatic Glucose Sensors: A Perspective and an Evaluation. *Electrochemical Science,* 5(2010)**,** 1246-1301.

Vesuvius. 2019. *Calcination*. Available: *https://www.vesuvius.com/en/our-solutions/de-de/industrial-processes/minerals-processing/calcination.html*. 1st May 2018.

Voutou, B. & Stefanaki, E.-C. 2008. Electron Microscopy: The basics. Physics of Advanced Materials Winter School, 1-11. Available: *https://pdfs.semanticscholar.org/576e/399e87efc2da56c2dc78c4c88d762e191886.pdf*. 12th July 2018.

Wang, G., He, X., Wang, L., Gu, A., Huang, Y., Fang, B., Geng, B. & Zhang, X. 2013a. Non-enzymatic electrochemical sensing of glucose. *Microchim Acta*, 180(3-4)**,** 161–186.

Wang, J.J., Hu, Yelin., Toth, R., Fortunato, G. & Braun, A. 2016. A facile nonpolar organic solution process of a nanostructured hematite photoanode with high efficiency and stability for water splitting. *Journal of Materials Chemistry, 4(*8)**,** 2821-2825.

Wang, Z. L., Yin, J. S. & Jiang, Y. D. 2000. EELS analysis of cation valence states and oxygen vacancies in magnetic oxides. *Micron,* 31(5)**,** 571-580.

Weaver, H., Hoflund, G. B., Minahan, D. M. & Salait, G. N. 2004. Electron energy loss spectroscopic investigation of Co metal, CoO and Co_3O_4 before and after Ar+ bombardment. *Applied Surface Science,* 235(4)**,** 420-448.

Wilson, R. & Turner, A. 1992. Glucose oxidase: an ideal enzyme. *Biosensors and Bioelectronics,* 7(3), 165-185.

World Health Organisation. 2016. *Diabetes Fact Sheet* [Online]. World Health Organization. Available: who.int/mediocentre/factsheets/fs312/enNovember2016. Accessed 12th August 2018.

Xiang, Q., Yu, J. & Wong, P.K. 2011. Quantitative characterisation of hydroxyl radicals produced by various photocatalysts. *Colloid and Interface Science*, 357(1), 163-167.

Yun, J. L, Lee, Y., Oh, D., Chen, T., Ceder, G. & Belcher, A. M. 2010. Biologically activated noble metal alloys at the nanoscale. Nano Letters, 10(7), 2433-2440.

Zhuang, Z., Su, X., Yuan, H., Sun, Q., Xiao, D. & Choi, M. M. F. 2007. An improved sensitivity non- enzymatic glucose sensor based on a CuO nanowire modified Cu electrode. *The Royal Society of Chemistry*, 133(1)**,** 126–132.

Zhou, C., Xu, L., Song, J., Xing, R., Xu, S., Liu, D. & Song, H. 2014. Ultrasensitive non-enzymatic glucose sensor based on three-dimensional network of ZnO-CuO hierarchical nanocomposites by electrospinning. *Scientific Reports*, 4(1)**,** 7382-7391.

Zhu, C., Yang, G., Li, H., Du, D. & Lin, Y. 2014. Electrochemical Sensors and Biosensors Based on Nanomaterials and Nanostructures. *Analytical Chemistry,* 87(1)**,** 230−249.

Zhu, H., LI, L., Zhou, W., Shao, Z. & Chen, X. 2016. Advances in non-enzymatic glucose sensors based on metal oxides. *Materials Chemistry B,* 46(4)**,** 7333-7349.

Zhu, Z., Gancedo, L. G., Flewitt, A. J., Xie, H., Moussy, F. & Milne, W. I. 2012. A Critical Review of Glucose Biosensors Based on Carbon Nanomaterials: Carbon Nanotubes and Graphene. *Sensors,* 12(5)**,** 5996-6022.

Zoski, C. G. 2007. *Handbook of Electrochemistry*. New Mexico: *Elsevier*.

~ Appendix ~

Appendix: Relevant Publication

Relevant publication: *Elemental Cu-doped Co_3O_4 thin film for highly sensitive non-enzymatic glucose detection*

Sensing and Bio-Sensing Research 23 (2019) 100262

Contents lists available at ScienceDirect

Sensing and Bio-Sensing Research

journal homepage: www.elsevier.com/locate/sbsr

Elemental Cu doped Co_3O_4 thin film for highly sensitive non-enzymatic glucose detection

Micaela Harry[a], Mahabubur Chowdhury[a,*], Franscious Cummings[b], Christopher J. Arendse[c]

[a] Department of Chemical Engineering, Cape Peninsula University of Technology, Cape Town 8000, South Africa
[b] Electron Microscope Unit, University of the Western Cape, Bellville 7535, South Africa
[c] Department of Physics and Astronomy, University of the Western Cape, Bellville 7535, South Africa

ARTICLE INFO

Keywords:
Co_3O_4
Non-enzymatic sensor
Glucose sensor
Thin film

ABSTRACT

We report on the non-enzymatic glucose sensing ability of elemental Cu doped Co_3O_4 thin film deposited on FTO in this study. A facile chemical solution method was used to substitute elemental Cu into the Co_3O_4 host lattice. The morphology of the electrode was characterized by XRD, SEM, HRTEM, SAED and EELS. The as prepared thin film exhibited very high sensitivity of 1850 μAcm^{-2} mM^{-1}, and linear range up to 7.6 mM. The sensor showed a limit of detection of 153 nM at a signal to noise ratio of 3. The developed sensor was used successfully to measure glucose level in human serum and spiked saliva samples.

1. Introduction

One of the major causes of death and disability in the world is diabetes mellitus. Currently there is no cure for diabetes mellitus and it is effectively controlled by regular monitoring of physiological blood glucose levels [1]. Traditional glucose sensors are enzymatic sensors; which utilizes glucose oxidase (GOx) on the electrode surface to oxidise glucose [2]. However challenges such as enzyme purification, intricate immobilization of enzyme and denaturing of enzyme limit the application of enzymatic sensors. Moreover, the need of redox shuttle to be present is the biggest barrier that hinders the sensitivity of this method [3–5]. Direct oxidation of glucose on the electrode surface in the absence of any enzyme (non-enzymatic sensor) is a current topic on interest, as it eliminates all the challenges associated with enzymatic sensors. Nanostructured metal oxides are more suitable for non-enzymatic glucose sensors as they possess good electrocatalytic properties, large surface areas and fast electron transfer [6]. In addition, nanostructured metal oxide materials can also counteract the drawbacks such as surface poisoning and reduction of the electrode [2]. High conductivity and catalytic activity are required for successful non-enzymatic glucose sensors. Various metal oxides such as $NiOH_2$ [7], Co_3O_4 [8], CuO, ZnO, SnO [9] etc. have been the subject of various studies for non-enzymatic glucose sensing applications. Among these, Co_3O_4 is of particular consideration due to its electro-catalytic properties, chemical stability and availability [10]. However, Co_3O_4 has low conductivity which results in a glucose sensor with low sensitivity as reported previously in literature [8,11,12]. Recently we have shown that elemental doping is a rational and effective approach to increase the electronic conductivity of Co_3O_4 [13,14]. Recently, Cu loading on Co_3O_4 support has been shown to increase hydrogen evolution due to the cooperative synergistic effect between Cu and Co_3O_4 [15]. Mehrabadi and co-authors have shown that $CuO_{0.3}CoO_{0.7}$ material showed enhanced gas sensing performance compared to pristine Co_3O_4 [16]. Thus, it is expected that the synergism from the combination of intrinsic and extrinsic Cu doping would be extremely interesting in glucose sensing applications and it is expected to achieve significantly improved performance when compared to pristine Co_3O_4.

Conventional electrode fabrication process for glucose sensing requires two step processing. Firstly, the catalysts are prepared in the form of nanoparticles and secondly it is immobilised on the electrode surface with a binder. The presence of additive material can produce contact resistance and obstruct reaction site as they are insulating and chemically inactive, which decreases the sensors performance [17–20]. Various advanced deposition techniques such as pulsed laser deposition (PLD), plasma sputtering, atomic layer deposition (ALD) have been used to fabricate metal oxide films. However, these techniques are capital investment intensive and requires frequent maintenance [21,22]. For the above-mentioned reasons, solution based process is a rational solution to the problem in the conventional systems.

In this study, we report on the facile solution processed deposition of Cu doped Co_3O_4 and its electrochemical glucose sensing ability. The as prepared Cu doped Co_3O_4 electrode showed high sensitivity,

* Corresponding author.
E-mail address: chowdhurym@cput.ac.za (M. Chowdhury).

https://doi.org/10.1016/j.sbsr.2019.100262
Received 19 November 2018; Received in revised form 4 February 2019; Accepted 7 February 2019

selectivity and stability.

2. Experimental procedure

2.1. Chemicals

Micasol detergent, ethanol (C_2H_5OH), fluorine doped tin oxide glass (FTO, 300 mm × 300 mm × 2 mm, surface resistivity ~7 Ω/sq), Cobalt (II) chloride hexahydrate ($CoCl_2.6H_2O$), sodium oleate ($C_{18}H_{33}NaO_2$), hexane (C_6H_{14}), Toluene (C_7H_8), cupric chloride ($CuCl_2.2H_2O$), glucose, fructose, sucrose, sodium chloride (NaCl), potassium chloride (KCl), acetaminophen ($C_8H_9NO_2$), uric acid ($C_5H_4N_4O_3$), ascorbic acid ($C_6H_8O_6$) and human serum were obtained from Sigma Aldrich South Africa and were used as it is without further purification.

2.2. Fabrication of the Cu doped Co_3O_4 electrode

2.2.1. Synthesis of copper doped Co_3O_4

The electrodes were fabricated in two steps. First, a cobalt oleate complex was synthesised by an ion exchange reaction between $CoCl_2.6H_2O$ and sodium oleate. For a typical synthesis, 40 mmol cobaltous chloride and 120 mmol sodium oleate were placed in a solution of 80 ml ethanol, 60 ml de-ionized water and 140 mL hexane. The solution was heated under reflux at 70 °C for 4 h. After refluxing, the upper organic layer containing cobalt oleate complex was washed 3 times in 30 mL distilled water in a seperatory funnel. The cobalt oleate complex was then placed in a petri dish and left to dry in the oven at 60 °C overnight. The residue was discarded appropriately. To prepare the Cu doped Co_3O_4 electrode, 0.09 g of cobalt oleate was dispersed in 0.5 mL toluene via sonication. Solution of $CuCl_2.2H_2O$ (in ethanol) was added to the cobalt oleate solution. The copper solution was added to the cobalt oleate solution at various volume percentages (98: 2 V/V, 90: 10 V/V, 85: 15 V/V, and 80: 20 V/V). This was done to vary the Cu concentration in the Co_3O_4 to find the optimum ratio of Cu: Co_3O_4 for enhanced electrochemical performance.

2.2.2. Electrode preparation

Rectangular pieces of FTO glasses were cut using a diamond glass cutter in accordance to the measurement of 4 cm length and 1.2 cm breath. The cut FTO glasses were cleaned via sonication by detergent for 10 min and rinsed with distilled water and dried under air. 50 µL of the precursor solution was deposited on the FTO glass by spin coating at 4000 rpm for 60 s. The film was then calcined at 350 °C for 10 min. The spin coating and calcination was repeated for $N = 1$ to 6 times as per the number of layers coated to evaluate the role of film thickness. The electrodes were calcined at 350 °C for 4 h at the final layer required. The pristine Co_3O_4 electrode was made the same as above except the fabrication solution was only cobalt oleate solution ($N = 1$ to $N = 5$).

2.2.3. Electrochemical measurements

All the electrochemical measurements were conducted using an Autolab PGSTAT302N potentiostat with Nova 2.0 software. A three electrode cell, consited of: Ag/AgCl (3 M) reference electrode, graphite rod as counter electrode and Cu:Co_3O_4 deposited FTO as working electrode was used for all electrochemical measurments. A quiescent 0.1 M NaOH solution was used as electrolyte for cyclic voltammetry and chronoamperometry measurements. Chronoamperometry was conducted under stirring and at an applied bias potential of + 0.65 V vs Ag/AgCl (3 M).

2.3. Surface characterization

X-ray diffraction (XRD) was used to identify the cobalt phase present in the as prepared electrode. The XRD patterns were recorded utilizing a PANalytical X'Pert PRO PW3040/60 diffractometer with Fe filtered Cu-Kα (λ = 0.154 nm) monochromated radiation source. Scanning electron microscopy (SEM) and energy dispersive X-ray spectroscopy (EDS) was conducted utilizing a Zeiss Auriga field-emission SEM, operated at 5 kV for imaging and 20 kV for EDS analysis. The EDS data was collected using an Oxford X-Max solid-state silicon drift detector, with an objective aperture of 60 µm and count rates between 60 and 120 s employed for high quality spectra. High resolution transmission electron microscopy (HR-TEM), selected area electron diffraction (SAED) and electron energy loss spectroscopy (EELS) data of the samples were collected using an FEI Tecnai F20 field emission gun TEM operated at 200 kV, equipped with a Gatan GIF-2001 energy filter. EELS was utilized to study the electron energy loss near edge fine structure (ELNEFS) signals of cobalt and oxygen ionization edges. Each spectrum was collected in normal parallel beam, bright-field TEM mode for 5 s. During TEM sample preparation, the sensing material was physically removed from the FTO substrates by scraping using a sharp edged razor blade in the presence of ethanol, thereby forming a concentrated solution; this was followed by ultra-sonication for 5 min. One drop of solution (~30 µl) was then drop casted onto a lacey carbon coated Ni grid (3 mm in diameter, 400 mesh) and completed by drying under a Xenon lamp for a further 5 min. Room temperature Hall effect measurements were conducted using an Ecopia Hall Effect Measurement System (HMS-3000 version 3.5) with 0.55 T magnetic field strength.

3. Results and discussion

3.1. Surface characterization of the modified Co_3O_4 electrode

The morphology and structure of the solution deposited film was evaluated by high resolution SEM and TEM. Fig. 1a & b represent the SEM image of the pristine and Cu doped electrodes, respectively. It can be seen from Fig. 1a that the deposited film of pristine Co_3O_4 is uniformly dispersed on the FTO. No hole or crack is observed from the SEM image, highlighting the consistency of the film thickness through the entire geometrical area. However, Cu doped Co_3O_4 film shows bigger nucleation sites through the entire film (Fig. 1b). The increased surface roughness is beneficial for electrochemical activities due to increased surface area [8]. The average film thickness on the Cu doped electrode is 1697 nm (Fig. 1c) and for the pristine electrode, the average film thickness is 357 nm (data not shown). This suggests successful incorporation of Cu into Co_3O_4 host lattice. TEM images of the Cu doped Co_3O_4 are presented in Fig. 1 (d & e). A uniform distribution of Cu was found (Fig. 1 f-h) from elemental X-ray mapping. Quantified EDS data (See supplementary data, Fig. S1) show that the Co and Cu X-ray signals are more or less one-to-one; this explains the relative uniform density of the colour maps for the respective elements.

Fig. 2 a & b represents the SAED patterns of the pristine and Cu doped Co_3O_4 electrode. The first four diffraction rings (Fig. 2a) are identified as that from the face centred cubic (fcc) Co_3O_4 crystal structure yielding $d_{111} = 0.474$ nm, $d_{220} = 0.291$ nm, $d_{311} = 0.249$ nm and $d_{400} = 0.205$ nm, respectively. From these values an average lattice constant of $a = 0.822 \pm 0.003$ nm was determined. Correspondingly, the Cu doped Co_3O_4 (Fig. 2b) electrode sample also exhibited the fcc crystal structure of Co_3O_4 but with a slight increase in the respective d-spacing to $d_{111} = 0.475$ nm, $d_{220} = 0.293$ nm, $d_{311} = 0.250$ nm and $d_{400} = 0.206$ nm. Due to this, there is a small expansion of the average lattice constant compared to the pristine Co_3O_4 sample, $a = 0.826 \pm 0.003$ nm. It can be observed from the XRD pattern (Fig. 2c) that the film contains the Co_3O_4 structure; regardless to the Cu doping. However, a slight increase in full-width-half-maxima can be observed for the Cu doped Co_3O_4 material. This phenomenon indicates strain in the Co_3O_4 matrix due to the successful addition of elemental Cu ions into the Co_3O_4 lattice. Also, the presence of (220), (311) and (400) peaks complements the observation from the TEM and SAED analysis.Fig. 3 compares the ELNEFS data of the Co $L_{3,2}$ ionization edge of the pristine (black curve) and Cu:Co_3O_4 (red curve) samples. Both

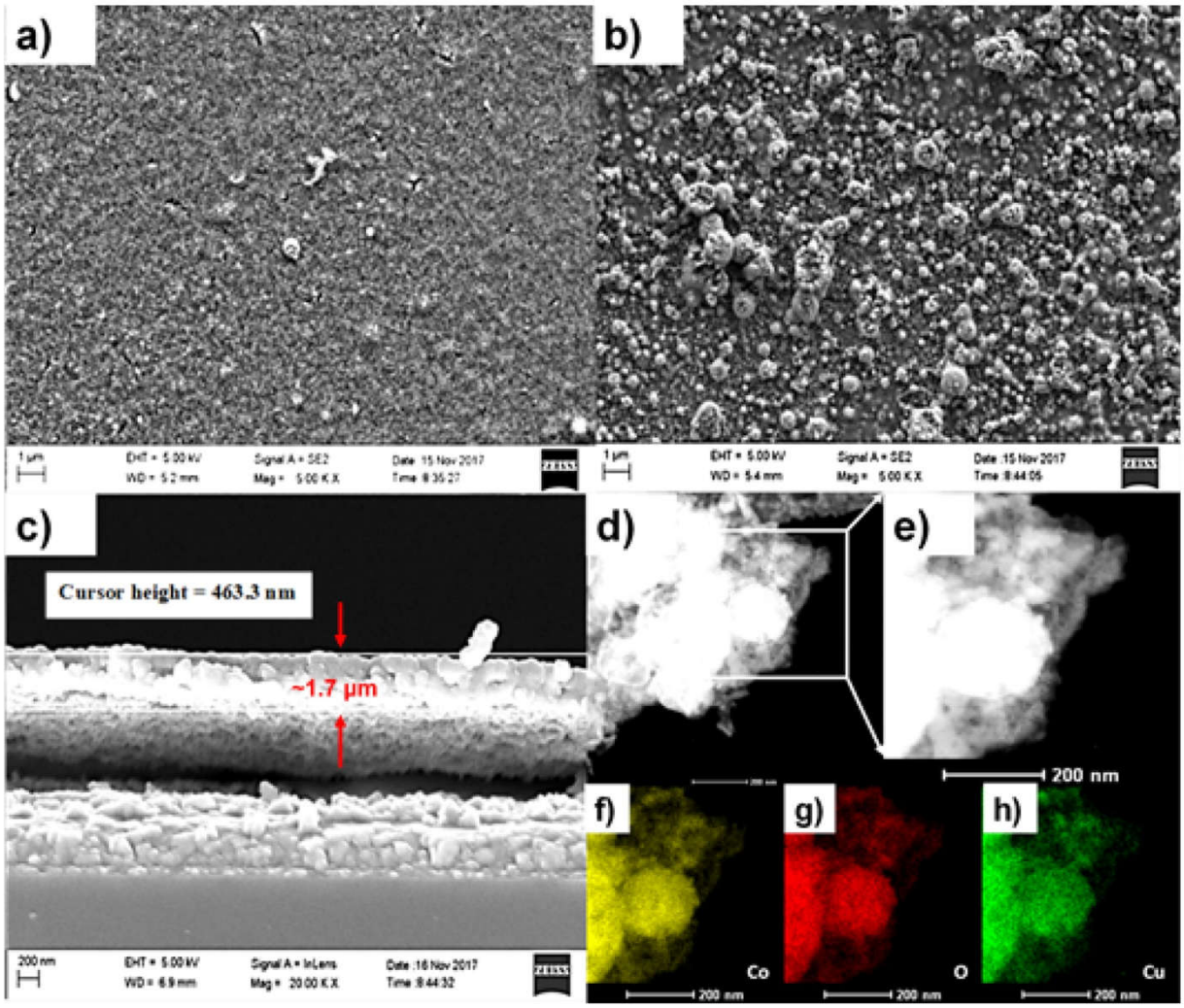

Fig. 1. SEM images of the film surface of pristine (a) Co_3O_4 and (b) Cu doped Co_3O_4; (c) cross sectional view of the Cu doped Co_3O_4 thin film; (d – h) TEM image and X-ray elemental distribution map of the Cu doped Co_3O_4 film.

materials show two sharp peaks at 783 (L_3) and 798 eV (L_2), which correspond to the Co $2p_{3/2}$ and Co $2p_{1/2}$ spin–orbit peaks of the Co_3O_4 spinel [23], respectively. In addition, it can be seen that the characteristic Cu $L_{3,2}$ edge at 931 eV is absent in the Cu:Co_3O_4 specimen, indicating that the Cu as identified in the X-ray elemental maps of Fig. 1, do not exist in either oxide or metallic form in the hybrid material. Rather, at closer inspection of the L_3/L_2 of the Co $L_{3,2}$, widely considered a fingerprint method for determining the Co valence state [23–26], a clearer understanding of the effect of the incorporation of the Cu in the Co_3O_4 matrix is developed. From Fig. 3 an L_3/L_2 ratio of 2.49 and 3.89 is determined for the pristine Co_3O_4 and Cu:Co_3O_4, respectively. The EELS spectra were normalised to the most intense ionization edge in order to compare the changes in the L_3/L_2 ratios in Fig. 3. To show this more clearly, two spectra have been added in the supplementary section (Fig. S2 and Fig. S3). In Fig. S2 it can be seen that the most intense (i.e. L_3) of the pure Co_3O_4 sample peaks at 783.4 eV with an electron count rate of 8051.48, whereas the L_2 edge peaks at 798 eV with a count of 3227.87. As such, an L_3/L_2 ratio for the pure Co_3O_4 sample of 8051.48/3227.87 = 2.494 is obtained. Similarly when doing the background subtraction of the raw Cu:Co_3O_4 spectrum (Fig. S3), an L_3/L_2 = 8617.400/2245.67 = 3.837 is obtained. The ratio of 2.49 is typical for cobalt oxides exhibiting cobalt ions in two oxidation states: one-third of the Co atoms being Co^{2+} in a tetrahedral coordination to oxygen and two thirds Co^{3+} in an octahedral oxygen environment [23,24]. The increase in the L_3/L_2 ratio for the Cu modified Co_3O_4 proves that a change in the $1/3Co^{2+}$ + $2/3Co^{3+}$ coordination occurred upon incorporation of the Cu ions in the Co_3O_4 matrix. The value of 3.89 is typical of pure Co^{2+} and in some instances Co^{4+} valence states [25,26]. However, considering the expansion in lattice parameter measured from the SAED results of Fig. 2 and the distribution of the Cu elements in the X-ray maps of Fig. 1, the increase in L_3/L_2 ratio, and subsequent change in valence state of the Co oxide, is attributed to doping by the Cu atoms.

3.2. Electrochemical behaviour of the Cu doped Co_3O_4 electrodes

Cyclic voltammetry (CV) was utilized to evaluate the performance of the Co_3O_4:Cu electrode for electrocatalytic oxidation of glucose in an alkaline solution of 0.1 M NaOH. Cyclic voltammetry was performed in the potential range between −0.2 V to 0.8 V vs. Ag/AgCl. Various ratios of Cu (98:2; 90:10; 85:15 and 80: 20; Co_3O_4:Cu) was introduced into the Co_3O_4 host lattice structure to find the optimum level of Cu doping for enhanced electrochemical activity. The 90:10 ratio of Co_3O_4:Cu depicted the highest electrochemical activity (current density response) in comparison to the other ratios studied (Fig. S4, supplementary document). Electrode film thickness plays a big role in enhanced electrochemical performance of any sensor. In this study, the electrode film thickness was controlled by increasing the no. of layers deposited (N = 1 to 6) on the FTO substrate. From the EIS study it was found that the resistance for charge transfer (R_{ct}) in 4 layer deposited electrode

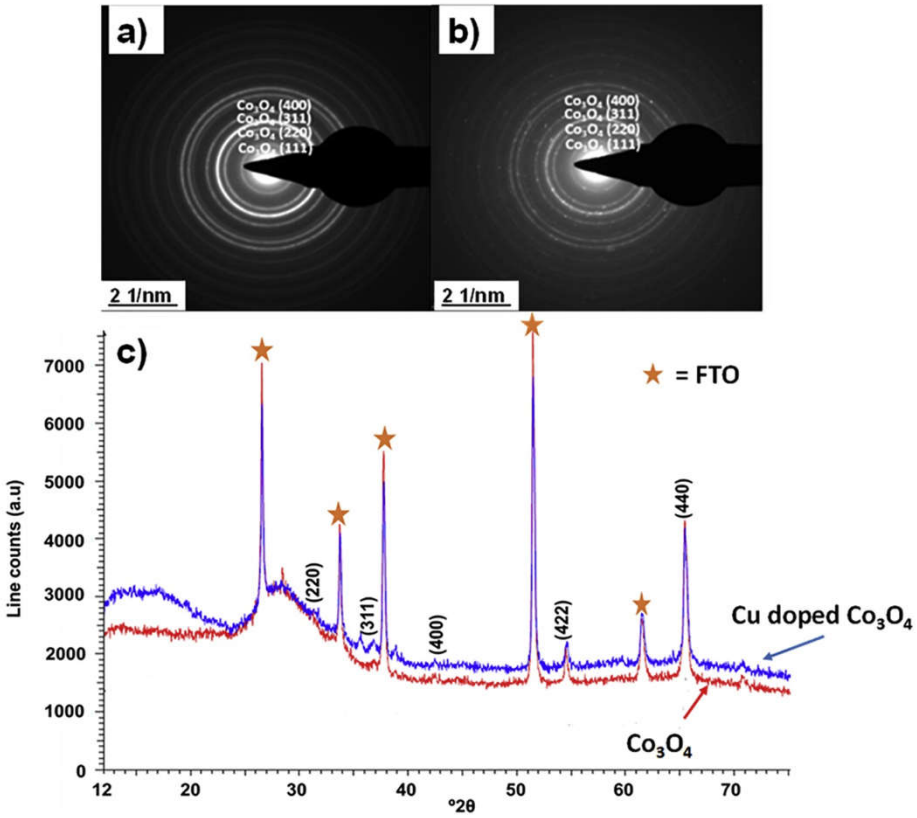

Fig. 2. (a) & (b) Selected area electron diffraction patterns for pristine and Cu doped Co_3O_4 electrode respectively, (c) XRD patterns of the pristine and Cu doped Co_3O_4 electrodes.

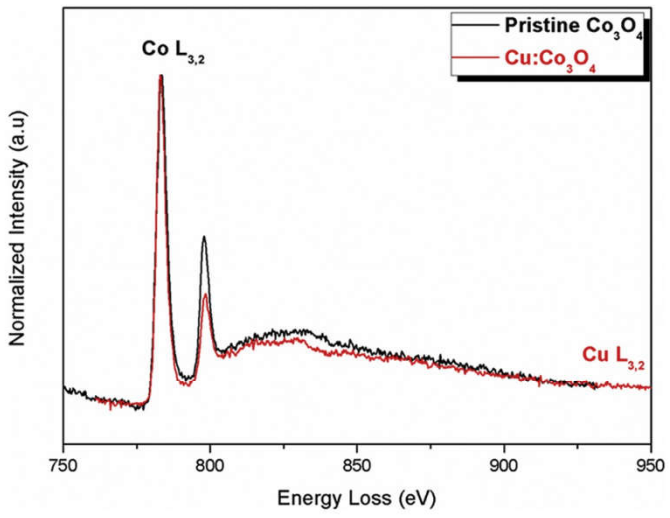

Fig. 3. Electron energy loss spectroscopy results comparing the Co $L_{3,2}$ ionization edge of the pristine Co_3O_4 sample to that of the Cu incorporated Co_3O_4 material.

was significantly lower (data not shown) than the other layers studied. Hence, the 4 layer deposited electrode showed the highest electrochemical activity (Fig. S5, supplementary document). All electrochemical results reported in this study were obtained using a 90:10 ratio of Co_3O_4:Cu with $N = 4$ electrode unless otherwise stated. A comparison between the CV of pristine Co_3O_4 and Cu doped Co_3O_4 highlighted the effect of Cu doping in Co_3O_4 host lattice structure, as the Cu doped Co_3O_4 showed enhanced electrochemical activity compared to pristine Co_3O_4 (Fig. S6, supplementary document). The pristine Co_3O_4 and Cu doped Co_3O_4 electrode exhibited a current density around 2.85 and 3.78 mA/cm^2 respectively in the presence of 5 mM glucose at +0,65 V. The presence of Cu doping in Co_3O_4 enhanced the catalytic oxidation current by 33%. It can be seen from Fig. 4a that there is a significant increase in the anodic current in the presence of 2 mM glucose compared to the absence of glucose. This highlights the glucose sensing ability of the as prepared electrode. Two pairs of redox peaks can be observed (Fig. 4a) due to the electrochemical redox reaction between Co_3O_4 and the OH^- ions [27]. The first pair of redox peaks (I/II) appeared in the relative low potential zone between +0.1 V to +0.3 V, and can be ascribed to the reversible transition between Co_3O_4 and CoOOH. The other set of redox peaks (III/IV) observed in the potential range of +0.6 to 0.7 V can be assigned to the conversion of CoOOH to Co_3O_4 [28]. Interestingly it can be observed from Fig. 4b that with increase in glucose concentration the anodic peak shifts towards more positive potential. The changes in CoO_2 and CoOOH species concentration result in the slight shift of the positive peak. The glucose oxidation mechanism can be summarized as follows:

$$Co_3O_4 + OH^- + H_2O \leftrightarrow 3CoOOH + e^- \quad (1)$$

$$CoOOH + OH^- \leftrightarrow CoO_2 + +H_2O + e^- \quad (2)$$

$$2CoO_2 + C_6H_{12}O_6 \rightarrow 2CoOOH + C_6H_{10}O_6 \quad (3)$$

The change in anodic and cathodic peak current at various scan rate is presented in Fig. 4c. A linear correlation exists between the peaks and the scan rate. This provides evidence of a fast electrochemical process and that the process is a surface controlled process of redox reaction [27].

The interfacial properties of the pristine Co_3O_4 and the modified Co_3O_4:Cu electrode were studied by electrochemical impedance spectroscopy (EIS) and presented in the form of Nyquist plot (Fig. 4d). The Nyquist diagrams did not exhibit a clear semicircle for both the pristine Co_3O_4 and Cu:Co_3O_4 electrodes. Exhibited semicircle and linear part at high and low frequency region can be attributed to charge transfer (R_{ct})

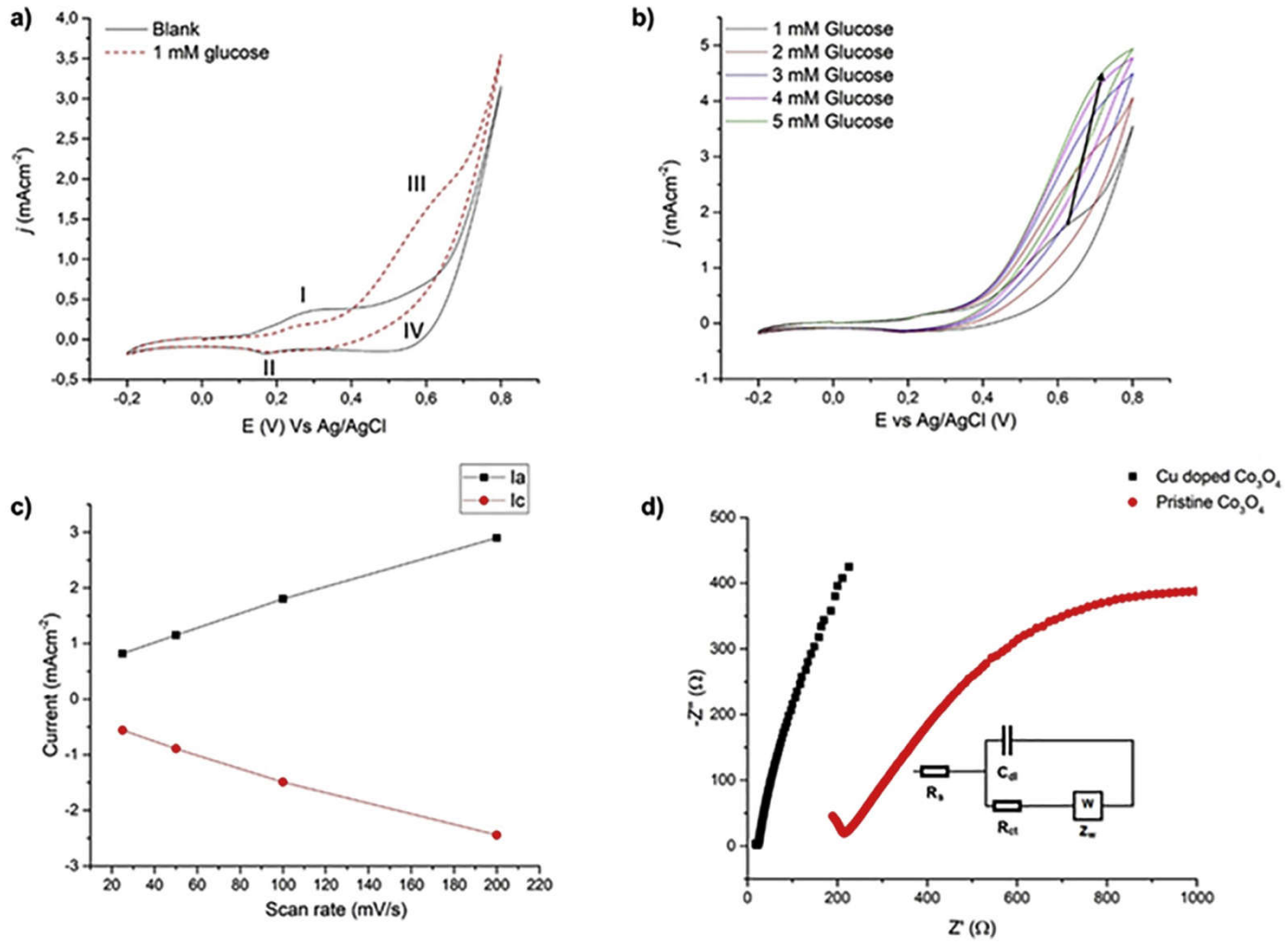

Fig. 4. Electrochemical behaviour of the Cu:Co_3O_4 thin film electrode in 0.1 M NaOH electrolyte solution; a) cyclic voltammogram of the pristine and Cu doped Co_3O_4 in the absence and presence of glucose at a scan rate of 25 mVs^{-1}, b) cyclic voltammetry of the Cu:Co_3O_4 thin film electrode in the presence of various glucose concentration at a scan rate of 25 mVs^{-1}, c) effect of scan rate on the electrochemical behaviour of Cu doped Co_3O_4 thin film electrode and d) Nyquist plot of pristine and Cu doped electrode.

and Warburg impedance (Z_w) respectively which provides indication of the electron transfer kinetics. It can be seen from Fig. 4d that the Cu:Co_3O_4 doped electrode exhibits a smaller semi-circle compared to the pristine electrode, highlighting higher electron transfer kinetics. Randle circuit (inset Fig. 4d) was used to calculate the R_{ct} values for both pristine (R_{ct} = 292 Ω) and Cu doped Co_3O_4 electrode (R_{ct} = 1.09 Ω). The Bode plot presented in supplementary document (Fig. S7) also shows that the charge transfer resistance decrease significantly with the presence of Cu in the Co_3O_4; highlighting the good electrochemical activity of the Cu doped $C_{o3}O_4$. Hall effect measurements were carried out to further evaluate the role of Cu doping in Co_3O_4 host lattice structure. The pristine Co_3O_4 sample was not very conductive, hence the input current was very low i.e. 0.2 μA. The Cu doped sample on the other hand displayed a greater conductivity thus the input current for conductivity measurement was in the range of 25–150 μA. The conductivity increased by three orders of magnitude with the addition of the Cu in Co_3O_4 and found to be 80 and 3.72×10^{-2} /Ωcm for Cu:Co_3O_4 and Co_3O_4, respectively. The increased conductivity is due to the successful Cu-doping of the Co_3O_4, as evinced by the increased carrier (electron) concentration from 1.69×10^{16} /cm^3 (for the pristine Co_3O_4) to 2.95×10^{19} /cm^3 (for the Cu: Co_3O_4). It should be noted that both films exhibited the n-type semiconductor behaviour of the electrodes.

3.3. Chronoamperometry study of the Cu doped Co_3O_4 electrodes

It was shown earlier (Fig. 4 a & b) that the oxidation peak of glucose was in the potential range of 0.6–0.7 V vs Ag/AgCl. Chronoamperometric (CA) detection of glucose was carried out (Fig. 5a) in the potential range of 0.6–0.8 V vs Ag/AgCl to evaluate the role of applied potential on the sensor sensitivity. Chronoamperometric measurement was performed under stirring at a successive addition interval of 30s. The sensor displayed a classical step style increase in current density after each successive addition of glucose at all applied potentials. The response time of the sensor in all cases were < 10 s. From the dose response curve presented in Fig. 5b it was observed that the sensor exhibits two distinctive linear ranges (18.3 μM to 1.44 mM and 1.44–7.36 mM). The sensitivity value was found to be larger in the low concentration range (18.3 μM - 1.44 mM) compared to higher concentration range (1.44–7.36 mM) for all applied potentials (table, inset Fig. 5b). The maximum sensitivity value was calculated to be 1850.4 $\mu Acm^{-2} mM^{-1}$ at +0.6 V (low range). However, the sensitivity in the second linear range increased with increasing applied potential. The reported sensitivity in this study was significantly higher compared to our previous studies [13,14]. The applied potential can be chosen depending on the application of the sensor. The limit of detection (LOD) was calculated utilizing the following equation.

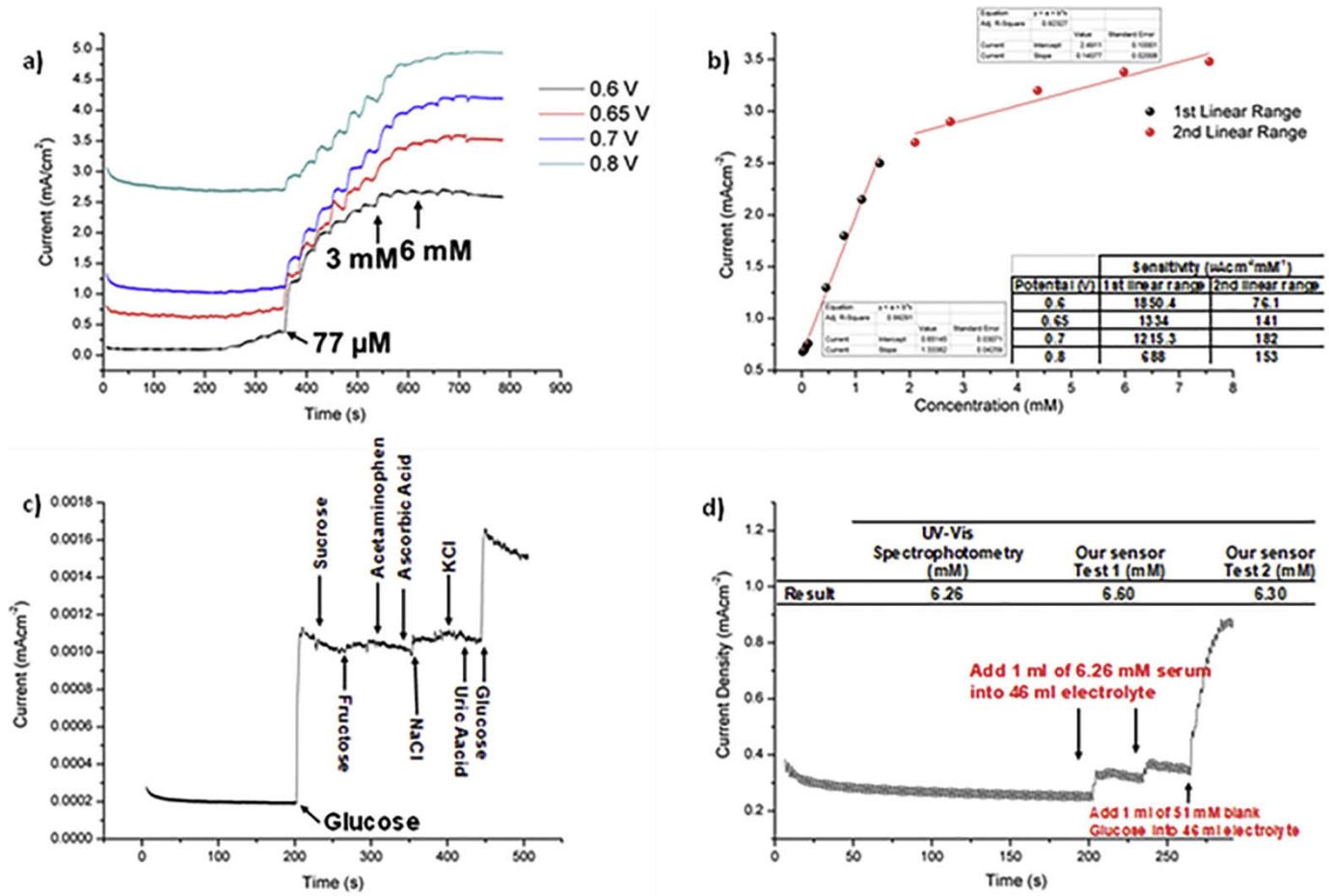

Fig. 5. a) Chrono amperometry of the electrode at different applied potential, b) typical dose response curve generated from CA at +0.65 V, c) Selectivity study of the as prepared electrode and d) comparison of sensor data with conventional glucose detection technique.

$$\mathrm{LOD} = \frac{3\sigma}{\mathrm{m}} \quad (4)$$

σ is the standard deviation of the sample linear range obtained after the addition of the glucose; m is the slope of the calibration curve. The extrapolated LOD was calculated to be 0.153 uM (S/N = 3). Table 1 shows a comparison of the applied potential of several typical non-enzymatic glucose electrodes. Compared with other studies, the present work exhibited high sensitivity and low detection limit with reasonable response time. Interference study (Fig. 5c) was conducted to evaluate the selectivity of the sensor in glucose detection due to the fact that the human blood contains other key species i.e. ascorbic acid (AA), acetaminophen (AC), uric acid (UA), fructose, sucrose, sodium chloride (NaCl) and potassium chloride (KCl). Interference study was conducted using a 1 mM glucose, 0.1 mM fructose, 0.1 mM sucrose, 0.1 mM AA, 0.1 mM AC, 100 mM NaCl and 100 mM KCl solutions respectively at an applied potential of +0.65 V. It can be seen that the sensors' response to glucose is significantly higher than other interference species. Electrode poisoning due to the presence of NaCl and KCl is a common phenomenon in the case of noble metal based sensors. The as developed sensor maintained good response when glucose was added after the successive addition NaCl and KCl and also other interference species. This proves that the developed sensor can be used for reliable measurement of

Table 1
Comparison of glucose detection performance of Cu:Co_3O_4 with other non-enzymatic sensors.

Material	Sensitivity ($\mu A cm^{-2} mM^{-1}$)	Response time (s)	LOD (µM)	Linear range	References
Co_3O_4: TiO_2	2008.82	≤ 5	0.34 µM	3 mM	[27]
Co_3O_4 nano-fibers	36.25	≤ 7	0.97 µM	–	[29]
Co_3O_4/PbO_2	460	≤ 2	0.31 µM	5 uM-1.2 mM	[30]
Co_3O_4-$Ni(OH)_2$	1.089	≤ 5	1.08 u µM	5 uM-40 uM	[31]
Sn: Co_3O_4	921/265	≤ 4	0.10 µM	2 uM-0.5 mM & 0.6 mM–5.5 mM	[14]
Zn: Co_3O_4	193	≤ 7	2.0 µM	5.5 mM–0.62 mM	[13]
Cu_2O-Cu	1620	–	49.0 µM	0–6 mM	[32]
Cu-Cu_2O nanoporous nanoparticles	123.8	–	0.05 µM	0.01–5.5 mM	[33]
Graphene wrapped Cu_2O nanotubes	285	≤ 9	0.003 µM	0.3–3.3 mM	[34]
Co_3O_4/GC	520.7	≤ 6	0.13 µM	< 2 mM	[35]
Cu: Co_3O_4	1850/76 1333/ 141	≤ 10	0.153 µM	18.3 µM-1.44 mM & 1.44 mM–7.6 mM	This work

Table 2
Detection of glucose in saliva sample ($n = 3$).

Spiked (mM)	Measured by Sensor (mM)	% Recovery
0.311	0.32	102
0.615	0.58	94.3
1.678	1.55	92.39

glucose in physiological samples. The good selectivity of the Cu:Co_3O_4 sensor towards glucose at +0.65 V can be attributed to the repelling effect at the Cu:Co_3O_4 surface as was first proposed by Ding and co-authors [8]. The results obtained from the interference study confirm that the developed method for electrode fabrication is suitable for making biosensors for glucose detection. The developed sensor was also applied to detect glucose in human serum sample. Fig. 5d exhibits the chrono amperometric response of the proposed sensor after successive addition of 1 mL serum (6.26 mM glucose concentration) in 46 mL of electrolyte solution. Clear increase in current response was observed after addition of human serum. The concentration of glucose in serum was measured by UV–vis spectrophotometry. The good agreement (Fig. 5d inset) between our proposed sensor and UV–vis spectrophotometry technique highlights the potential application of the non-enzymatic glucose sensor. In order to develop a non-invasive route for glucose detection, the sensor was used to detect glucose in spiked human saliva as a proof of concept. The saliva samples were spiked with different amount of known glucose concentration for electrochemical analysis. Table 2 shows that the obtained recovery is in the range of 92–97%. This highlights the sensor's potential application in glucose detection of real samples.

3.4. Reproducibility, repeatability, stability and shelf life of the proposed sensor

Reproducibility of glucose sensors is vital for the accurate measurement of analyte concentrations. Four individual electrodes were prepared accordingly and tested with 1 mM glucose at 25 mV/s. The anodic oxidation current peaks were then compared for inter electrode reproducibility. The percentage relative standard deviation (% R.S.D) was calculated to be 9% for four sensors. Repeatability tests were performed by measuring the current response of the electrode in 1 mM glucose solution ($n = 5$). Before each measurement, the sensor wash washed with distilled water and dried under air flow to be tested in freshly prepared 1 mM glucose solution immediately. The % R.S.D. was calculated to be 10% between five repeats of the same electrode (Supplementary document, Fig. S8). Chemical stability of the sensor was determined by cyclic voltammetry for 100 cycles (Supplementary document, Fig. S8) in a 1 mM glucose solution at a scan rate of 25 mV/s. It can be seen that no new redox pairs were found even though the anodic current decreases slightly. Hence it can be concluded that the chemical stability of the sensor is good. The shelf life of the sensor was evaluated over a four-week period. The sensor was tested, washed with distilled water and stored under ambient conditions after testing each week. The sensor maintained 80% of the initial current response after the four-week period (data not shown). This highlights the long term storage and testing ability of the proposed sensor.

4. Conclusion

In this study, elemental Cu was successfully substituted into the lattice structure of Co_3O_4 by a chemical solution method. Introduction of Cu resulted in increased electrical conductivity, charge career density and decreased charge transfer resistance in Co_3O_4. This ultimately resulted in enhanced electrochemical activity when compared to pristine Co_3O_4. The as developed Cu doped Co_3O_4 sensor, showed very high sensitivity of 1850 $\mu Acm^{-2} Mm^{-1}$ with a limit detection of 0.153 μM and, was used successfully to measure glucose concentration in human serum and spiked saliva sample.

Acknowledgments

Mahabubur Chowdhury would like to thank the National Research Foundation of South Africa for financial assistance (Grant no: 88220).

Conflicts of interest

The author declares no conflicts of interest.

Appendix A. Supplementary data

Supplementary data to this article can be found online at https://doi.org/10.1016/j.sbsr.2019.100262.

References

[1] J. Luo, H. Zhang, S. Jiang, J. Jiang, X. Liu, Facile one-step electrochemical fabrication of a non-enzymatic glucose-selective glassy carbon electrode modified with copper nanoparticles and graphene, Microchim. Acta 177 (2012) 485–490.
[2] P. Si, Y. Huang, T. Wanga, J. Ma, Nanomaterials for electrochemical non-enzymatic glucose biosensors, RSC Adv. (2012).
[3] J. Li, Y. Li, Y. Zhang, G. Wei, Highly sensitive molecularly imprinted electrochemical sensor based on the double amplification by an inorganic Prussian blue catalytic polymer and the enzymatic effect of glucose oxidase, Anal. Chem. 84 (2012) 1888–1893.
[4] C. Chen, Q. Xie, D. Yang, H. Xiao, Y. Fu, Y. Tan, S. Yao, Recent advances in electrochemical glucose biosensors: a review, RSC Adv. 3 (2013) 4473–4491.
[5] Z. Li, Y. Xin, Z. Zhang, H. Wu, P. Wang, Rational design of binder-free noble metal/metal oxide arrays with nanocauliflower structure for wide linear range nonenzymatic glucose detection, Sci. Rep. 5 (2015) 10617.
[6] C. Zhu, G. Yang, H. Li, D. Du, Y. Lin, Electrochemical sensors and biosensors based on nanomaterials and nanostructures, Anal. Chem. 87 (2014) 230–249.
[7] C.-Y. Ko, J.-H. Huang, S. Raina, W.P. Kang, A high performance non-enzymatic glucose sensor based on nickel hydroxide modified nitrogen-incorporated nanodiamonds, Analyst 138 (2013) 3201–3208.
[8] Y. Ding, Y. Wang, L. Su, M. Bellagamba, H. Zhang, Y. Lei, Electrospun Co3O4 nanofibers for sensitive and selective glucose detection, Biosens. Bioelectron. 26 (2010) 542–548.
[9] S.N.A. Mohd Yazid, I. Md Isa, S. Abu Bakar, N. Hashim, S. Ab Ghani, A review of glucose biosensors based on graphene/metal oxide nanomaterials, Anal. Lett. 47 (2014) 1821–1834.
[10] C.-W. Kung, C.-Y. Lin, Y.-H. Lai, R. Vittal, K.-C. Ho, Cobalt oxide acicular nanorods with high sensitivity for the non-enzymatic detection of glucose, Biosens. Bioelectron. 27 (2011) 125–131.
[11] L.T. Hoa, J.S. Chung, S.H. Hur, A highly sensitive enzyme-free glucose sensor based on Co3O4 nanoflowers and 3D graphene oxide hydrogel fabricated via hydrothermal synthesis, Sensors Actuators B Chem. 223 (2016) 76–82.
[12] T. Liangliang, H. Gege, C. Yanhua, W. Shenping, S. Yongyao, Y. Hengqing, Y. Cong, C. Yanling, L. Lu, Co_3O_4 based non-enzymatic glucose sensor with high sensitivity and reliable stability derived from hollow hierarchical architecture, Nanotechnology 29 (2018) 075502.
[13] M. Chowdhury, F. Cummings, M. Kebede, V. Fester, Binderless solution processed Zn doped Co3O4 film on FTO for rapid and selective non-enzymatic glucose detection, Electroanalysis 29 (2017) 578–586.
[14] M. Chowdhury, C. Ossinga, F. Cummings, J. Chamier, M. Kebede, Novel Sn doped Co3O4 thin film for nonenzymatic glucose bio-sensor and fuel cell, Electroanalysis 29 (2017) 1876–1886.
[15] Y. Yamada, K. Yano, Q. Xu, S. Fukuzumi, Cu/Co3O4 nanoparticles as catalysts for hydrogen evolution from Ammonia borane by hydrolysis, J. Phys. Chem. C 114 (2010) 16456–16462.
[16] Z.S. Mehrabadi, A. Ahmadpour, N. Shahtahmasebi, M.M.B. Mohagheghi, Synthesis and characterization of Cu doped cobalt oxide nanocrystals as methane gas sensors, Phys. Scr. 84 (2011) 015801.
[17] H.S. Jeon, M.S. Jee, H. Kim, S.J. Ahn, Y.J. Hwang, B.K. Min, Simple chemical solution deposition of Co3O4 thin film electrocatalyst for oxygen evolution reaction, ACS Appl. Mater. Interfaces 7 (2015) 24550–24555.
[18] H. Shi, G. Zhao, Water oxidation on spinel NiCo2O4 nanoneedles anode: microstructures, specific surface character, and the enhanced electrocatalytic performance, J. Phys. Chem. C 118 (2014) 25939–25946.
[19] C. Yuan, H.B. Wu, Y. Xie, X.W. Lou, Mixed transition-metal oxides: design, synthesis, and energy-related applications, Angew. Chem. Int. Ed. 53 (2014) 1488–1504.
[20] M. Cabo, E. Pellicer, E. Rossinyol, M. Estrader, A. Lopez-Ortega, J. Nogues, O. Castell, S. Surinach, M.D. Baro, Synthesis of compositionally graded nanocast NiO/NiCo2O4/Co3O4 mesoporous composites with tunable magnetic properties, J. Mater. Chem. 20 (2010) 7021–7028.
[21] M.E. Donders, H.C.M. Knoops, M.C.M. Van, W.M.M. Kessels, P.H.L. Notten, Remote

plasma atomic layer deposition of Co3O4 thin films, Journal of Electrochemical Society 158 (2011) G92–G96.
[22] W. Estrada, M.C.A. Fantini, S.C. de Castro, C.N. Polo da Fonseca, A. Gorenstein, Radio frequency sputtered cobalt oxide coating: structural, optical, and electrochemical characterization, J. Appl. Phys. 74 (1993) 5835–5841.
[23] Z.L. Wang, J.S. Yin, Y.D. Jiang, EELS analysis of cation valence states and oxygen vacancies in magnetic oxides, Micron 31 (2000) 571–580.
[24] H.A.E. Hagelin-Weaver, G.B. Hoflund, D.M. Minahan, G.N. Salaita, Electron energy loss spectroscopic investigation of co metal, CoO, and Co3O4 before and after Ar+ bombardment, Appl. Surf. Sci. 235 (2004) 420–448.
[25] B.M. Abu-Zied, S.M. Bawaked, S.A. Kosa, W. Schwieger, Effect of microwave power on the thermal genesis of Co3O4 nanoparticles from cobalt oxalate micro-rods, Appl. Surf. Sci. 351 (2015) 600–609.
[26] D. Barreca, A. Gasparotto, O.I. Lebedev, C. Maccato, A. Pozza, E. Tondello, S. Turner, G. Van Tendeloo, Controlled vapor-phase synthesis of cobalt oxide nanomaterials with tuned composition and spatial organization, CrystEngComm 12 (2010) 2185–2197.
[27] Z. Gao, L. Zhang, C. Ma, Q. Zhou, Y. Tang, Z. Tu, W. Yang, L. Cui, Y. Li, TiO2 decorated Co3O4 acicular nanotube arrays and its application as a non-enzymatic glucose sensor, Biosens. Bioelectron. 80 (2016) 511–518.
[28] I.G. Casella, M. Gatta, Study of the electrochemical deposition and properties of cobalt oxide species in citrate alkaline solutions, J. Electroanal. Chem. 534 (2002) 31–38.
[29] Y. Ding, Y. Wang, L. Su, M. Bellagamba, H. Zhang, Y. Lei, Electrospun Co3O4 nanofibers for sensitive and selective glucose detection, Biosens. Bioelectron. 26 (2010) 542–548.
[30] X. Chen, G. Wu, Z. Cai, M. Oyama, X. Chen, Advances in enzyme-free electrochemical sensors for hydrogen peroxide, glucose, and uric acid, Microchim. Acta 181 (2013) 689–705.
[31] M. Rahman, A.J.S. Ahammad, J.-H. Jin, S.J. Ahn, J.-J. Lee, A comprehensive review of glucose biosensors based on nanostructured metal-oxides, Sensors 10 (2010) 4855–4886.
[32] G. Wang, X. He, L. Wang, A. Gu, Y. Huang, B. Fang, B. Geng, X. Zhang, Non-enzymatic electrochemical sensing of glucose, Microchim. Acta 180 (2013) 161–186.
[33] Y. Zhao, Y. Li, Z. He, Z. Yan, Facile preparation of Cu–Cu_2O nanoporous nanoparticles as a potential catalyst for non-enzymatic glucose sensing, RSC Adv. 3 (2013) 2178–2181.
[34] J. Luo, S. Jiang, H. Zhang, J. Jiang, X. Liu, A novel non-enzymatic glucose sensor based on Cu nanoparticle modified graphene sheets electrode, Anal. Chim. Acta 709 (2012) 47–53.
[35] C. Hou, Q. Xu, L. Yin, X. Hu, Metal–organic framework templated synthesis of Co3O4 nanoparticles for direct glucose and H2O2 detection, Analyst 137 (2012) 5803–5808.